

INITIATION OF WATER HAMMER IN
HORIZONTAL OR NEARLY-HORIZONTAL PIPES
CONTAINING STEAM AND SUBCOOLED WATER

by

ROBERT WILLIAM BJORGE

S.B., Massachusetts Institute of Technology
(1978)

S.M., Massachusetts Institute of Technology
(1979)

Submitted to the Department of
Mechanical Engineering
in Partial Fulfillment of the
Requirements of the
Degree of

DOCTOR OF PHILOSOPHY

at the

MASSACHUSETTS INSTITUTE OF TECHNOLOGY

January 1983

(c) Robert W. Bjorge 1982

The author hereby grants to M.I.T. permission to reproduce
and distribute copies of this document in whole or in part.

Signature of Author



Department of Mechanical Engineering
September 9, 1982

Certified by

Thesis Supervisor

Accepted by

Chairman, Mechanical Engineering Department Committee

Archives

MASSACHUSETTS INSTITUTE
OF TECHNOLOGY

APR 20 1983

INITIATION OF WATER HAMMER IN
HORIZONTAL OR NEARLY-HORIZONTAL PIPES
CONTAINING STEAM AND SUBCOOLED WATER

by

ROBERT WILLIAM BJORGE

Submitted to the Department of Mechanical Engineering
on September 9, 1982 in partial fulfillment of the
requirements for the Degree of Doctor of Philosophy in
Mechanical Engineering

ABSTRACT

Water slug formation in a stratified countercurrent flow of steam and subcooled water in a horizontal or nearly-horizontal pipe traps a large steam bubble, which then collapses rapidly and causes a water hammer. This water hammer initiating mechanism has been studied experimentally and analytically.

A low pressure steam-water laboratory apparatus was constructed. Measurements of liquid depth, critical inlet water flow rate for water hammer initiation, liquid temperature rise along the pipe, and the location of water slug formation were made.

A one-dimensional two-phase flow model was developed which predicts steam flow and liquid depth profiles in a circular pipe. The model uses available shear stress and interfacial heat transfer correlations. Given the steam flow and liquid depth, a criterion for stratified-slug flow regime transition is applied at each location along a pipe to determine if water slug formation (leading to a condensation water hammer) will occur.

Calculations were made with the analytical model and compare favorably with the experimental results. Numerical studies were carried out to examine the effect of modifying various parameters (e.g., inlet water subcooling) on the predicted water hammer region boundaries for the low pressure system. The model was applied to two high pressure nuclear reactor systems which had experienced condensation water hammer events. A step-by-step procedure is presented for use by the piping system designer to prevent condensation water hammers of the type studied here.

Thesis Supervisor: Dr. Peter Griffith

Title: Professor of Mechanical Engineering

TO MY PARENTS
WILSON AND RUTH BJORGE

ACKNOWLEDGEMENTS

The author wishes to express his sincere appreciation for the advice and inspiration given by Professors Peter Griffith, Warren Rohsenow, Henry Paynter, and Peter Huber.

Mr. Bill Finley worked with the author on construction of the experimental apparatus. His ideas, suggestions, and assistance were invaluable.

This research was sponsored by Boston Edison Company and Northeast Utilities, Inc. The author gratefully acknowledges the support of the National Science Foundation in the form of a Graduate Fellowship.

BIOGRAPHICAL SKETCH

The author was born in Medford, Oregon on April 20, 1957. He was raised and attended elementary and secondary school in Eugene, Oregon. He attended the University of Oregon in 1974 and entered MIT in 1975, where he graduated in 1978 with the degree of Bachelor of Science in Nuclear Engineering. During the summers of 1977 and 1978, he worked in the Reactor Analysis and Safety Division at Argonne National Laboratory. He was awarded a National Science Foundation Graduate Fellowship to attend MIT, and in 1979 received the degree of Master of Science in Mechanical Engineering. For two years, he worked for the Medium Steam Turbine Department of General Electric Company in Lynn, Massachusetts, resuming his graduate studies in 1981.

TABLE OF CONTENTS

	<u>Page</u>
ABSTRACT.....	2
ACKNOWLEDGEMENTS.....	4
BIOGRAPHICAL SKETCH.....	5
LIST OF FIGURES.....	8
LIST OF TABLES.....	12
NOMENCLATURE.....	13
I. INTRODUCTION.....	19
A. Historical background.....	19
B. The present work.....	23
II. EXPERIMENTAL STUDIES.....	25
A. Experimental apparatus.....	25
B. High speed photographs.....	28
C. Air-water liquid depth tests.....	34
D. Steam-water tests.....	34
E. Liquid exit temperature tests.....	42
F. Discussion of experimental uncertainties..	42
III. THE ANALYTICAL MODEL.....	49
A. Foundations of the model.....	49
B. Derivation of the governing equations.....	53
C. Determination of Momentum and Heat Fluxes.	59
D. A criterion for water hammer initiation...	69
IV. THE NUMERICAL SOLUTION.....	74
A. The approach used.....	74
B. The computer program.....	79

	<u>Page</u>
V. NUMERICAL RESULTS.....	85
A. Comparison with data.....	85
B. Studies using the computer model.....	91
VI. CONCLUSIONS.....	107
REFERENCES.....	109
APPENDIX A. Computer Program Listings.....	112
APPENDIX B. Determination of c_1 from Critical Inlet Water Flow Rate Data.....	122
APPENDIX C. Computed Results for Low Pressure Sample Case.....	123
APPENDIX D. Computed Results for Low Pressure Sample Case with Vented Steam.....	131
APPENDIX E. Computed Results for PWR Steam Generator Sample Case.....	139
APPENDIX F. Computed Results for Millstone #1 Isolation Condenser Sample Case.....	147
APPENDIX G. Design Procedure for Water Hammer Avoidance.....	155

LIST OF FIGURES

<u>Figure</u>		<u>Page</u>
I-1	Original and modified feedwater lines to Steam Generator No. 22 of Indian Point Unit No. 2, taken from Cahill (1974).....	20
II-1	Schematic diagram of the experimental apparatus.....	26
II-2	Photographs of test section.....	27
II-3	Water slug formation and periodic water hammer in the 2.0 m pipe.....	30,31
II-4	Details of water slug formation in the 1.6 m pipe.....	33
II-5	Measurement of liquid depth using a scale wrapped around the pipe.....	35
II-6	Time to cessation of water hammers after shutoff of inlet water flow.....	41
II-7	Idealized model of brass pipe used in estimating the effect of tangential conduction.....	45
III-1	Flow geometry selected for analysis.....	50
III-2	Control volume used for global energy balance.....	55
III-3	Differential control volumes used for derivation of fundamental differential equations.....	55
III-4	Ratio of Taitel-Dukler (1976) to Mishima-Ishii (1980) stability parameter for given flow conditions.....	72
IV-1	Pipe length divided into finite difference sections (not necessarily of equal length).....	75
IV-2	Geometric formulae for a circular cross-section of a stratified flow.....	77

<u>Figure</u>		<u>Page</u>
IV-3	Sample computer run for typical conditions of low pressure experiments.....	80
V-1	Comparison of liquid depths predicted by computer model with air-water test data of Table II-1.....	86
V-2	Comparison of measured with predicted critical inlet water flow rates for water hammer initiation.....	88
V-3	Comparison of measured with predicted "exit" liquid temperatures, using the CHOP computer program with $c_1 = 2.5$	90
V-4	Calculated effect of pipe length on the water hammer region, low pressure experiments.....	94
V-5	Calculated effect of pipe diameter on the water hammer region, low pressure experiments.....	95
V-6	Calculated effect of pipe inclination on the water hammer region, low pressure experiments.....	96
V-7	Calculated effect of inlet water subcooling on the water hammer region, low pressure experiments.....	97
V-8	Calculated effect of saturation temperature on the water hammer region, low pressure experiments.....	99
V-9	Calculated effect of vented steam flow on the water hammer region, low pressure experiments.....	100
V-10	Calculated effect of pipe length on the water hammer region for the PWR steam generator feed pipe described by Block, et al. (1977).....	102
V-11	Calculated effect of inlet water subcooling on the water hammer region for the PWR steam generator feed pipe described by Block, et al. (1977).....	104

<u>Figure</u>		<u>Page</u>
V-12	Simplified diagram of isolation condenser supply line in Millstone #1 nuclear power plant.....	105
C-1	Dimensionless steam flow rate profile for low pressure sample case.....	127
C-2	Dimensionless liquid temperature profile for low pressure sample case.....	128
C-3	Dimensionless liquid depth profile for low pressure sample case.....	129
C-4	Taitel-Dukler stability parameter profile for low pressure sample case.....	130
D-1	Dimensionless steam flow rate profile for low pressure sample case with vented steam.....	135
D-2	Dimensionless liquid temperature profile for low pressure sample case with vented steam.....	136
D-3	Dimensionless liquid depth profile for low pressure sample case with vented steam.....	137
D-4	Taitel-Dukler stability parameter profile for low pressure sample case with vented steam.....	138
E-1	Dimensionless steam flow rate profile for PWR steam generator sample case.....	143
E-2	Dimensionless liquid temperature profile for PWR steam generator sample case.....	144
E-3	Dimensionless liquid depth profile for PWR steam generator sample case.....	145
E-4	Taitel-Dukler stability parameter profile for PWR steam generator sample case.....	146

<u>Figure</u>		<u>Page</u>
F-1	Dimensionless steam flow rate profile for Millstone #1 isolation condenser sample case.....	151
F-2	Dimensionless liquid temperature profile for Millstone #1 isolation condenser sample case.....	152
F-3	Dimensionless liquid depth profile for Millstone #1 isolation condenser sample case.....	153
F-4	Taitel-Dukler stability parameter profile for Millstone #1 isolation condenser sample case.....	154

LIST OF TABLES

<u>Table</u>		<u>Page</u>
II-1	Measured Liquid Depths: Air-Water Tests.	36
II-2	Measured Critical Inlet Water Flow Rates for Water Hammer Initiation.....	39
II-3	Measured Exit Liquid Temperatures.....	43

NOMENCLATURE

a_1	constant in Equation (III-36)
a_2	constant in Equation (III-39)
A_L	liquid flow area (m^2)
A_L^*	dimensionless liquid flow area, $A_L/(\pi D^2/4)$
A_S	steam flow area (m^2)
A_S^*	dimensionless steam flow area, $A_S/(\pi D^2/4)$
A_S'	steam flow area above a wave crest in Equation (III-63) (m^2)
b	width of a rectangular channel (m)
c_1	constant in Equations (III-60) and (III-61) which modifies the rectangular channel heat transfer coefficient for use in a circular pipe
c_{PL}	liquid specific heat ($J \cdot kg^{-1} \cdot K^{-1}$)
\bar{c}_{PL}	liquid specific heat at the average of the steam and liquid temperatures ($J \cdot kg^{-1} \cdot K^{-1}$)
d_{hyd}	hydraulic depth, A_L/S_I (m)
d_L	liquid depth in a circular pipe (m)
d_L^*	dimensionless liquid depth, d_L/D
D	pipe diameter (m)
D_h	hydraulic diameter (m)
$D_{h,L}$	liquid hydraulic diameter, defined by Equation (III-53) (m)
$D_{h,S}$	steam hydraulic diameter, defined by Equation (III-54) (m)
f	friction factor
f_A	friction factor in Equation (III-31)
Fr	Froude number, defined by Equation (III-19)
g	gravitational acceleration ($m \cdot s^{-2}$)

h	heat transfer coefficient ($W \cdot m^{-2} \cdot K^{-1}$)
h	height of a rectangular channel (m)
h'	interfacial heat transfer coefficient before correction for condensation in Equation (III-41) ($W \cdot m^{-2} \cdot K^{-1}$)
h_I	interfacial condensation heat transfer coefficient, defined by Equation (III-10) ($W \cdot m^{-2} \cdot K^{-1}$)
h_L	liquid heat transfer coefficient, for use in estimating heat transfer to wall ($W \cdot m^{-2} \cdot K^{-1}$)
h_o	outside heat transfer coefficient due to natural convection, used in Equation (II-6) ($W \cdot m^{-2} \cdot K^{-1}$)
h_S	steam heat transfer coefficient, for use in estimating heat transfer to wall ($W \cdot m^{-2} \cdot K^{-1}$)
h_x	heat transfer coefficient at axial location x ($W \cdot m^{-2} \cdot K^{-1}$)
i_{fg}	enthalpy of vaporization ($J \cdot kg^{-1}$)
i_L	liquid enthalpy ($J \cdot kg^{-1}$)
i_{LO}	inlet liquid enthalpy ($J \cdot kg^{-1}$)
i_S	steam enthalpy ($J \cdot kg^{-1}$)
k_L	liquid thermal conductivity ($W \cdot m^{-1} \cdot K^{-1}$)
k_{Lex}	thermal conductivity of Lexan, $.288 W \cdot m^{-1} \cdot K^{-1}$
k_M	metal (brass) thermal conductivity, $128.1 W \cdot m^{-1} \cdot K^{-1}$
k_S	steam thermal conductivity ($W \cdot m^{-1} \cdot K^{-1}$)
l	macroscale of turbulence in Equation (III-41) (m)
L	pipe length (m)
\dot{m}_L	liquid mass flow rate ($kg \cdot s^{-1}$)
\dot{m}_L^*	dimensionless liquid mass flow rate, \dot{m}_L / \dot{m}_{LO}
\dot{m}_{LO}	inlet liquid mass flow rate ($kg \cdot s^{-1}$)
\dot{m}_S	steam mass flow rate ($kg \cdot s^{-1}$)

\dot{m}_S^*	dimensionless steam mass flow rate, \dot{m}_S/\dot{m}_{LO}
\dot{m}_{SO}	vented steam mass flow rate ($\text{kg} \cdot \text{s}^{-1}$)
n	direction component normal to a surface
n	number of nodes in the finite difference mesh of Figure IV-1
N_{MI}	Mishima-Ishii stratified-slug flow regime transition parameter, defined by Equation (III-65)
N_{TD}	Taitel-Dukler stratified-slug flow regime transition parameter, defined by Equation (III-62)
Nu	Nusselt number, defined by Equation (III-57)
Nu'	rectangular channel Nusselt number, defined by Equation (III-48)
Nu_t	turbulence Nusselt number in Equation (III-41), $h' l/k_L$
$(\overline{Nu})_x$	Nusselt number, averaged from the steam and water inlet in a cocurrent flow to the axial location x
p	pressure (Pa)
p	pass counter in numerical solution algorithm
Pr	Prandtl number, $\mu c_p/k$
Pr_L	liquid Prandtl number, $\mu_L c_{PL}/k_L$
Pr_S	steam Prandtl number, $\mu_S c_{PS}/k_S$
$(\overline{Pr}_L)_x$	liquid Prandtl number, averaged from the steam and water inlet in a cocurrent flow to the axial location x
q	heat flux ($\text{W} \cdot \text{m}^{-2}$)
q^*	dimensionless condensation rate, defined by Equation (III-19)
q_{cond}	heat transferred by tangential conduction, in Equation (II-5) (W)
q_I	heat transferred by interfacial condensation, in Equation (II-5) (W)
r	damping factor in Equation (IV-6)

Ra_L	liquid Rayleigh number used in Equation (II-7)
Re	Reynolds number, $\rho V D/\mu$
Re_L	liquid Reynolds number, defined by Equation (III-55)
Re_L'	rectangular channel liquid Reynolds number, defined by Equation (III-46)
$(\overline{Re}_L)_x$	liquid Reynolds number, averaged from the steam and water inlet in a cocurrent flow to the axial location x
Re_S	steam Reynolds number, defined by Equation (III-56)
Re_S'	rectangular channel steam Reynolds number, defined by Equation (III-47)
$(\overline{Re}_S)_x$	steam Reynolds number, averaged from the steam and water inlet in a cocurrent flow to the axial location x
Re_t	turbulence Reynolds number in Equation (III-41), $l V/\nu$
S_I	interface perimeter at a cross section (m)
S_I^*	dimensionless interface perimeter, S_I/D
S_L	liquid wall perimeter at a cross section (m)
S_L^*	dimensionless liquid wall perimeter, S_L/D
S_S	steam wall perimeter at a cross section (m)
S_S^*	dimensionless steam wall perimeter, S_S/D
$(\overline{St})_x$	Stanton number, $Nu/(Re_L Pr_L)$, averaged from the steam and water inlet in a cocurrent flow to the axial location x
t	fluid layer thickness in a rectangular channel (m)
t_L	liquid layer thickness in a rectangular channel (m)
t_S	steam layer thickness in a rectangular channel (m)
T_A	ambient temperature (K)
T_L	liquid bulk temperature (K)

T_L^*	dimensionless liquid bulk temperature, defined by Equation (III-19)
T_{LO}	inlet liquid temperature (K)
T_M	metal (brass) temperature (K)
T_S	steam bulk temperature (K)
U	overall heat transfer coefficient, defined by Equation (II-6) ($W \cdot m^{-2} \cdot K^{-1}$)
V_I	interface velocity ($m \cdot s^{-1}$)
V_L	liquid bulk velocity ($m \cdot s^{-1}$)
V_S	steam bulk velocity ($m \cdot s^{-1}$)
x	axial position (m)
x^*	dimensionless axial position, x/D

Greek letters

α	void fraction, A_S^*
β	angle defined in Figure IV-2
ϵ_h	eddy diffusivity of heat
ζ	dimensionless quantity defined by Equation (III-24)
θ	pipe inclination, defined in Figure III-1
K_L	effective turbulent thermal conductivity, defined by Equation (III-37)
μ_L	liquid viscosity ($kg \cdot m^{-1} \cdot s^{-1}$)
μ_S	steam viscosity ($kg \cdot m^{-1} \cdot s^{-1}$)
ρ_L	liquid density ($kg \cdot m^{-3}$)
ρ_S	steam density ($kg \cdot m^{-3}$)
τ_A	non-condensing interfacial shear stress, defined by Equation (III-30) ($N \cdot m^{-2}$)
τ_I	interfacial shear stress ($N \cdot m^{-2}$)

τ_I^*	dimensionless interfacial shear stress, defined by Equation (III-19)
τ_L	liquid wall shear stress ($N \cdot m^{-2}$)
τ_L^*	dimensionless liquid wall shear stress, defined by Equation (III-19)
τ_S	steam wall shear stress ($N \cdot m^{-2}$)
τ_S^*	dimensionless steam wall shear stress, defined by Equation (III-19)
ν	dynamic viscosity, μ/ρ
ϕ	dimensionless quantity, defined by Equation (III-19)
χ	angle defined in Figure II-5
ψ	dimensionless quantity, defined by Equation (III-19)
ω_0	dimensionless temperature difference, defined by Equation (III-19)
$\bar{\omega}_1$	dimensionless temperature difference, defined by Equation (III-19)
$\bar{\omega}_2$	dimensionless temperature difference, defined by Equation (III-19)

CHAPTER I

INTRODUCTION

A. Historical background

Much of today's interest in condensation water hammer in horizontal or nearly-horizontal pipes containing steam and subcooled water can be traced to an incident which occurred at the Indian Point Unit No. 2 pressurized water reactor nuclear power station on November 13, 1973. The sequence of events was described by Cahill (1974):

"Following a turbine trip at 7:40 a.m., due to high water level in Steam Generator No. 23, and subsequent reactor trip at 7:46 a.m., due to "low-low" water level in Steam Generator No. 21, a break occurred in the feedwater line to Steam Generator No. 22 just inside containment near the feedwater line penetration . . . It was noted that the feedwater line to Steam Generator No. 22 experienced a shaking accompanied by a loud noise at about the time of reactor trip."

The feedwater line involved is shown as the "original line" in Figure I-1, taken from Cahill (1974). When the steam generator water level drops below the level of the feedwater supply pipe, the pipe drains, establishing a stratified flow in which water flows into the steam generator and steam is drawn into the pipe and condenses on the water surface. Cahill (1974) suggested that the steam velocity at some

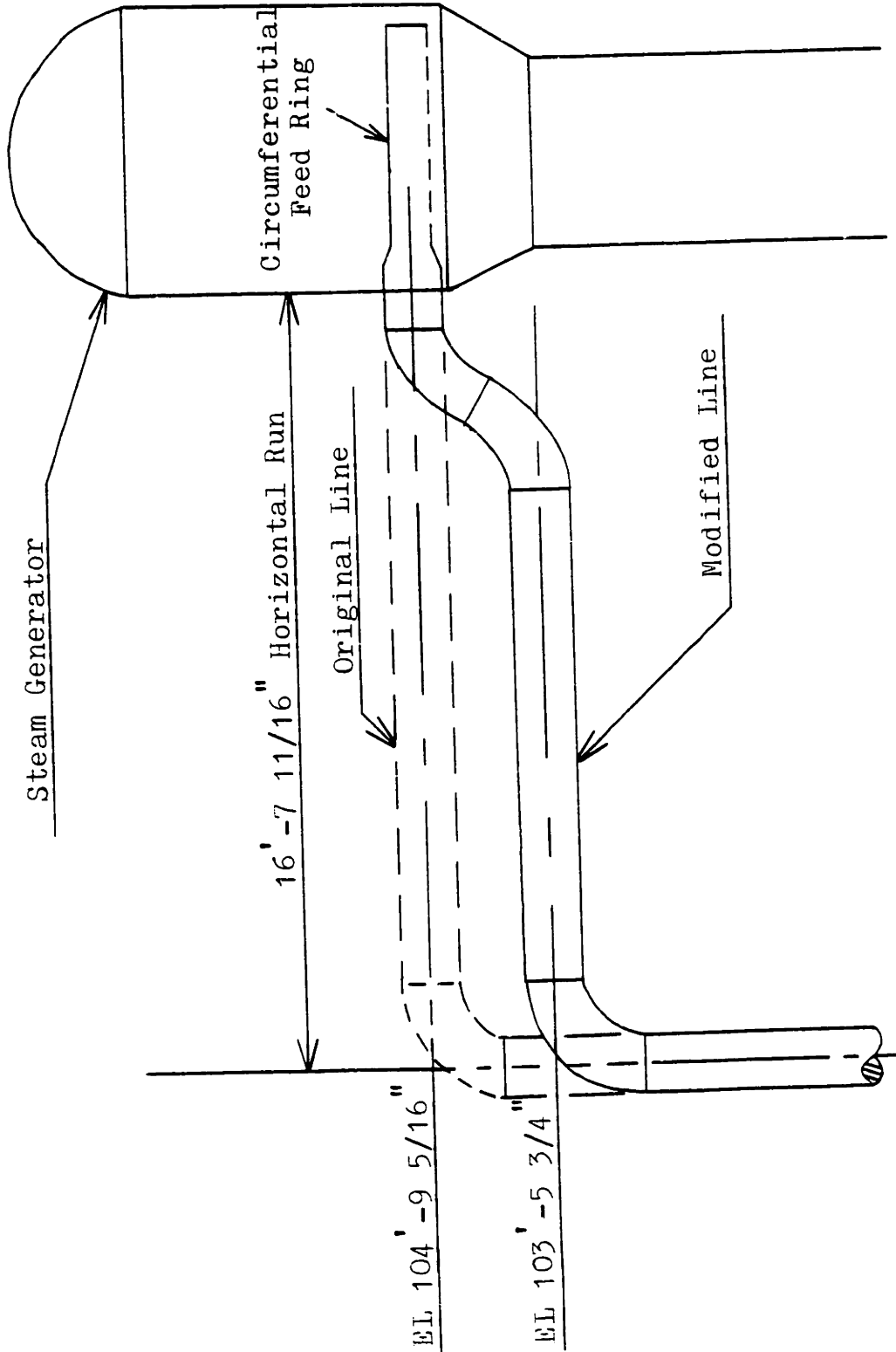


Figure I-1. Original and modified feedwater lines to Steam Generator No. 22 of Indian Point Unit No. 2, taken from Cahill (1974).

location could become high enough to cause water slug formation and a subsequent rapid steam bubble collapse leading to water hammer. Photographs of water slug formation were obtained in an air-water-vacuum laboratory system and provided the first evidence of this water hammer initiating mechanism. Cahill (1974) reported that the feedwater piping was modified as shown in Figure I-1 to prevent drainage of the feedwater line. No water hammer problems have been encountered with the new design. It should be pointed out that after entering the steam generator, the water drains through holes in a circumferential feed ring, so it is conceivable that water slug formation could occur in the feed ring, even with the modified feed pipe.

The Indian Point incident led Westinghouse to undertake a study of the problem. The mechanism identification and air-water-vacuum work done by Westinghouse was discussed by Cahill (1974). Roidt (1975) obtained further evidence of the water hammer initiating mechanism in a small scale steam-water system and investigated experimentally the pressure history during steam bubble collapse and the effect of top-discharge "J-tubes" in the feed ring on preventing pipe drainage and thereby water hammer initiation. The pressure history and peak pressure measurements were described by Roidt (1975) as suspect because of the presence of noncondensable gases in the system. Roidt (1975) also presented a theory to model the steam bubble collapse. However, no

attempt was made to quantify the water hammer initiating mechanism of water slug formation.

With the goal of improving the understanding of water hammer in PWR steam generators, the U. S. Nuclear Regulatory Commission funded a study by Creare, Inc., which was reported by Block, et al. (1977). Areas examined include incident reports from operating plants, vendor hardware and operating recommendations, the water hammer initiating mechanism, the steam bubble collapse process, and the potential for structural damage. Steam-water tests were performed, using simplified models of the feedwater pipe and feed ring system. This report is the most comprehensive study to date of the condensation water hammer problem. Block, et al. (1977) described the elements required to quantitatively predict water hammer initiation, but said that the understanding of interfacial transport phenomena at that time was inadequate to permit such a prediction.

Gruel, et al. (1981) studied the impulses generated by condensation water hammers and the associated piping system deflections. If the reader is concerned about the potential consequences of condensation water hammer, this work should be consulted.

Jones (1981) constructed an early version of the apparatus used in the present study and obtained films of water hammer initiation during water flow transients, as well as pressure traces of water hammer events.

B. The present work

This study was undertaken with the objective of describing quantitatively the initiating mechanism of steam bubble collapse-induced water hammer in a horizontal or nearly-horizontal pipe which supplies subcooled water to a steam-filled chamber. With this information, it is expected that designers will be able to avoid condensation water hammer problems in future steam power plants and that operators will be able to prevent or reduce the risk of condensation water hammer in existing plants.

The initiating mechanism consisting of water slug formation that was identified by previous researchers is studied here in a low pressure laboratory apparatus. Several tests are described, including measurements of the critical inlet water flow rate for water hammer initiation.

A one-dimensional stratified flow analysis is developed which predicts the liquid depth and steam flow rate variation along a circular pipe.⁽¹⁾ Given this information, a criterion for localized water slug formation is selected and applied to predict water hammer initiation.

The original analytical model developed here to predict condensation water hammer initiation is verified by comparison with the results of several different experiments.

⁽¹⁾ Although the circular pipe is studied here, the same approach may be used to analyze pipes of other cross-sections.

Then, the effect of varying each of several flow parameters is predicted using the model. Potential applications to high pressure systems are discussed, areas where further work should be considered are identified, and a step-by-step approach is presented for the plant designer and operator to follow in evaluating the susceptibility of a piping system to condensation and the effects of different water hammer prevention strategies.

CHAPTER II
EXPERIMENTAL STUDIES

A. Experimental apparatus

1. Hardware description. A schematic diagram of the experimental apparatus used in this study is shown in Figure II-1. The test section design is an extension of that of Jones (1981). Two views of the test section are shown in Figure II-2.

The test section includes 1.22 m of 0.0381 m I. D. transparent Lexan pipe, supported by Plexiglas disks held by steel cables, and 0.78 m of 0.0381 m I. D. brass pipe, located as shown in Figure II-1. The brass pipe enters the steam tank flush with the inside wall of the tank.

To study the effect of pipe length on water hammer initiation, 0.40 m of brass pipe was removed from the test section nearest the steam tank for one series of tests. Thus, tests were run with total test section lengths of 2.0 m and 1.6 m.

Steam is supplied to the tank by MIT steam lines, with a typical air volume fraction of 10^{-4} . Pressure in the tank is controlled by a Watts Model 145M1 pressure regulator in the steam supply line. The tank is kept drained by a Hoffman Model 603B inverted bucket steam trap. A steam vent is provided at the left end of the test section for use in purging the system of air. Adjustable supports are used to regulate the test section inclination.

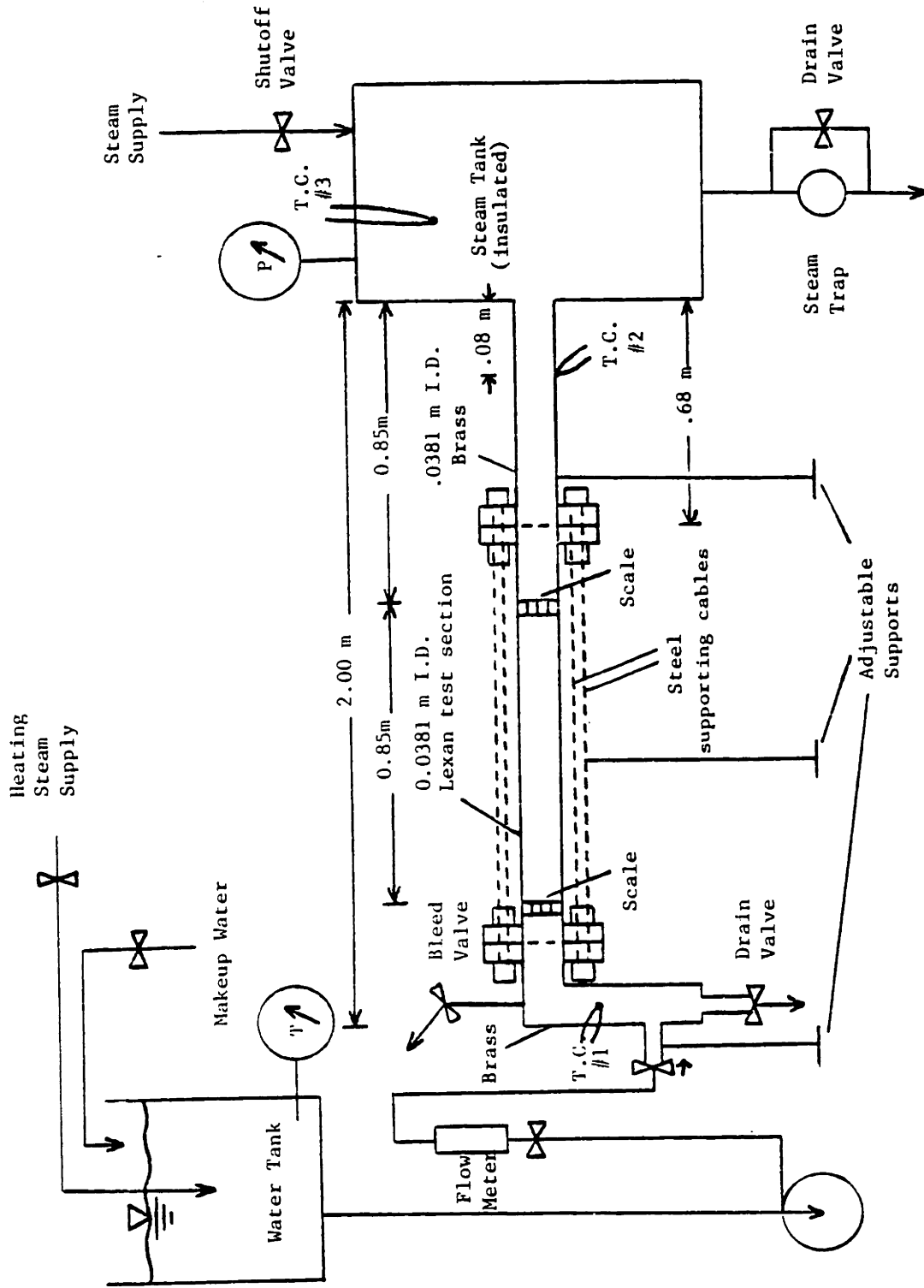
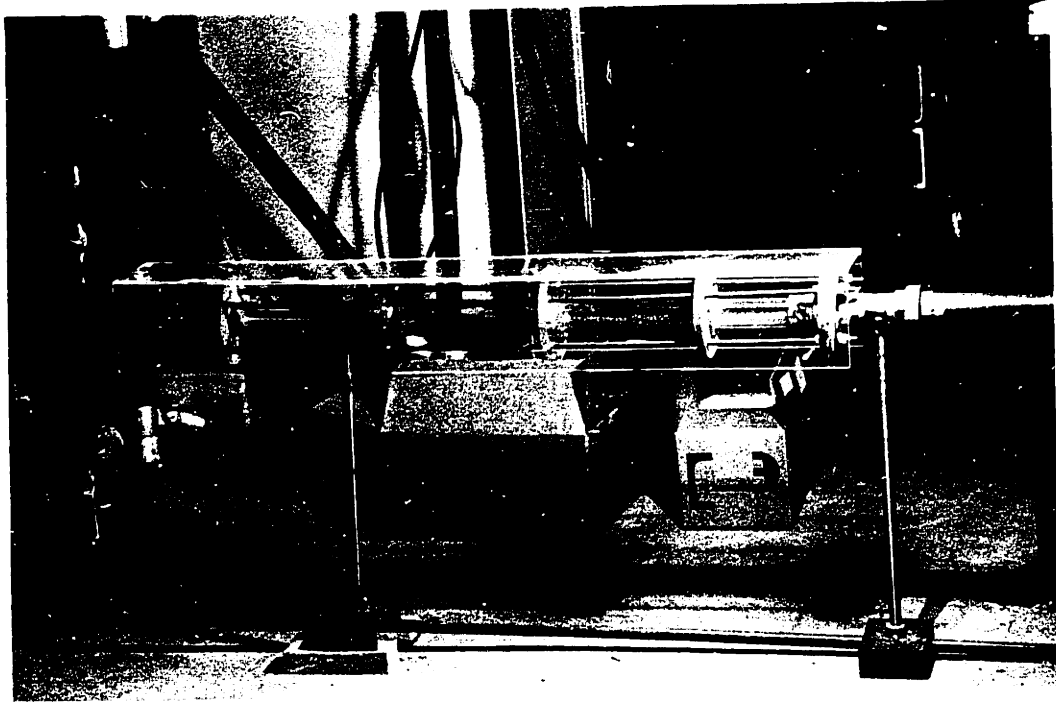
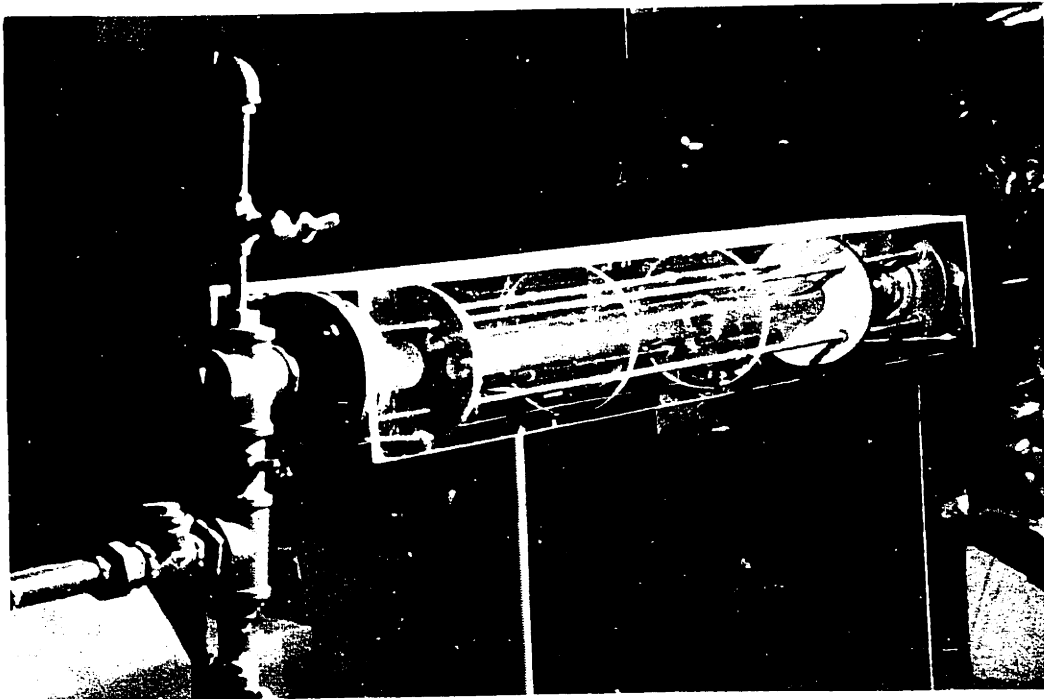


Figure II-1. Schematic diagram of the experimental apparatus.



a. Side view.



b. View from water inlet.

Figure II-2. Photographs of test section.

Subcooled water, heated with steam to the desired temperature, is pumped into the test section. Flow rate is controlled with a Jenkins 106-A, 119-A Steam Disc valve with a throttling seat. Steam backflow into the water supply piping is prevented by a check valve.

2. Instrumentation. A Fischer-Porter flowmeter (Tube FP-3/4-27-G-10/80, Float GNSVT-56) with a full scale flow of $3.19 \times 10^{-4} \text{ m}^3 \cdot \text{s}^{-1}$ and an accuracy of $\pm 6 \times 10^{-6} \text{ m}^3 \cdot \text{s}^{-1}$ is used to measure the water flow into the test section. Copper-constantan thermocouples sense the water supply (T. C. #1 in Figure II-1) and steam tank (T. C. #3) temperatures. For one series of tests, an additional thermocouple (T. C. #2), covered with insulation, was used to sense the outer wall temperature at the bottom of the brass pipe 0.08 m upstream of the pipe exit. An Omega Model 400A digital readout, with switchable input, is used to obtain temperatures from the thermocouple voltages.

Steam tank pressure is measured by a pressure gauge (U. S. Gauge No. 33003) with an accuracy of $\pm 8 \times 10^3 \text{ Pa}$. Paper scales wrapped around the Lexan pipe at 0.85 m and 1.70 m from the pipe exit are used to measure liquid depths.

B. High speed photographs

Films of steam-water interactions in the test section were taken on Kodak Double-X Negative 16 mm film (No. 7222) with a Hycam high speed movie camera. The films show a side view of the end of the transparent part of the test section

nearest the steam-filled tank. The camera speed was set at 100 frames per second, and a timer flashing at 100 Hz was used to mark the film so that its exact speed could be determined.

The sequence of events which occurs in a pipe after the inlet water flow rate has been increased in a quasi-steady manner to just above the critical value for water hammer initiation (for given test conditions) is shown in Figures II-3a through II-3r. These photographs are from films taken of the 2.0 m long horizontal test section with temperatures $T_S = 394$ K and $T_{LO} = 289$ K. The time elapsed after the first frame is shown for each. The water flows from left to right, and the steam flows from right to left and condenses on the water surface. Initially (Figures II-3a through II-3e), waves grow on the steam-water interface due to the coupling between increasing condensation heat transfer and increasing steam velocity. When the local steam velocity becomes high enough to cause transition from stratified flow to slug flow, a water slug is formed (Figure II-3f). This slug traps a steam bubble, which collapses rapidly (Figures II-3g and II-3h), resulting in a water hammer. After a period of violent mixing (Figures II-3i and II-3j), the pipe becomes filled with water for about two-thirds of its length and nearly empty of water for the remainder (Figure II-3k). Gravity waves then propagate in both directions (Figures II-3l and II-3m), seeking to reestablish a stratified flow.

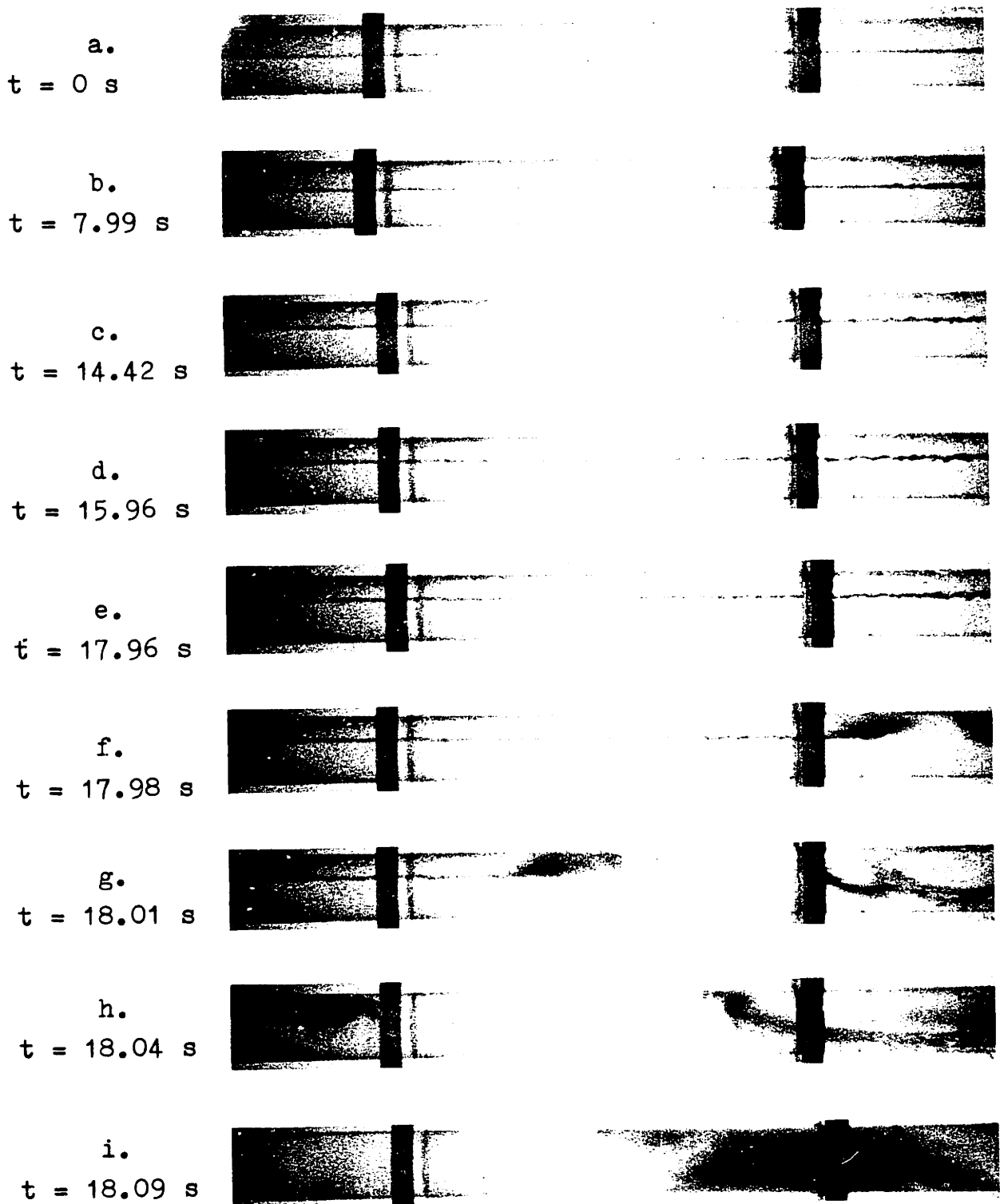


Figure II-3. Water slug formation and periodic water hammer in the 2.0 m pipe. Field of view is .73 to 1.09 m from the pipe exit.

j.
t = 18.16 s



k.
t = 18.43 s



l.
t = 18.51 s



m.
t = 19.41 s



n.
t = 20.41 s



o.
t = 20.53 s



p.
t = 20.66 s



q.
t = 20.68 s



r.
t = 20.70 s

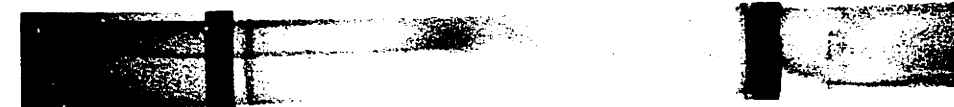


Figure II-3 (continued)

However, before the left-running wave reaches the end of the pipe, wave growth occurs (Figures II-3n through II-3p), and another water slug forms (Figure II-3q) and collapses (Figure II-3r). This periodic water hammer then may continue indefinitely.

The instability which leads to formation of a water slug is shown in more detail in Figures II-4a through II-4e. These photographs were taken of the 1.6 m long horizontal test section, with $T_S = 394$ K and $T_{LO} = 294$ K. The time elapsed after the first frame is shown for each. In Figures II-4a and II-4b, a large surface wave is seen traveling to the left. In Figure II-4c, this wave approaches the top of the pipe, forming a water slug, as seen in Figure II-4d. A second water slug also forms (Figure II-4e), as bubble collapse gets under way.

The photographs shown here verify that localized water slug formation is the initiating mechanism for steam bubble collapse-induced water hammer in horizontal or nearly-horizontal pipes. The observed location where a water slug forms can be quantified for the two cases photographed. In the 2.0 m test section, with $T_S = 394$ K and $T_{LO} = 289$ K, the water slug forms just to the right of the field of view, roughly 0.70 m upstream of the pipe exit. In the 1.6 m test section, with $T_S = 394$ K and $T_{LO} = 294$ K, the water slug forms roughly 0.50 m upstream of the pipe exit.

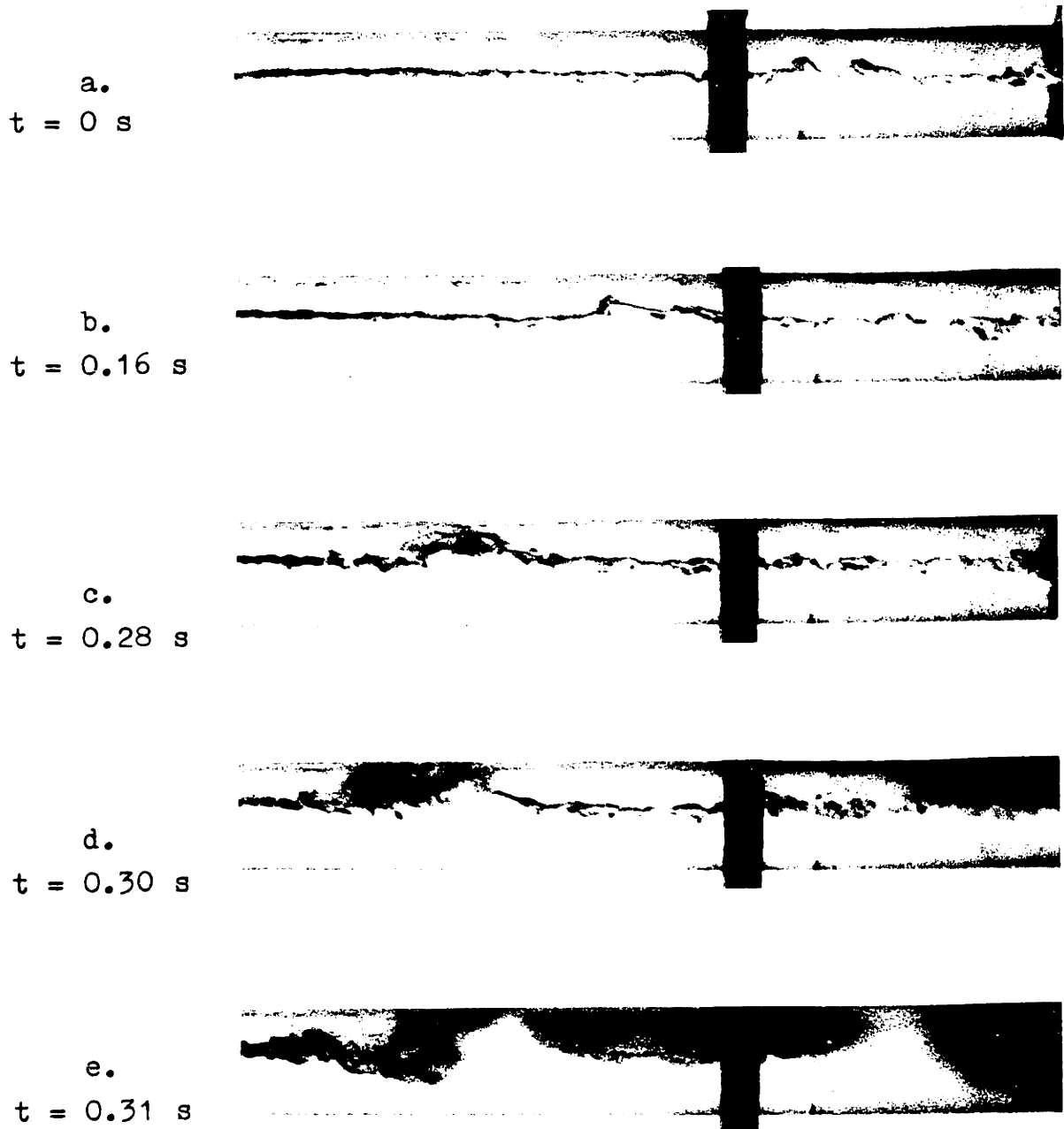


Figure II-4. Details of water slug formation in the 1.6 m pipe. Field of view is .33 to .63 m from the pipe exit.

C. Air-water liquid depth tests

When steam flows in a pipe and condenses on the water surface, the liquid depth is affected by wall friction in the steam and liquid, interfacial friction, and the condensation rate. To provide a useful check on the liquid wall friction computation and the numerical solution method, liquid depth data for the air-water system were obtained.

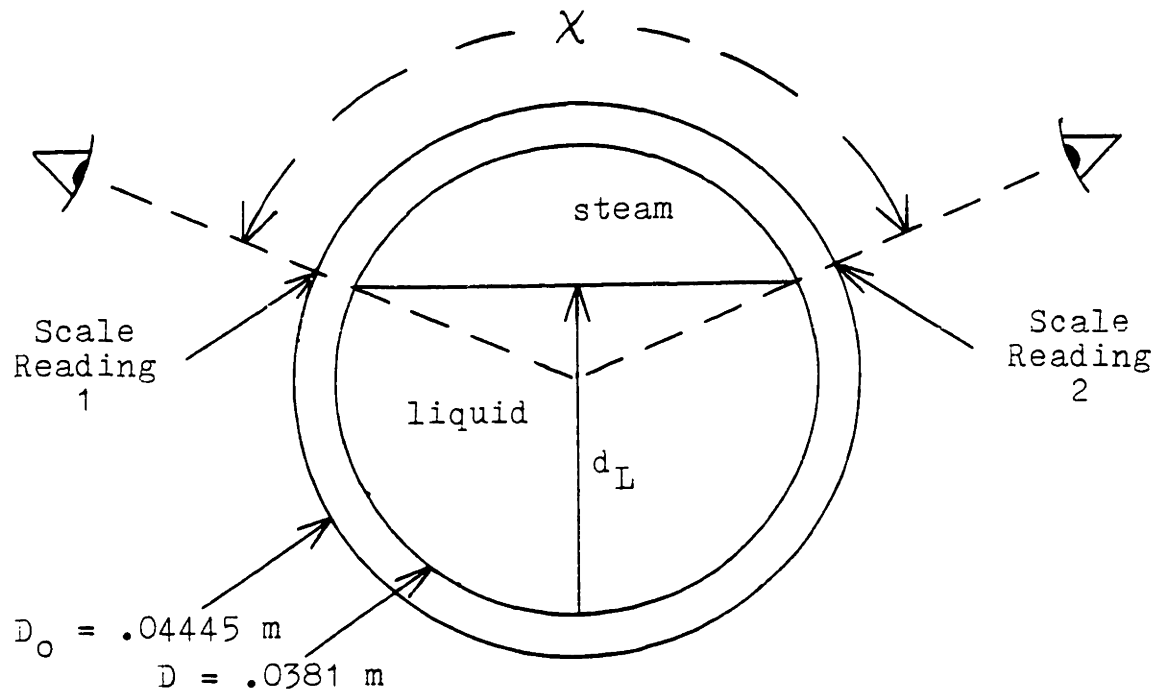
Using a scale wrapped around the outside of the Lexan pipe, liquid depths can be measured as shown in Figure II-5. From each side of the pipe, the observer looks radially inward at the gas-liquid interface and records the corresponding scale reading. The dimensionless liquid depth is then calculated as

$$d_L^* = 0.5 \left\{ 1 + \cos \left[(\text{Reading 1} - \text{Reading 2}) / D_o \right] \right\} \quad (\text{II-1})$$

Air water liquid depth data were collected in the 2.0 m test section at 0.85 m and 1.70 m from the pipe exit for several water flow rates and three pipe inclinations. The data obtained are shown in Table II-1.

D. Steam-water tests

1. Experimental procedure. By adjusting the supports, the test section was brought to the desired inclination with the help of a level and a meterstick. The water supply tank was filled with water and heated to the desired temperature. With all drain and vent valves opened, steam was admitted to the steam tank and test section. When steam began to vent



$$0.5 X D_o = \text{Scale Reading 1} - \text{Scale Reading 2}$$

$$d_L/D = 0.5 (1 + \cos (X/2))$$

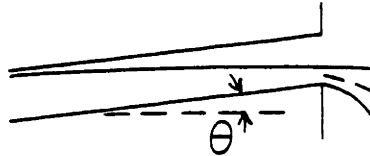
Figure II-5. Measurement of liquid depth using a scale wrapped around the pipe.

Table II-1

MEASURED LIQUID DEPTHS: AIR-WATER TESTS

Pipe Inclination (radians)	Inlet Water Temp. (K)	Inlet Water Flow ($\text{kg}\cdot\text{s}^{-1}$)	Measured d_L^* at	
			0.85 m ⁽²⁾	1.70 m ⁽²⁾
0	284.8	0.064	0.374	0.465
0	283.7	0.096	0.453	0.565
0	283.4	0.128	0.558	0.655
0	283.2	0.159	0.632	0.752
0	283.2	0.191	0.679	0.832
+0.0035	295.4	0.032	0.397	0.532
+0.0035	285.9	0.064	0.495	0.678
+0.0035	282.0	0.096	0.594	0.766
+0.0035	280.4	0.128	0.666	0.854
+0.0035	279.8	0.159	0.734	0.948
-0.0030	285.4	0.064	0.303	0.374
-0.0030	283.7	0.096	0.344	0.465
-0.0030	282.0	0.128	0.428	0.552
-0.0030	282.0	0.159	0.490	0.644
-0.0030	282.0	0.191	0.571	0.713

(1) Pipe inclination, θ , is defined as follows:



(2) Distance from pipe exit.

into the room (after most of the air had been displaced), the drain valves were closed, but the vent valve was left open for another 2 to 3 minutes to purge any remaining air from the system. The vent valve was then closed until only a wisp of steam was visible leaving the test section. This venting was done to prevent the buildup of air during the tests. The steam pressure regulator was adjusted (and further adjusted during tests, when necessary) to maintain a steam tank pressure of about 2.05×10^5 Pa.⁽¹⁾

The water pump was then activated, causing water to flow into the test section, dump into the steam tank, and drain out through the steam trap. Water flow rate, water inlet temperature, and steam tank temperature and pressure were recorded temporarily and the flow was observed for several minutes to determine if a water hammer event would occur. If none did, the water flow rate was increased slightly (in steps of $3.2 \times 10^{-6} \text{ m}^3 \cdot \text{s}^{-1}$) and the observation process repeated. When a water hammer did occur, the associated test conditions were recorded permanently. These conditions were therefore the measured conditions for the (quasi-steady) initiation of water hammer. It was observed that if the water flow rate was increased rapidly it was possible to initiate water hammer at a lower flow rate.

⁽¹⁾ Operation at higher pressures was precluded by the 395 K temperature limit of the Lexan pipe used.

2. Results. Critical inlet water flow rate data were collected at a steam temperature of roughly 394 K, inlet water temperatures of roughly 289 K, 322 K, 339 K, and 355 K, pipe inclinations of +0.003, 0, and -0.003, and test section lengths of 2.0 m and 1.6 m. Each case was run three times to ensure the reproducibility of results. Little variation was seen between the critical water flow rates of these duplicate runs. The data collected were therefore averaged. Measured steam tank temperatures were never more than 3 K above the saturation temperatures corresponding to measured steam tank pressures. Steam conditions were taken to be saturated at the average of the two temperatures. Little error is introduced by this assumption.

The experimental results are summarized in Table II-2. Decreasing the inlet water temperature, increasing the pipe length, and increasing the pipe inclination are each seen to reduce the critical inlet water flow rate for water hammer initiation.

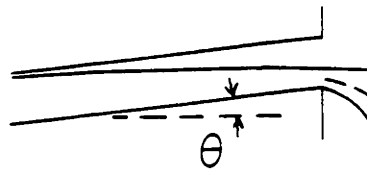
The transition from stratified to slug flow which initiates condensation water hammer occurs when the steam velocity exceeds a critical value at the location of slug formation. In the flow pattern studied here, the local steam velocity depends on the local steam mass flow rate and flow area. The trends observed experimentally can be qualitatively explained by this mechanism:

Table II-2

MEASURED CRITICAL INLET WATER FLOW RATES
FOR WATER HAMMER INITIATION

<u>Pipe Length (m)</u>	<u>Inlet Water Temp. (K)</u>	<u>Steam Temp. (K)</u>	<u>Pipe⁽¹⁾ Inclination</u>	<u>Crit. Water Flow Rate (kg·s⁻¹)</u>
1.6	288.9	394.4	0	0.0807
1.6	323.7	395.6	0	0.0875
1.6	339.8	396.1	0	0.0903
1.6	357.0	397.0	0	0.1077
2.0	288.0	394.5	0	0.0573
2.0	323.0	395.9	0	0.0738
2.0	339.5	396.6	0	0.0830
2.0	353.9	395.9	0	0.1130
2.0	284.5	396.3	+0.003	0.0520
2.0	323.3	395.7	+0.003	0.0675
2.0	340.4	396.6	+0.003	0.0704
2.0	353.2	396.3	+0.003	0.0691
2.0	286.1	396.3	-0.003	0.0573
2.0	323.5	395.9	-0.003	0.0728
2.0	340.7	396.0	-0.003	0.0914
2.0	355.4	396.7	-0.003	0.1161

(1) Pipe inclination, θ , is defined as follows:



- i. Decreasing the inlet water temperature causes more steam to be condensed. The critical steam velocity is thus reached at a larger steam flow area. This corresponds to a reduced inlet water flow rate.
2. Increasing the pipe length increases the steam condensed, since the surface area for interfacial condensation increases. The critical steam velocity is thus reached at a larger steam flow area. This corresponds to a reduced inlet water flow rate.
3. Increasing the pipe inclination increases the liquid depth for a given inlet water flow rate, thus decreasing the steam flow area. Thus, a lower inlet water flow rate is required to reach the critical steam velocity.

Once periodic water hammer begins, reducing the inlet water flow rate below that required for water hammer initiation does not stop it. In fact, even if the inlet water flow is shut off, as much as several minutes elapse before the water hammers cease. The time to cessation of water hammers after shutoff of inlet water flow was measured in the 2.0 m and 1.6 m horizontal pipes for four inlet water temperatures. The results are shown in Figure II-6. As the subcooling is increased, more time is required for water hammers to stop because the inventory of water in the pipe takes longer to

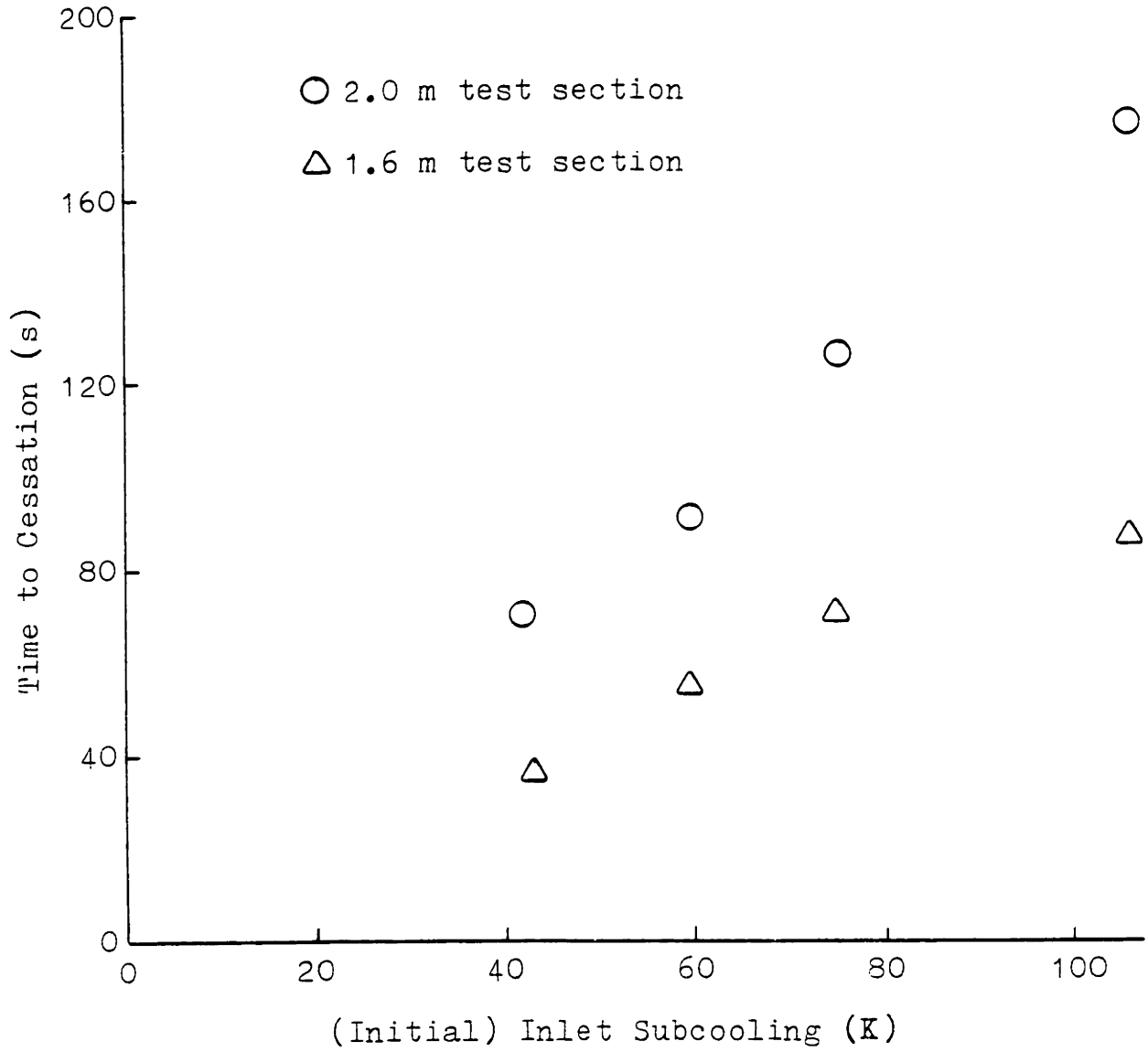


Figure II-6. Time to cessation of water hammers after shutoff of inlet water flow.

heat up to near the saturation temperature. In the longer pipe, more time is required for water hammers to stop because the initial inventory of subcooled water is greater.

E. Liquid exit temperature tests

1. Experimental procedure. One thermocouple (T. C. #2 in Figure II-1) senses the outside wall temperature of the brass pipe 0.08 m upstream of the pipe exit. The difference between this temperature measurement and the local bulk liquid temperature is examined in Section II.F.1 and shown to be small.

For four inlet water temperatures in the 1.60 m horizontal test section, water temperatures near the exit were measured over a range of inlet water flow rates below the critical inlet water flow rate for water hammer initiation. The test procedure was that outlined in Section II.D.

2. Results. The temperature data collected are shown in Table II-3. Greater water flow rates experience a smaller temperature rise. Increasing the inlet water temperature also decreases the temperature rise, even when it is expressed as a fraction of the maximum possible temperature rise,

$$T_S - T_{LO}$$

F. Discussion of experimental uncertainties

In the experiments conducted here, there are uncertainties (in addition to instrumentation inaccuracies) associated with the measurement of exit liquid temperature, liquid depth,

Table II-3

MEASURED EXIT LIQUID TEMPERATURES⁽¹⁾

<u>Inlet Water Flow (kg·s⁻¹)</u>	<u>Inlet Water Temp. (K)</u>	<u>Exit Water Temp. (K)</u>	<u>Steam Temp. (K)</u>	<u>$\frac{(T_{L,ex} - T_{LO})}{(T_S - T_{LO})}$</u>
0.0381	300.9	354.3	395.6	0.564
0.0445	299.8	352.0	395.3	0.547
0.0509	298.2	349.3	395.0	0.528
0.0572	297.6	348.2	394.5	0.522
0.0636	296.5	345.9	393.9	0.508
0.0380	324.3	363.2	397.4	0.532
0.0443	325.9	362.6	397.2	0.514
0.0506	325.9	361.5	397.0	0.500
0.0569	325.4	359.8	396.5	0.484
0.0633	324.8	358.7	396.1	0.476
0.0696	324.8	357.6	395.6	0.463
0.0378	339.3	370.4	398.2	0.528
0.0441	341.5	368.7	397.8	0.483
0.0504	341.5	367.6	397.9	0.463
0.0567	341.5	366.5	397.9	0.443
0.0630	340.9	365.4	397.5	0.432
0.0693	340.4	364.8	396.9	0.432
0.0376	357.0	376.5	398.3	0.471
0.0439	358.2	375.9	398.3	0.443
0.0502	357.6	374.3	398.3	0.410
0.0564	357.0	372.6	398.3	0.377
0.0627	356.5	371.5	398.0	0.361
0.0690	355.9	372.0	398.0	0.383

(1) "Exit" water temperature is actually the measured temperature 0.08 m upstream of the exit. Tests were run in the 1.8 m test section with an ambient temperature of 298 K.

and pipe inclination. The effect of heat losses to the surroundings also should be examined.

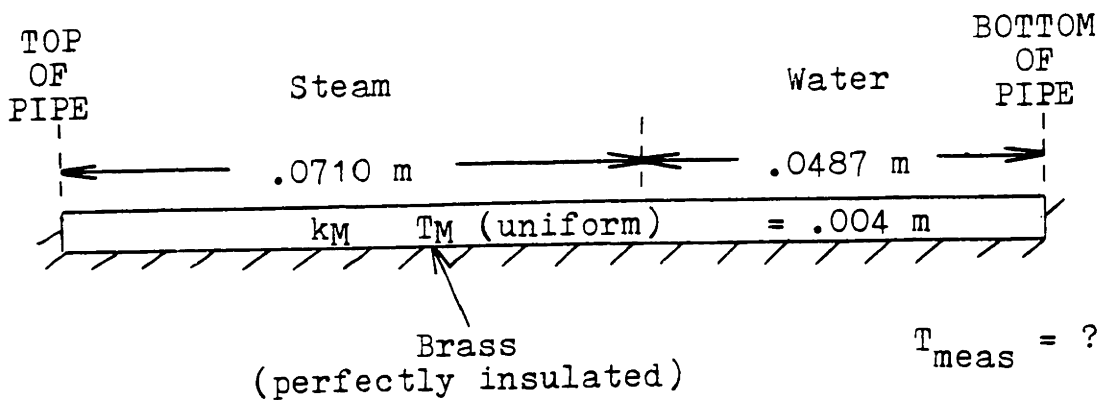
1. Liquid exit temperature. A copper-constantan thermocouple (T. C. #2 in Figure II-1) is located on the outer wall at the bottom of the brass pipe 0.08 m upstream of the pipe exit. This thermocouple is intended to provide a measurement of the local bulk liquid temperature. It is wrapped with many layers of insulating tape, minimizing heat loss to the room. However, the effect of tangential conduction in the brass on this temperature reading needs to be determined.

Figure II-7 shows an idealized model of the situation. The brass section shown is a rectangular block which contacts the steam and water over the same perimeter as in the pipe and has the same thickness as the pipe. It is taken to be perfectly insulated from the room. The data shown are taken from a numerical calculation using the methods outlined in Chapter IV. Symbols are explained in the Nomenclature, and all the quantities are expressed in SI units.

Using the turbulent forced convection heat transfer correlation of Dittus and Boelter (1930),

$$Nu = 0.023 Re^{0.8} Pr^{0.4} , \quad (II-2)$$

the liquid and steam heat transfer coefficients are found to be:



$A_L = 3.632 \times 10^{-4}$	$T_A = 297.04$
$A_S = 7.769 \times 10^{-4}$	$T_S = 394.47$
$m_L = 5.381 \times 10^{-2}$	$T_L = 344.57$
$m_S = 4.808 \times 10^{-3}$	$S_L = 4.868 \times 10^{-2}$
$L = 975.94$	$S_I = 3.647 \times 10^{-2}$
$S = 1.166$	$S_S = 7.102 \times 10^{-2}$
$V_L = 1.518 \times 10^{-1}$	$D_{h,L} = 1.706 \times 10^{-2}$
$V_S = 5.308$	$D_{h,S} = 2.891 \times 10^{-2}$
$L = 3.978 \times 10^{-4}$	$Re_L = 6,353$
$S = 1.288 \times 10^{-5}$	$Re_S = 13,890$
$k_L = .663$	$Pr_L = 2.513$
$k_S = 2.680 \times 10^{-2}$	$Pr_S = 1.021$
$k_M = 128.1$	

Figure II-7. Idealized model of brass pipe used in estimating the effect of tangential conduction.

$$\begin{aligned} h_L &= 1425 \text{ W} \cdot \text{m}^{-2} \cdot \text{K}^{-1} \\ h_S &= 44.3 \text{ W} \cdot \text{m}^{-2} \cdot \text{K}^{-1} . \end{aligned} \quad (\text{II-3})$$

An upper bound on the heat transferred by tangential conduction is obtained by taking the metal temperature, T_M , to be uniform. The following equation is obtained from a heat balance on the brass:

$$T_M = \frac{h_L S_L T_L + h_S S_S T_S}{h_L S_L + h_S S_S} \quad (\text{II-4})$$

Using this equation, $T_M = 346.7 \text{ K}$ is calculated for the conditions of Figure II-7. This differs from the local bulk liquid temperature by only 2.2 K. Since this is a worst case calculation, T. C. #2 should provide a good approximation to the local bulk liquid temperature.

The ratio of the upper bound on the heat transferred by tangential conduction to the interfacial condensation heat transfer is

$$\frac{q_{\text{cond, max}}}{q_I} = \frac{h_S S_S (T_S - T_M)}{h_I S_I (T_S - T_L)} . \quad (\text{II-5})$$

The value of h_I calculated by the computer model of Chapter IV is $3575 \text{ W} \cdot \text{m}^{-2} \cdot \text{K}^{-1}$. Substitution in Equation (II-5) gives a ratio of 0.02. Since this is an upper bound, the effect of tangential conduction on the condensation rate in the brass pipe is negligible. Since the thermal conductivity of Lexan is much less than that of brass, tangential conduction in the Lexan is inconsequential.

2. Liquid depth. The presence of a meniscus increases the elevation at which the liquid contacts the wall above the liquid surface elevation away from the wall. As a result, liquid depths measured using the technique of Section II.C will be greater than the actual liquid depths. Also, since the contact angle of the gas-liquid interface with the wall is constant, the measurement error should increase as the liquid depth approaches the top of the pipe.

3. Pipe inclination. The range of pipe inclinations studied was from -0.003 to $+0.003$ radians. This corresponds to a 6 mm change in elevation over the length of the 2.0 m test section. It is believed that the accuracy associated with the test section inclination was about ± 2 mm, due to measurement uncertainty and pipe warping during tests. Thus, the uncertainty in pipe inclination is roughly ± 0.001 radians.

4. The effect of heat loss to the room. To obtain an upper bound on the heat lost to the room, suppose the heat transfer coefficient inside the pipe is very large. Then, treating the pipe wall as thin, the overall heat transfer coefficient is given by

$$\frac{1}{U} = \frac{1}{h_o} + \frac{\delta}{k_{Lex}}, \quad (\text{II-6})$$

where h_o is the outside heat transfer coefficient, δ is the Lexan wall thickness, and k_{Lex} is the Lexan thermal conductivity ($0.288 \text{ W} \cdot \text{m}^{-1} \cdot \text{K}^{-1}$). Using the equation cited by

Rohsenow and Choi (1961) for natural convection outside a horizontal pipe,

$$\text{Nu} = 0.56 \text{ Ra}_L^{0.25} , \quad (\text{II-7})$$

with $T_S = 400 \text{ K}$, $T_A = 295 \text{ K}$, and $D_o = 0.04445 \text{ m}$, one obtains $h_o = 9.16 \text{ W} \cdot \text{m}^{-2} \cdot \text{K}^{-1}$. Then, using Equation (II-6) and the relation

$$q = U (T_S - T_A) , \quad (\text{II-8})$$

the heat flux is $q = 1040 \text{ W} \cdot \text{m}^{-2}$. The total heat loss to the room from the pipe is then

$$Q = \pi D L q = 270 \text{ W} . \quad (\text{II-9})$$

For the conditions given, the total interfacial heat exchange is about 10,000 W. Thus the maximum heat loss to the room is less than 3 percent of the interfacial condensation heat transfer. Since the average inside wall temperature is much less than the steam temperature (due to the presence of cold liquid and the finite inside heat transfer coefficient), heat losses to the room through the Lexan pipe are unimportant. Since water slug formation occurs in the Lexan pipe, heat losses to the room through the brass pipe near the steam tank have little effect.

CHAPTER III
THE ANALYTICAL MODEL

A. Foundations of the model

1. The system analyzed. An analytical model has been developed in this research which predicts the onset of condensation water hammer in a horizontal or nearly-horizontal circular pipe supplying subcooled water to a steam-filled chamber. The flow geometry analyzed is shown in Figure III-1. The system parameters which the analysis will require as inputs are:

- (1) Pipe length, L
- (2) Pipe diameter, D
- (3) Pipe inclination, θ
- (4) Steam temperature, T_S (saturated)
- (5) Inlet water temperature, T_{LO}
- (6) Inlet water mass flow rate, \dot{m}_{LO}
- (7) Vented steam mass flow rate, \dot{m}_{SO}

2. The method of analysis. The mass, momentum, and energy conservation equations for a one-dimensional stratified two-phase flow can be solved numerically to provide the liquid depth, liquid temperature, and steam mass flow rate at all locations along the pipe. Then, a stratified-slug flow regime transition criterion can be applied to determine the location, if any, where a water slug will form. This localized water slug formation was shown in Section II.B to be the mechanism which initiates the condensation water

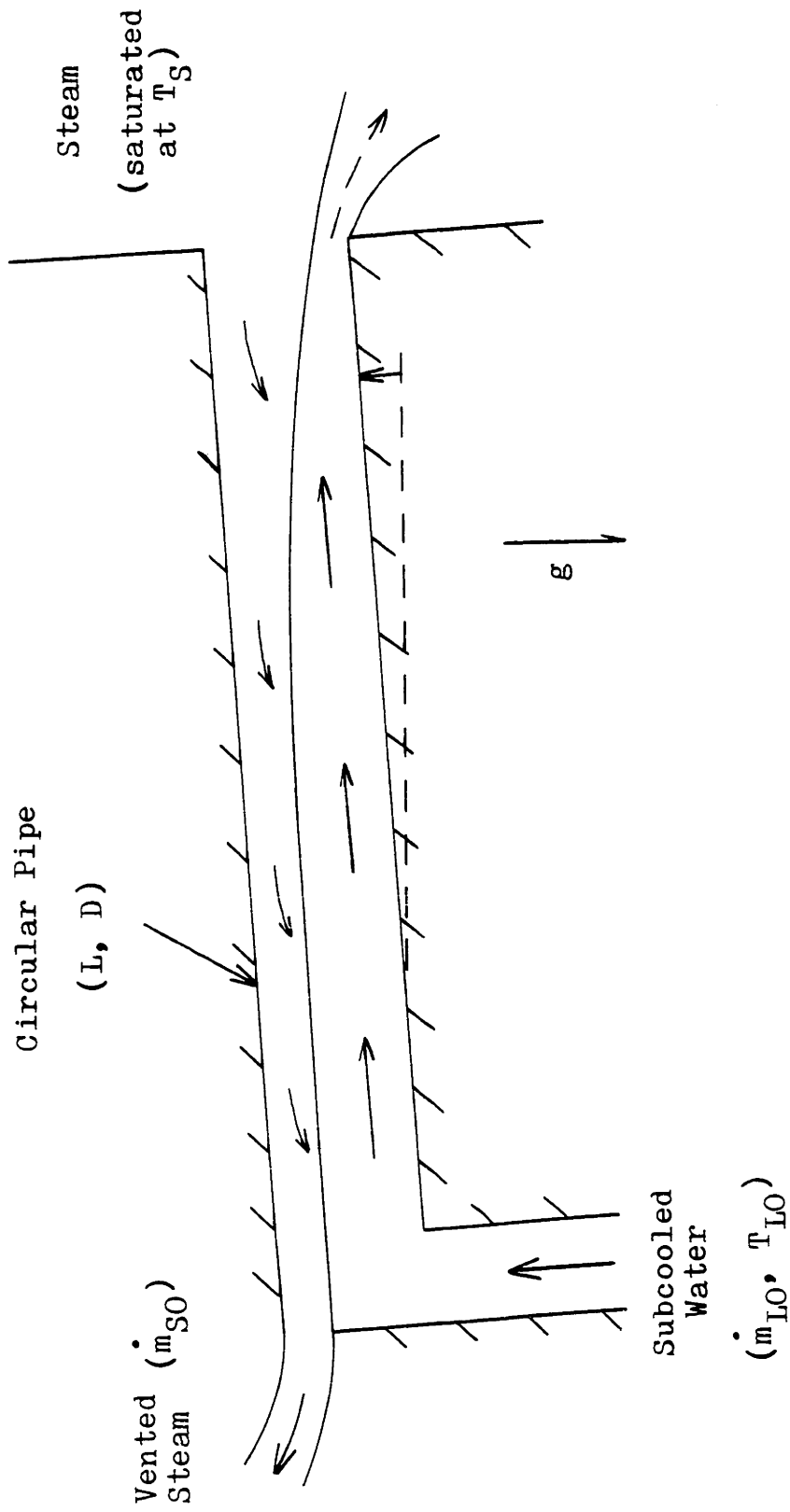


Figure III-1. Flow geometry selected for analysis.

hammer.

Stratified flow in the absence of condensation is the well-known problem of open-channel flow. The one-dimensional flow assumption to be used in the present analysis is equivalent to the "parallel movement" assumption of Bélanger (1828), later termed "gradually-varied flow" by Boussinesq (1877). The equation of gradually-varied flow in a circular pipe is:

$$(1 - Fr^2) \frac{d(d_L^*)}{dx^*} = -\tau_L^* . \quad (\text{III-1})$$

The engineering analysis of open channel flow, as described by Bakhmeteff (1932), consists of dividing a channel length into relatively long sections of gradually-varied flow and relatively short sections containing abrupt changes, such as hydraulic jumps, weirs, and overfalls. Any device which has a fixed relation between liquid depth and liquid flow rate is called a control. A control provides a boundary condition for the solution of Equation (III-1). In the case of the free overfall, the depth and flow rate are related by the requirement that the energy of the liquid stream is a minimum at the overfall. This can be shown to require $Fr^2 = 1$ at the overfall.

Given Equation (III-1) and the free overfall control, an expression for τ_L^* is required. A turbulent pipe flow correlation may be used, provided the appropriate hydraulic diameter is used.

The integration of Equation (III-1) must, in general, be carried out numerically, using a finite difference technique. Since the equation is singular at $Fr^2 = 1$, the boundary condition is usually taken as $Fr^2 = 1 - \delta$, where δ is small. A finite difference mesh may be specified in terms of liquid depth or distance from the overfall. Specifying the mesh in terms of liquid depth has the advantage of giving accurate results with a uniform mesh. Since the pipe length is often known, specifying the mesh in terms of distance along the pipe and using a non-uniform mesh is also accurate, and has the advantage of providing data at the same locations for each case examined. Further information on open-channel flow analysis and numerical methods may be found in Chow (1959) and Henderson (1966).

Interfacial shear, the pressure gradient along the pipe, and the addition of liquid by condensation combine to increase the complexity of the one-dimensional stratified flow equations for the steam-water system. However, the numerical solution methods used in open-channel flow remain useful.

In this chapter, the governing equations for the steam-water system are derived and expressed in dimensionless form. The method follows that of Linehan, et al. (1970), who studied cocurrent stratified flow condensation in a horizontal rectangular channel. The liquid and steam wall shear stresses, interfacial shear stress, and condensation heat transfer coefficient are examined and a suitable correlation for each

is selected from the literature. Finally, a stratified-slug flow regime transition criterion is selected.

B. Derivation of the governing equations

The flow geometry analyzed here was shown in Figure III-1. The following simplifying assumptions will be made:

1. The flow is steady, and can be treated as one-dimensional in both velocity and temperature.
2. The pipe is circular, and its inclination is small.
3. The steam is saturated, and its temperature is constant along the pipe.
4. The ratio of steam to liquid density is small.
5. The liquid depth at the pipe discharge is critical, and the gradually-varied flow assumption is applied over the entire pipe.

By considering steady flow, the analysis is considerably simplified but will be unable to predict the effect of inlet water flow rate transients on water hammer initiation. Use of the gradually-varied flow assumption near the pipe exit will produce inaccurate results within 2 to 3 hydraulic depths of the exit, but well upstream, where water slug formation occurs, the error will be small.

Consider a control volume extending from the water inlet

to an arbitrary location along the pipe, as shown in Figure III-2. A mass balance gives

$$\dot{m}_S + \dot{m}_{LO} = \dot{m}_L + \dot{m}_{SO} . \quad (\text{III-5})$$

An energy balance gives

$$\dot{m}_S i_S + \dot{m}_{LO} i_{LO} = \dot{m}_{SO} i_S + \dot{m}_L i_L . \quad (\text{III-6})$$

Combining Equations (III-5) and (III-6),

$$\dot{m}_L = \dot{m}_{LO} \left[1 + \frac{(i_L - i_{LO})}{(i_S - i_L)} \right] . \quad (\text{III-7})$$

Since \dot{m}_{LO} , i_{LO} , and i_S are known, Equation (III-7) relates the local liquid enthalpy (or temperature) to the local liquid mass flow rate.

Next, consider the liquid and steam control volumes in Figure III-3, of differential length δx . An energy balance on the liquid gives

$$\dot{m}_L i_L + \delta \dot{m}_L i_S = (\dot{m}_L + \delta \dot{m}_L) (i_L + \delta i_L) , \quad (\text{III-8})$$

and, with $\delta i_L = c_{PL} \delta T_L$,

$$\frac{dT_L}{dx} = \frac{(i_S - i_L)}{\dot{m}_L c_{PL}} \frac{d\dot{m}_L}{dx} . \quad (\text{III-9})$$

The interfacial condensation heat transfer coefficient, h_I , is used to determine $d\dot{m}_L/dx$, yielding

$$\frac{d\dot{m}_L}{dx} = \frac{h_I S_I (T_S - T_L)}{i_{fg}} . \quad (\text{III-10})$$

Inserting Equation (III-9) into Equation (III-10), one

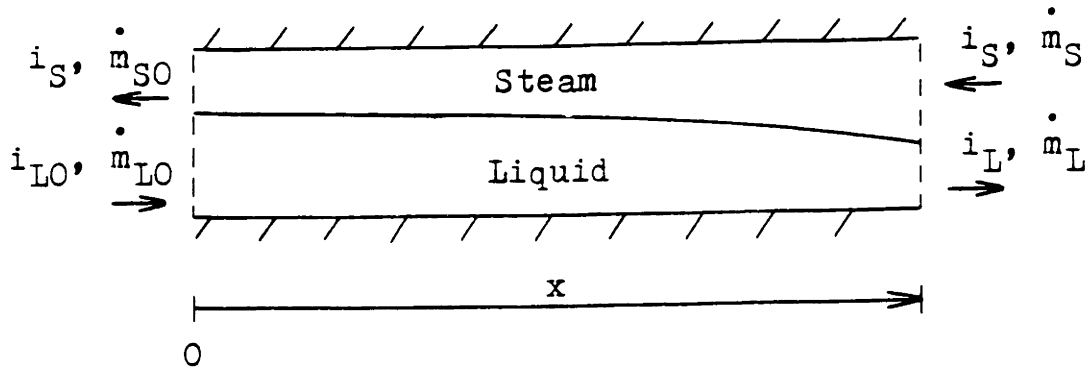


Figure III-2. Control volume used for global energy balance.

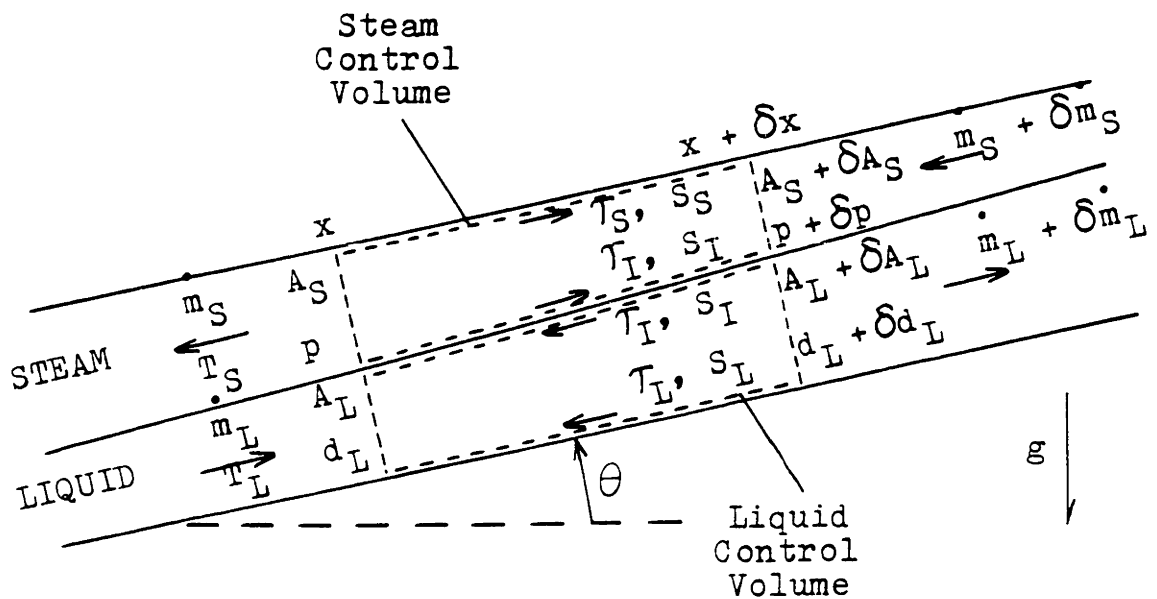


Figure III-3. Differential control volumes used for derivation of fundamental differential equations.

obtains

$$\frac{dT_L}{dx} = \frac{(i_S - i_L) h_I S_I (T_S - T_L)}{\dot{m}_L c_{PL} i_{fg}} \quad (\text{III-11})$$

Define \bar{c}_{PL} as the liquid specific heat at the average of the steam and liquid temperatures and use the approximation

$$i_S - i_L = i_{fg} + \bar{c}_{PL} (T_S - T_L) . \quad (\text{III-12})$$

Inserting this into Equation (III-11),

$$\frac{dT_L}{dx} = \frac{h_I S_I (T_S - T_L)}{\dot{m}_L c_{PL}} \left[1 + \frac{\bar{c}_{PL} (T_S - T_L)}{i_{fg}} \right] \quad (\text{III-13})$$

A momentum balance on the liquid gives

$$-(\tau_L S_L + \tau_I S_I) \delta x - A_L \delta p - g \theta \rho_L A_L \delta x - \rho_L g \delta d_L A_L = \frac{(\dot{m}_L + \delta \dot{m}_L)^2}{\rho_L (A_L + \delta A_L)} - \frac{\dot{m}_L^2}{\rho_L A_L} - V_I \delta \dot{m}_L . \quad (\text{III-14})$$

Using the relation $\delta A_L = S_I \delta d_L$, this equation can be manipulated to give

$$-(\tau_L S_L + \tau_I S_I) - A_L \frac{dp}{dx} - \rho_L g \theta A_L = \rho_L g A_L \frac{d(d_L)}{dx} + \frac{2 \dot{m}_L}{\rho_L A_L} \frac{d\dot{m}_L}{dx} - \frac{\dot{m}_L^2 S_I}{\rho_L A_L^2} \frac{d(d_L)}{dx} - V_I \frac{d\dot{m}_L}{dx} . \quad (\text{III-15})$$

A momentum balance on the steam gives

$$(\tau_S S_S + \tau_I S_I) \delta x - A_S \delta p = \frac{(-\dot{m}_S - \delta \dot{m}_S)^2}{\rho_S (A_S + \delta A_S)} - \frac{\dot{m}_S^2}{\rho_S A_S^2} + V_I \delta \dot{m}_S . \quad (\text{III-16})$$

Using the relations $\delta A_S = -S_I \delta d_L$ and $\delta \dot{m}_S = \delta \dot{m}_L$, this equation can be manipulated to give

$$\frac{dp}{dx} = \frac{1}{A_S} (\tau_S s_S + \tau_I s_I) - \frac{2 \dot{m}_S}{\rho_S A_S^2} \frac{d\dot{m}_L}{dx} - \frac{\dot{m}_S^2 s_I}{\rho_S A_S^3} \frac{d(d_L)}{dx} - \frac{V_I}{A_S} \frac{d\dot{m}_L}{dx} \quad (\text{III-17})$$

Inserting Equation (III-17) into Equation (III-15), using the relation $\dot{m} = \rho V A$, and neglecting the terms involving V_I , one obtains

$$\left\{ 1 - \frac{\dot{m}_L^2 s_I}{\rho_L^2 g A_L^3} \left[1 + \frac{A_L}{A_S} \left(\frac{\rho_S v_S^2}{\rho_L v_L^2} \right) \right] \right\} \frac{d(d_L)}{dx} = - \frac{1}{\rho_L g} \left(\frac{\tau_L s_L}{A_L} + \frac{\tau_S s_S}{A_S} + \frac{\tau_I s_I}{A_L} + \frac{\tau_I s_I}{A_S} \right) - \theta + \frac{2 \dot{m}_L}{\rho_L^2 g A_L^2} \left[\frac{A_L}{A_S} \left(\frac{v_S}{v_L} \right) - 1 \right] \frac{d\dot{m}_L}{dx} \quad (\text{III-18})$$

In the work of Linehan, et al. (1970) for cocurrent flow, $V_I = 1.14 V_L$ was used. In a countercurrent flow, this value is inappropriate. Trial calculations using $V_I = V_L$ showed that the contribution of the terms involving V_I was small, so they have been removed from the equation.

It is useful to transform these governing equations into a dimensionless form. Define dimensionless variables as follows:

$$\begin{aligned} d_L^* &= d_L/D & T_L^* &= (T_L - T_{LO})/(T_S - T_{LO}) \\ x^* &= x/D & Nu &= h_I D_{h,L}/k_L \\ \alpha &= A_S/(\pi D^2/4) & q^* &= h_I A_L (T_S - T_L)/(\dot{m}_L i_{fg}) \\ \dot{m}_L^* &= \dot{m}_L/\dot{m}_{LO} & \phi &= \frac{(1 - \alpha)}{\alpha} \frac{\rho_S v_S^2}{\rho_L v_L^2} \\ \dot{m}_S^* &= \dot{m}_S/\dot{m}_{LO} & \psi &= \frac{(1 - \alpha)}{\alpha} \frac{v_S}{v_L} \end{aligned}$$

$$\begin{aligned}
\tau_L^* &= \tau_L S_L / (\rho_L g A_L) & \omega_0 &= \frac{c_{PL}|_{T_L} (T_S - T_{LO})}{i_{fg}} \\
\tau_S^* &= \tau_S S_S / (\rho_S g A_S) & \bar{\omega}_1 &= \frac{c_{PL}|_{(T_S+T_L)/2} (T_S - T_L)}{i_{fg}} + 1 \\
\tau_I^* &= \tau_I S_I / (\alpha \rho_L g A_L) & \bar{\omega}_2 &= \frac{c_{PL}|_{(T_L+T_{LO})/2} (T_L - T_{LO})}{i_{fg}} \\
Fr^2 &= \dot{m}_L^2 S_I / (\rho_L^2 g A_L^3)
\end{aligned}
\tag{III-19}$$

The governing equations then become

$$\left[1 - Fr^2 (1 + \phi) \right] \frac{d(d_L^*)}{dx^*} = -\tau_L^* - \tau_I^* - \tau_S^* - \theta + \frac{2 Fr^2 q^* (\psi - 1)}{2 Fr^2 q^* (\psi - 1)}
\tag{III-20}$$

$$\frac{d(T_L^*)}{dx^*} = q^* \left(\frac{S_I D}{A_L} \right) \left(\frac{\bar{\omega}_1}{\bar{\omega}_0} \right)
\tag{III-21}$$

$$\dot{m}_S^* = \frac{\dot{m}_{SO}}{\dot{m}_{LO}} + \frac{\bar{\omega}_2}{\bar{\omega}_1}
\tag{III-22}$$

in dimensionless form. Note that Equation (III-20) reduces to Equation (III-1), the equation of gradually-varied open-channel flow, when no steam flow is present.

The boundary condition on liquid temperature is

$$T_L^* = 0 \quad \text{at } x^* = 0
\tag{III-23}$$

The boundary condition on liquid depth is the free overfall "control," which specifies that the critical depth of an open-channel flow is reached at the overfall. From Equation (III-20), this means that

$$\zeta = 1 - Fr^2 (1 + \phi) = 0 \quad \text{at } x^* = L/D
\tag{III-24}$$

Equations (III-20) through (III-22), together with the boundary conditions (III-23) and (III-24), are the fundamental relations which describe the model of the flow of Figure III-1. In addition to fluid properties, the quantities τ_L , τ_I , τ_S , and h_I must be specified to permit the solution of the problem. The determination of these quantities is discussed next, in Section III.C. For the cases examined here, local Reynolds numbers exceeded 3500 for each phase, and turbulent flow was therefore present. This was confirmed by inspection of the water flow in the transparent test section.

C. Determination of Momentum and Heat Fluxes

1. Liquid and steam wall shear stresses. The wall shear stress for each phase is calculated using the turbulent pipe flow friction factor equation shown in Rohsenow and Choi (1961), where

$$\tau = \frac{f}{8} \rho v^2 , \quad (\text{III-25})$$

and

$$f = 0.3164 \text{ Re}^{-0.25} , \quad (\text{III-26})$$

where

$$\text{Re}_S = \frac{\rho_S v_S D_{h,S}}{\mu_S} \quad \text{Re}_L = \frac{\rho_L v_L D_{h,L}}{\mu_L} \quad (\text{III-27})$$

and

$$D_{h,S} = \frac{4 A_S}{S_S + S_I} \quad D_{h,L} = \frac{4 A_L}{S_L + S_I} \quad (\text{III-28})$$

are used for the stratified flow case as an approximation. Since the liquid is not a thin film, the wall-layer model used by Linehan, et al. (1970) was not used here.

2. Interfacial shear stress. Linehan, et al. (1970) proposed a linear superposition of the non-condensing interfacial shear stress, τ_A , and the suction parameter, of the form

$$\tau_I = \tau_A + \frac{v_S}{S_I} \frac{dm_L}{dx}, \quad (\text{III-29})$$

where

$$\tau_A = \frac{f_A}{8} \rho_S v_S^2, \quad (\text{III-30})$$

$$f_A = 9.26 \times 10^{-6} \text{Re}_L' + 0.0524, \quad (\text{III-31})$$

and

$$\text{Re}_L' = \frac{\dot{m}_L}{\mu_L b}, \quad (\text{III-32})$$

where b is the width of a rectangular channel. Equation (III-31) was obtained by correlation of data in a rectangular channel with a 10 to 1 aspect ratio. Using a method described in Section III.C.3, Equation (III-31) may be converted to

$$f_A = 4.86 \times 10^{-6} \text{Re}_L + 0.0524 \quad (\text{III-33})$$

for a pipe of arbitrary cross-section (used here for the

circular pipe). The interfacial shear stress, τ_I , is then given by Equations (III-29), (III-30), and (III-33).

Since the development of the model presented here, Jensen and Yuen (1982) have reported on their study of interfacial heat, mass, and momentum transport. One of their conclusions is a tentative recommendation of the Linehan, et al. (1970) interfacial shear stress calculation method which is used here.

3. Condensation heat transfer coefficient. The first theoretical analysis of condensation on liquid films was done by Nusselt (1916), who examined laminar flow due to gravity on a vertical surface and on the outside of a horizontal tube, in the absence of interfacial shear. Nusselt obtained the equation

$$\frac{h_x x}{k_L} = \left[\frac{\rho_L (\rho_L - \rho_S) g i_{fg} x^3}{4 \mu_L k_L (T_S - T_W)} \right]^{0.25} \quad (\text{III-34})$$

for laminar film condensation on a vertical surface. The derivation of Equation (III-34) and a discussion of suggested improvements to the equation may be found in Rohsenow and Choi (1961).

With the objective of advancing the art of condenser design, considerable research has been done on condensation heat transfer with diabatic walls. Laminar flow forced convection condensation inside a horizontal and inclined tube with a liquid layer at the bottom of the tube was studied by Chaddock (1955), Chato (1960), and Rufer and

Kezios (1967). As in the present work, the similarity to open-channel flow was noted by these authors. Considerable work has also been done on annular flow forced convection condensation, including that of Traviss, et al. (1972). For the most part, these analyses have dealt with heat transfer across thin films. For example, Chaddock (1955) neglected heat transfer through the liquid layer at the bottom of the pipe and applied a Nusselt-type analysis to the thin liquid film on the remainder of the pipe's circumference.

More recently, however, researchers have begun to examine the condensation heat transfer between a vapor and a turbulent subcooled liquid layer with adiabatic walls. Linehan, et al. (1970) expressed the condensation heat flux in terms of an effective turbulent thermal conductivity, K_L :

$$q_c = \left(K_L \frac{\partial T_L}{\partial n} \right) \Big|_t \quad (\text{III-35})$$

Using the mean liquid velocity, V_L , and a mixing length equal to the liquid depth, t , the eddy diffusivity of heat is expressed as

$$\epsilon_h = a_1 t V_L . \quad (\text{III-36})$$

Since

$$K_L \Big|_t = K_L = \rho_L c_{PL} \epsilon_h , \quad (\text{III-37})$$

$$K_L \Big|_t = a_1 k_L \text{Re}_L' \text{Pr}_L . \quad (\text{III-38})$$

Linehan, et al. (1970) further assumed that

$$\frac{\partial T_L}{\partial n} = \frac{T_S - T_L}{a_2 t} \quad (\text{III-39})$$

to obtain the result

$$\text{Nu}' = 0.0073 \text{Re}_L' \text{Pr}_L, \quad (\text{III-40})$$

where the constant 0.0073 was obtained by correlation of experimental data.

Bankoff, et al. (1978) and Thomas (1979) applied the analogy between mass transfer in gas absorption by a turbulent liquid and heat transfer in condensation on a turbulent liquid. Brumfield, et al. (1975, 1976) had obtained mass transfer coefficients by looking at "small-scale" and "large-scale" turbulence, and the analogous dimensionless heat transfer equation for the "small-eddy" case was shown to be

$$\text{Nu}_t = 0.25 \text{Re}_t^{0.75} \text{Pr}_L^{0.5}, \quad (\text{III-41})$$

where $\text{Nu}_t = h' l / k_L$, Re_t is the turbulence Reynolds number, $l V / \nu$, h' is the interfacial heat transfer coefficient before correction for condensation, V is the turbulence intensity, and l is the macroscale of turbulence. One way to correct for condensation is to use the Colburn analogy between heat and momentum transfer and apply Equation (III-29).

A complete review of turbulent gas absorption analyses and their application to condensation on turbulent subcooled

liquids may be found in Jensen and Yuen (1982). A briefer review is presented by Bankoff (1980). One consequence of these studies is that the interfacial condensation heat transfer coefficient should correlate well with Re_L and Pr_L when heat transfer is governed by liquid phase turbulence. The vapor phase also affects the condensation rate by ruffling the interface, so a correlation of the form

$$Nu = a Re_L^b Re_S^c Pr_L^d \quad (III-42)$$

has been used by most researchers.

Studies of interfacial condensation heat transfer in stratified flow of steam and subcooled water have been reported recently by Lee, et al. (1979), Lim, et al. (1981), and Jensen and Yuen (1982) for cocurrent flow and by Segev and Collier (1980), Segev, et al. (1981), and Bankoff, et al. (1982) for countercurrent flow. These researchers conducted their experiments in rectangular channels, with aspect ratios ranging from 3:1 to 10:1.

For cocurrent condensation in a horizontal channel, Lee, et al. (1979) obtained a correlation of quantities averaged from the steam and water inlet ($x = 0$):

$$(\overline{St})_x = 0.0045 (\overline{Re}_S)_x^{1/3} (\overline{Re}_L)_x^{-0.29} \quad (III-43)$$

Also, using laser-doppler measurements to estimate the turbulence quantities l and V , reasonable agreement was found between the data and Equation (III-41).

Further work by Lim, et al. (1981) resulted in the correlations:

$$(\overline{Nu})_x = 0.0344 (\overline{Re}_S)_x^{0.58} (\overline{Re}_L)_x^{0.42} (\overline{Pr}_L)_x^{0.3} \quad (\text{III-44})$$

(rough interface)

$$(\overline{Nu})_x = 0.631 (\overline{Re}_S)_x^{0.58} (\overline{Re}_L)_x^{0.09} (\overline{Pr}_L)_x^{0.3} \quad (\text{III-45})$$

(smooth interface)

Jensen and Yuen (1982) presented a detailed study of interfacial shear stresses and condensation rates in horizontal stratified cocurrent flow in a rectangular channel. Several turbulent transport theories are discussed, with the objective of obtaining a unified theory for heat, mass, and momentum transfer at the interface between a gas and a turbulent liquid.

Work on countercurrent flow condensation on a turbulent subcooled liquid in stratified flow has sought correlations of the local heat transfer coefficient in terms of local dimensionless quantities. In rectangular channels, all of the authors have used the definitions

$$Re_L' = \frac{\rho_L V_L t_L}{\mu_L}, \quad (\text{III-46})$$

$$Re_S' = \frac{\rho_S V_S t_S}{\mu_S}, \text{ and} \quad (\text{III-47})$$

$$Nu' = \frac{h_I t_L}{k_L}. \quad (\text{III-48})$$

Segev and Collier (1980) performed tests in a horizontal rectangular channel with a 3 to 1 aspect ratio and found

their data were correlated by

$$\text{Nu}' = 5.06 \times 10^{-5} \text{Re}_S'^{0.012} \text{Re}_L'^{1.45} \text{Pr}_L'^{0.55} \quad (\text{III-49})$$

(smooth interface)

$$\text{Nu}' = 6.11 \times 10^{-6} \text{Re}_S'^{0.58} \text{Re}_L'^{1.21} \text{Pr}_L'^{0.10} \quad (\text{III-50})$$

(rough interface)

Water slug formation and the consequent water hammer were also seen in the test section. Segev, et al. (1981) later reported the results of further tests at inclinations of 17 and 45 degrees from the horizontal, including more correlations.

The results of similar, but more extensive, tests on countercurrent condensation in a rectangular channel with a 10 to 1 aspect ratio were reported by Bankoff, et al. (1982). Condensation heat transfer data were correlated by

$$\text{Nu}' = 0.173 \text{Re}_S'^{0.027} \text{Re}_L'^{0.49} \text{Pr}_L'^{0.42} \quad (\text{III-51})$$

(smooth interface)

$$\text{Nu}' = 0.34 \times 10^{-9} \text{Re}_S'^{2.1} \text{Re}_L'^{0.56} \text{Pr}_L'^{1.16} \quad (\text{III-52})$$

(rough interface)

Experimental data on water hammer initiation (in a nearly horizontal channel) and flooding (in moderately inclined and vertical channels) were also collected. The water hammer initiation data appear to have been taken at ratios of liquid depth to channel height less than 0.5, since the

Taitel-Dukler (1976) stability criterion is shown to predict higher critical steam flow rates than that of Mishima and Ishii (1979) when compared with the data (see Figure III-4 in Section III.D).

The Bankoff, et al. (1982) correlation for counter-current condensation in a rectangular channel will be used as the basis for calculating the condensation rates in the circular pipe geometry of the present model. Because the aspect ratio studied by Bankoff, et al. is large, secondary flows should have less of an effect on the heat transfer rate, and the dependence on the dimensionless variables shown by Equations (III-51) and (III-52) should be more accurate than that shown by Equations (III-49) and (III-50).

In a pipe of arbitrary cross-section, the following definitions, analogous to Equations (III-46) through (III-48), are made:

$$D_{h,L} = \frac{4 A_L}{S_L + S_I} \quad (\text{III-53})$$

$$D_{h,S} = \frac{4 A_S}{S_S + S_I} \quad (\text{III-54})$$

$$Re_L = \frac{m_L D_{h,L}}{\mu_L A_L} \quad (\text{III-55})$$

$$Re_S = \frac{m_S D_{h,S}}{\mu_S A_S} \quad (\text{III-56})$$

$$Nu = \frac{h_I D_{h,L}}{k_L} \quad (\text{III-57})$$

If the liquid layer thickness, t_L , is taken to be one-half the height of the rectangular channel, for $b/h = 10$ as in

Bankoff, et al. (1982),

$$D_{h,L} = 1.905 t_L \quad (\text{III-58})$$

$$D_{h,S} = 1.905 t_S \quad (\text{III-59})$$

If t were very small, D_h would equal $2.0 t$. If t were equal to the channel height, D_h would equal $1.818 t$. Thus, little error is introduced by use of Equations (III-58) and (III-59) for typical values of t_L and t_S . Using these definitions, Equations (III-51) and (III-52) may be modified to give the following expressions for a pipe of arbitrary cross-section (used here for the circular pipe):

$$\text{Nu} = 0.236 c_1 \text{Re}_S^{0.027} \text{Re}_L^{0.49} \text{Pr}_L^{0.42} \quad (\text{III-60})$$

(smooth interface)

$$\text{Nu} = 1.17 \times 10^{-10} c_1 \text{Re}_S^{2.1} \text{Re}_L^{0.56} \text{Pr}_L^{1.16} \quad (\text{III-61})$$

(rough interface)

Here, c_1 is a constant multiplier, expected to be greater than 1.0, which accounts for the presence of secondary flows in a partially-filled circular pipe which are not present in a wide rectangular channel. In Chapter V, a best fit of water hammer initiation data gives $c_1 = 2.5$. This is also shown to provide good agreement with exit liquid temperature data taken in the circular pipe used in the present study. Since the rough and smooth interface regimes are not quantified, a conservative calculation

method (from the point of view of water slug formation prediction) is used. The higher value of Nu, whether from Equation (III-60) or (III-61) is used in the present model. The test conditions were such that the smooth interface expression, Equation (III-60), governed all the calculations which were compared with data. Thus, the validity of using $c_1 = 2.5$ in Equation (III-61) is unknown.

D. A criterion for water hammer initiation

1. Water slug formation. Suppose that, for a given set of flow and system conditions, the model of Sections III.B and III.C has been used to predict the variation of liquid depth and steam mass flow rate along a pipe. The location, if any, of water slug formation (which leads to steam bubble collapse-induced water hammer) can then be predicted, given a suitable criterion for stratified-slug flow regime transition. If stratified-slug transition is predicted at any location along the pipe, water hammer is expected. As the inlet water flow rate is increased in small steps (and the model applied at each flow rate), the location where stratified-slug transition appears first is the predicted location of water slug formation.

The stratified-slug transition criterion of Taitel and Dukler (1976) was selected for use here. The boundary between stratified and slug flow is given by

$$N_{TD} = \frac{\phi Fr^2}{(1 - d_L^*)^2} = 1.0 \quad (\text{III-62})$$

for a horizontal or nearly-horizontal circular pipe, where the notation of the present study has been used.⁽¹⁾

Equation (III-62) is obtained by a force balance between the pressure difference over a wave due to the Bernoulli effect and the gravity force on the wave. Taitel and Dukler (1976) also assume (without theoretical justification) that the ratio of the steam flow area above a wave crest, A_S' , to the steam flow area away from the wave, A_S , is

$$\frac{A_S'}{A_S} = 1 - d_L^* . \quad (\text{III-63})$$

An alternative stratified-slug transition criterion which was examined is that of Mishima and Ishii (1980) for a horizontal rectangular channel:

$$V_S = 0.487 \sqrt{\rho_L g h_S / \rho_S} \quad (\text{III-64})$$

Equation (III-64) was derived from a stability analysis of waves of finite amplitude and specified wavelength done by Kordyban and Ranov (1970), with the hypothesis that the wavelength associated with slug formation is that which has the largest growth rate. Equation (III-64), derived theoretically, is virtually identical to the Wallis-Dobson (1973) correlation, which has a constant of 0.500 instead of 0.487 and was obtained from experimental data. By analogy with the Kelvin-Helmholtz instability formulae for

(1) The reader should note that in the Taitel and Dukler (1976) paper, the final form of this equation is misprinted and in error by a factor of α .

small-amplitude, long wavelength disturbances in (1) a rectangular channel and (2) a circular pipe, the Mishima-Ishii stratified-slug transition criterion may be written as

$$N_{MI} = 4.216 \phi Fr^2 = 1 \quad (\text{III-65})$$

for the circular pipe. Comparison with the Taitel-Dukler criterion, Equation (III-62), shows that, for given flow conditions,

$$\frac{N_{TD}}{N_{MI}} = \frac{0.2372}{(1 - d_L^*)^2} \quad (\text{III-66})$$

Equation (III-66) is plotted in Figure III-4. Since each stability parameter contains the square of the steam velocity, the difference in predicted critical steam velocity between the two is not as great as it appears for d_L^* less than about 0.6. However, as d_L^* increases above 0.6, the discrepancy becomes very large.

Use of the Taitel-Dukler criterion provided better agreement between predictions and critical inlet water flow rate data. As shown in Appendix B, the rms deviation of data from the predictions of the Taitel-Dukler criterion with $c_1 = 2.5$ is 13.6 percent. The rms deviation of data from the predictions of the Mishima-Ishii criterion with its optimum value of $c_1 = 2.8$ is 18.5 percent. The Taitel-Dukler criterion, Equation (III-62), is therefore used in the model to predict water slug formation and the initiation of water hammer.

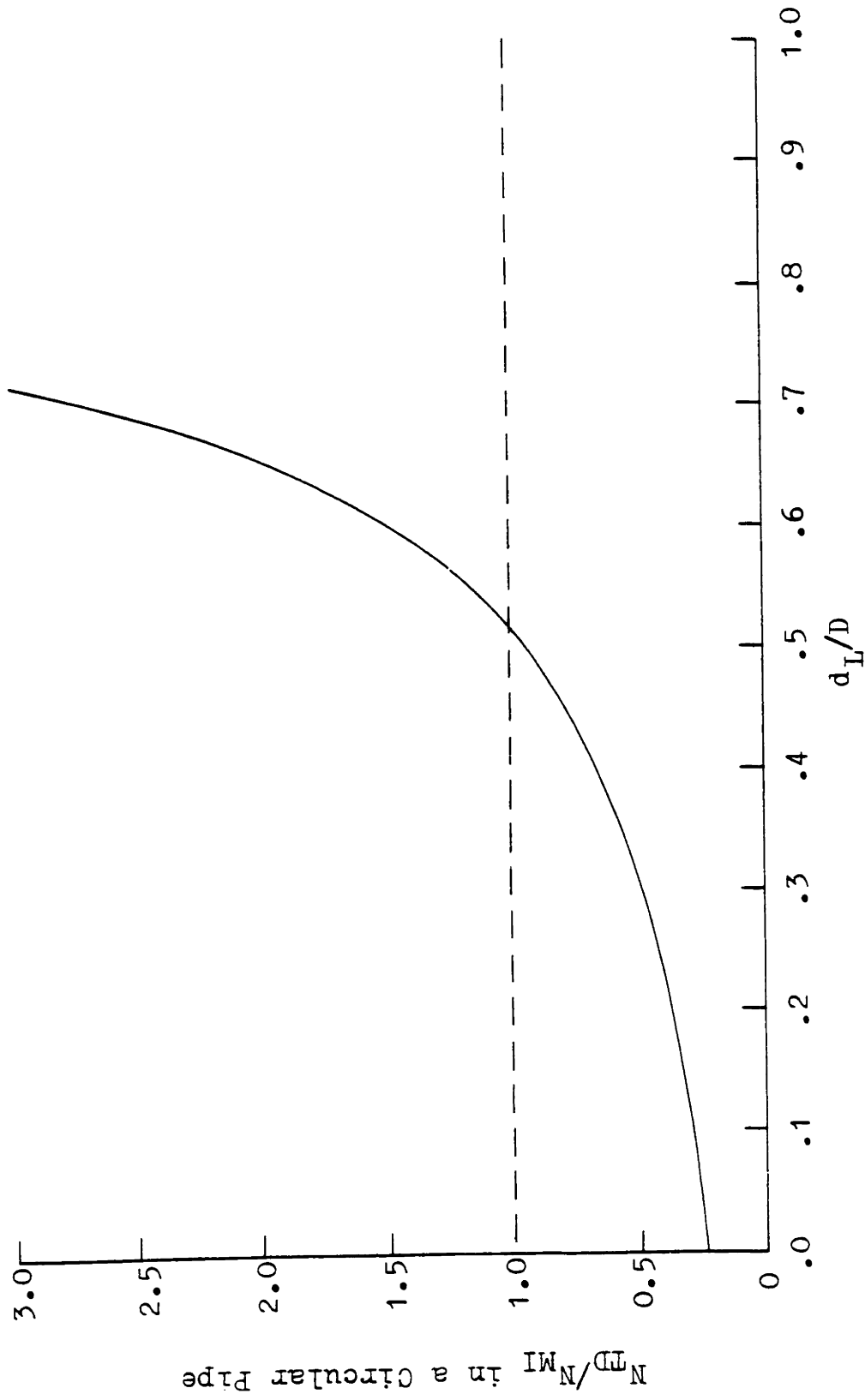


Figure III-4. Ratio of Taitel-Dukler (1976) to Mishima-Ishii (1980) stability parameter for given flow conditions.

2. Pipe-full limit. One means to prevent condensation water hammer in the flow geometry studied here is to ensure that the pipe runs full at all times. This problem was studied by Wallis, et al. (1977). Their criterion for the minimum water flow rate necessary to run the pipe full may be expressed as

$$\frac{16 \dot{m}_{LO}^2}{\pi^2 \rho_L^2 g D^5} = 0.25 \quad (\text{III-67})$$

The region where water hammer is predicted to occur is thus bounded by the stratified flow breakdown on the one hand and the pipe-full limit on the other.

CHAPTER IV

THE NUMERICAL SOLUTION

A. The approach used

1. Application of the finite difference method. The objective here is the numerical solution of Equations (III-20) through (III-22), subject to the boundary conditions of Equations (III-23) and (III-24), and with the momentum and heat flux quantities calculated as described in Section III.C. In order to obtain results at the same locations along a pipe for different flow conditions, the finite difference mesh is specified in terms of distance rather than liquid depth. The pipe length is divided into $n-1$ small sections (not necessarily of equal length) as shown in Figure IV-1.

An explicit finite difference method is then applied. Starting with the boundary condition $T_L^* = 0$ at $x^* = 0$, liquid temperatures are calculated for each node, proceeding in the direction of increasing x^* and using a finite difference approximation to Equation (III-21):

$$T_{L,i+1}^* = T_{L,i}^* + \left[q^* \left(\frac{S_I D}{A_L} \right) \left(\frac{\bar{\omega}_1}{\omega_0} \right) \right]_i (x_{i+1}^* - x_i^*) \quad (IV-1)$$

Equation (III-22) is used to compute $\dot{m}_{S,i+1}$, given $T_{L,i+1}^*$. Fluid properties, \mathcal{T}_L^* , \mathcal{T}_3^* , \mathcal{T}_I^* , and Nu are calculated for node $i+1$, using $T_{L,i+1}^*$. Initially, $d_L^* = 0.5$ is assumed at all nodes. The "rightward sweep" using Equation (IV-1) then provides an approximate temperature profile along the pipe.

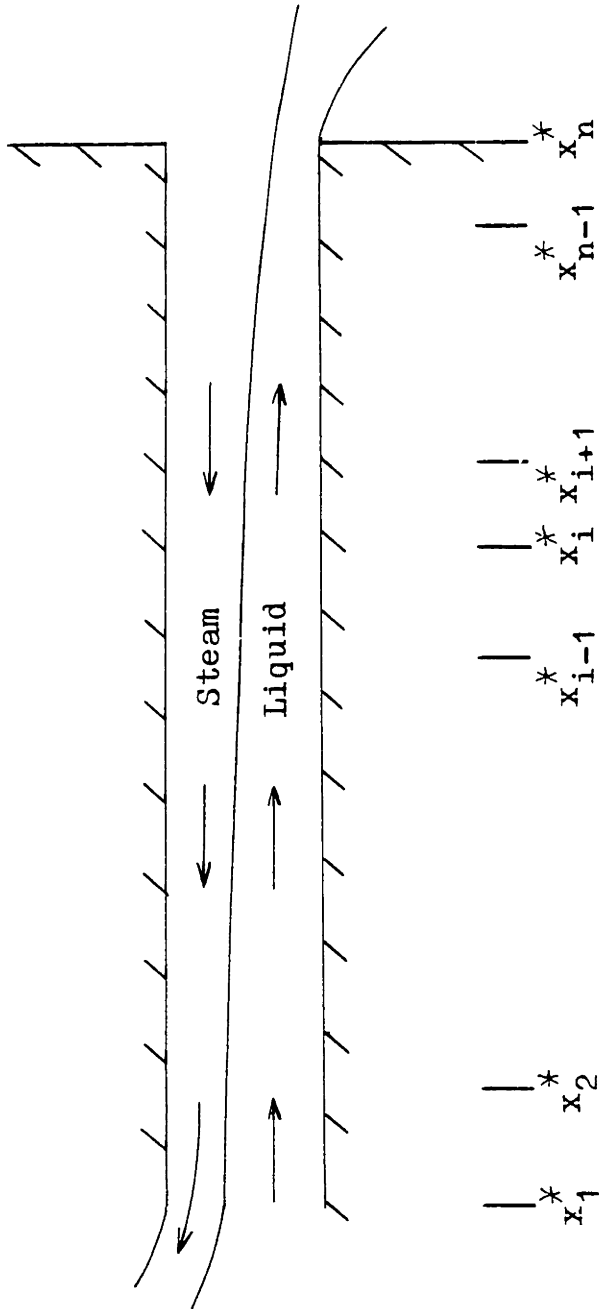


Figure IV-1. Pipe length divided into finite difference sections (not necessarily of equal length).

Since the boundary condition $\zeta = 0$ at $x^* = L/D$ is a singular point of Equation (III-20), the actual boundary condition used in the numerical solution is

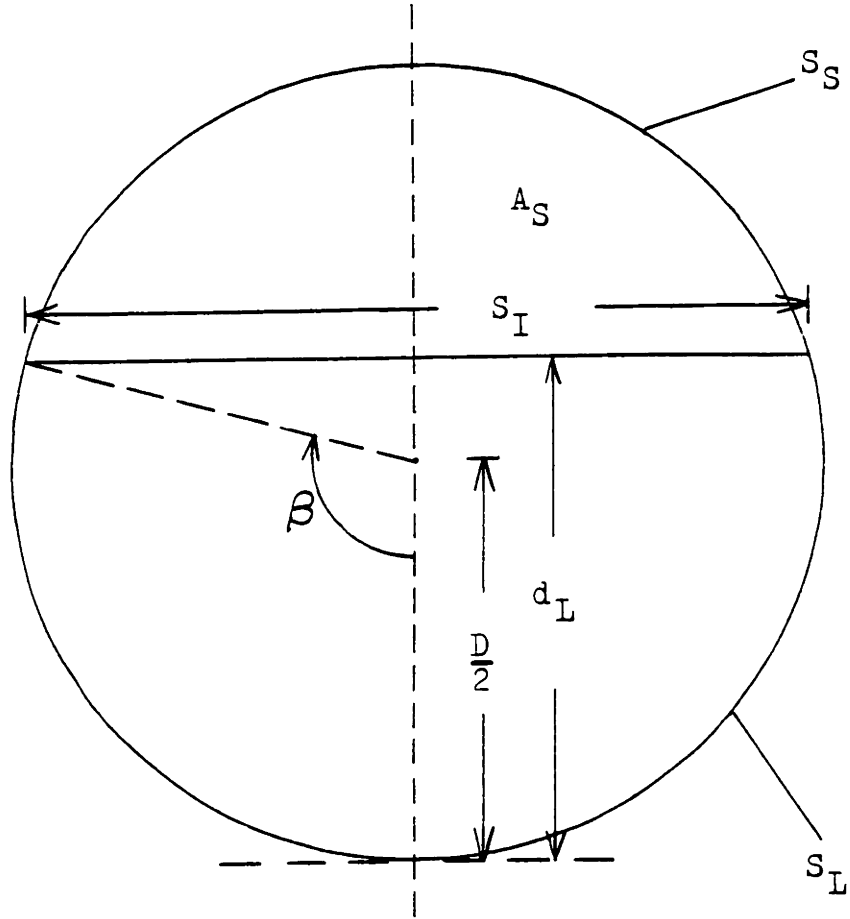
$$\zeta = 0.075 \text{ at } x^* = L/D . \quad (\text{IV-2})$$

The value of 0.075 was selected because it minimized the inlet liquid depth for the number of nodes used. If more nodes were used, a smaller value of ζ could be used in Equation (IV-2). Since the one-dimensional flow model is invalid near $\zeta = 0$ and since water slug formation usually occurs well away from the pipe discharge, $\zeta = 0.075$ provides sufficient accuracy.

Equation (IV-2) is solved iteratively for the liquid depth at $x^* = L/D$. Then, liquid depths are calculated for each node, proceeding in the direction of decreasing x^* and using a finite difference approximation to Equation (III-20):

$$d_{L,i-1}^* = d_{L,i}^* - \left[\frac{-\tau_L^* - \tau_I^* - \tau_S^* - \theta + 2 \text{Fr}^2 q^* (\psi - 1)}{\zeta} \right]_i (x_i^* - x_{i-1}^*) \quad (\text{IV-3})$$

Local geometric quantities, τ_L^* , τ_S^* , τ_I^* , and Nu are calculated for node $i-1$, using $d_{L,i-1}^*$. The formulae shown in Figure IV-2 are used to compute local geometric quantities. The "leftward sweep" using Equation (IV-3) provides an approximate liquid depth profile along the pipe. Successive "rightward" and "leftward" sweeps are made until these con-



$$\begin{array}{ll}
 d_{L*} = d_L/D & \beta = \cos^{-1} (1 - 2 d_{L*}) \\
 S_{I*} = S_I/D & S_{L*} = \beta \\
 S_{L*} = S_L/D & S_{S*} = \pi - \beta \\
 S_{S*} = S_S/D & S_{I*} = \sin \beta \\
 A_{S*} = A_S / (\pi D^2 / 4) & A_{L*} = (2\beta - \sin 2\beta) / (2\pi) \\
 A_{L*} = A_L / (\pi D^2 / 4) & A_S = 1 - A_{L*}
 \end{array}$$

Figure IV-2. Geometric formulae for a circular cross-section of a stratified flow.

vergence criteria are satisfied at all nodes on the pth pass:

$$\frac{(T_L^*)_p - (T_L^*)_{p-1}}{(T_L^*)_p} < 0.0001 \quad (\text{IV-4})$$

$$\frac{(d_L^*)_p - (d_L^*)_{p-1}}{(d_L^*)_p} < 0.0001 \quad (\text{IV-5})$$

2. Behavior of the solution procedure. To obtain converged results, updated temperatures were damped using the formula

$$(T_L^*)_p = (T_L^*)_{\text{calc}} (1 - r) + (T_L^*)_{p-1} r, \quad (\text{IV-6})$$

where $(T_L^*)_{\text{calc}}$ is the result calculated on the pth pass using Equation (IV-1). Values of r used varied from 0 (no damping) to 0.1.

In some cases, oscillations in liquid depth from pass to pass prevented convergence. This problem was solved by specifying a maximum liquid depth. That is, if the liquid depth calculated by Equation (IV-3) is greater than the specified maximum, it is set equal to the maximum. This maximum liquid depth is chosen to be greater than any converged liquid depth and thus only influences the first several passes of the solution procedure.

In the adiabatic case, no damping is required, and only 2 passes are needed to obtain convergence. With condensation, from 10 to 40 passes were required to obtain convergence. For given conditions, there was observed to be an optimum value of r in Equation (IV-6) which minimized the number

of passes required.

3. Accuracy of the solution. The accuracy of any finite difference technique is affected by the nodal spacing. Studies were made to show the number of nodes required to give accurate results. It was found that, since the liquid depth varies rapidly near the pipe discharge ($\zeta = 0$), the nodal spacing should be smaller in that region. Liquid depths within less than 1 percent of those achieved with half the nodal spacing were achieved using 50 nodes, with 40 intervals of equal length, the rightmost divided into 10 equal subintervals. This nodal arrangement was selected for use in the computer program described in Section IV.B. If this nodal arrangement were to prove inadequate for some conditions, a reduced nodal spacing could be used.

B. The computer program

1. Program function. The solution algorithm described in Section IV.A was implemented on the MIT Joint Computer Facility VAX time-sharing system in FORTRAN. Computer program listings are shown in Appendix A. A sample run, showing data entry and output file creation, is shown in Figure IV-3.

The main program, CHOP (Countercurrent Horizontal Pipe), requests the input variables listed in Section III.A.1, plus
 DZETAOUT, the value of ζ at $x^* = L/D$ (e.g., 0.075)
 TDAMP, the value of r in Equation (IV-6)
 DMAX, the maximum value of d_L^* (typically 0.95
 unless reduced to obtain convergence)

```
$ RUN CHOP
ENTER L,D,DZETAOUT,TDAMP,DMAX
2,.0381,.075,.05,.95
ENTER TSAT, TL0, WL, WS, THETA, DHMOD
396.0,336.0,.086,0,0,2.5
  1      0.55089      0.13492
  2      0.67375      0.28745
  3      0.75384      0.37328
  4      0.65471      0.39950
  5      0.65711      0.40263
  6      0.66906      0.40299
  7      0.67079      0.40377
  8      0.66854      0.40411
  9      0.66803      0.40407
 10      0.66839      0.40402
 11      0.66852      0.40402
 12      0.66847      0.40403
 13      0.66844      0.40403
 14      0.66844      0.40403
DO YOU WISH A PLOT?
'YES'
PLOT DMS?
'YES'
PLOT DTL?
'YES'
PLOT DDL?
'YES'
PLOT DUKLER?
'YES'
DO YOU WISH A PRINT?
'YES'
FORTRAN STOP
```

Figure IV-3. Sample computer run for typical conditions of low pressure experiments.

DHMOD, the constant c_1 in Equations (III-66) and (III-67) (e.g., 2.5; see Section V.A.2)

Given the saturated steam temperature, steam properties are calculated using polynomial approximations. The "primary" dimensionless variables (dimensionless liquid temperature, dimensionless liquid depth, and dimensionless steam mass flow rate) are initialized before the first pass to these values at each of the 50 nodes:

$$DTL(I) = 0. \quad (IV-7)$$

$$DDL(I) = 0.5 \quad (IV-8)$$

$$DMS(I) = 0.000001 + XWS/XWL \quad (IV-9)$$

The subroutine "EVAL" is called after this initialization and again whenever any of the primary variables is recomputed. EVAL calculates the liquid properties (ρ_L , μ_L , k_L , c_{pL} , and Pr_L), τ_L^* , τ_S^* , τ_I^* , and Nu at each node.

The solution proceeds as outlined in Section IV.A, with alternating "leftward" and "rightward" sweeps. To provide feedback to the user, an iteration print is made after each complete (leftward plus rightward) pass, as shown in Figure IV-3. This print displays the number of the pass, the inlet dimensionless liquid depth, and the outlet dimensionless liquid temperature. If the iteration print shows that the solution procedure is not converging, the run is stopped and started over, using a different value of the damping factor and/or the maximum liquid depth.

When a converged result is obtained, the Taitel-Dukler stability parameter (N_{TD} in Equation III-62) is calculated for each node. The subroutine "OUTPUT" and its subroutine "PLOTR" are then called. As shown in Figure IV-3, the user may request a plot of DTL, DMS, DDL, and/or the Taitel-Dukler parameter. A printout of the input data, fluid property information, calculated primary variables, and the calculated values of τ_L^* , τ_S^* , τ_I^* , and Nu may also be requested. The printout and plots produced from the computer run of Figure IV-3 are shown in Appendix C.

2. Prediction of water hammer initiation. Localized water slug formation, leading to a steam bubble collapse-induced water hammer, is expected when the Taitel-Dukler parameter exceeds 1.0 at any node. Define the critical value of any one of the input parameters as that which separates the water hammer region from the stable region when the other input parameters are held constant. This critical value is found by running CHOP several times until the value of the varied input parameter produces a maximum Taitel-Dukler parameter just greater than 1.0. Such a procedure was followed to obtain the critical conditions used as input in Figure IV-3.

The critical inlet water flow rate is often of interest since, in an existing piping system, it may be the only parameter which can be controlled to prevent water hammer. However, at the design stage, the piping geometry and the

water inlet temperature also may be adjusted.

3. An "absolute" stability boundary. It was observed in Section II.D that if the inlet water flow rate is increased rapidly, water hammer initiation can occur at lower inlet water flow rates than in the quasi-steady case examined experimentally and analytically here. This is due to the rapid variation of liquid depths and condensation rates with time associated with the filling of the pipe.

Although it does not consider these transient effects, a simple approach can be used to provide a bound on the water hammer region which may be sufficiently conservative. If the inlet water flow is immediately heated to saturation, a known constant steam flow will exist along the pipe. The liquid depths can be calculated in one "leftward" sweep and the location of the maximum Taitel-Dukler parameter will be at the water inlet, where the liquid depth is greatest. Of course, water slug formation at the water inlet is of no significance. However, if a water slug will not form, even with these assumptions, it is plausible that water hammer initiation will not occur, even under transient conditions.

The result of the calculations described in this part is termed the "absolute stability limit." A simpler program than CHOP could be written to calculate this limit, but CHOP may be used by specifying a very large heat transfer coefficient (e.g., DHMOD = $c_1 = 10,000$) which gives $T_L^* = 1.0$ at the second node. A number of calculations are presented

in Chapter V using both $DHMOD = c_1 = 2.5$ (the "metastable-unstable limit") and the "absolute stability limit." The critical water flow rates predicted by the "absolute stability limit" are on the order of one-half those predicted by the "metastable-unstable limit."

CHAPTER V
NUMERICAL RESULTS

A. Comparison with data

1. Air-water liquid depth tests. The computer program CHOP can be used to predict the liquid depth profile in an air-water test. The saturation temperature is set to 0.01 K above the liquid inlet temperature, so that the steam flow is negligible. Using this method, liquid depths at 0.85 m and 1.70 m from the discharge of the 2.0 m test section were calculated for the test conditions of Table II-1.

A plot of measured vs. predicted dimensionless liquid depths is shown in Figure V-1. At 0.85 m from the pipe exit good agreement is seen. At 1.70 m from the pipe exit the measured liquid depths are somewhat higher than predicted, particularly for higher liquid depths. This is believed to be due partly to entrance effects (not considered in the computer model), which can greatly increase wall shear stresses for about 10 or 20 L/D's from the water inlet, and partly to the measurement uncertainties discussed in Section II.F.2. This discrepancy is small enough that it is not expected to greatly affect prediction of the stability of a stratified flow well downstream. These air-water tests therefore provide confirmation of the liquid wall shear stress relation and the computational methods used.

2. Water hammer initiation tests. The computer program CHOP was used to predict the critical inlet water

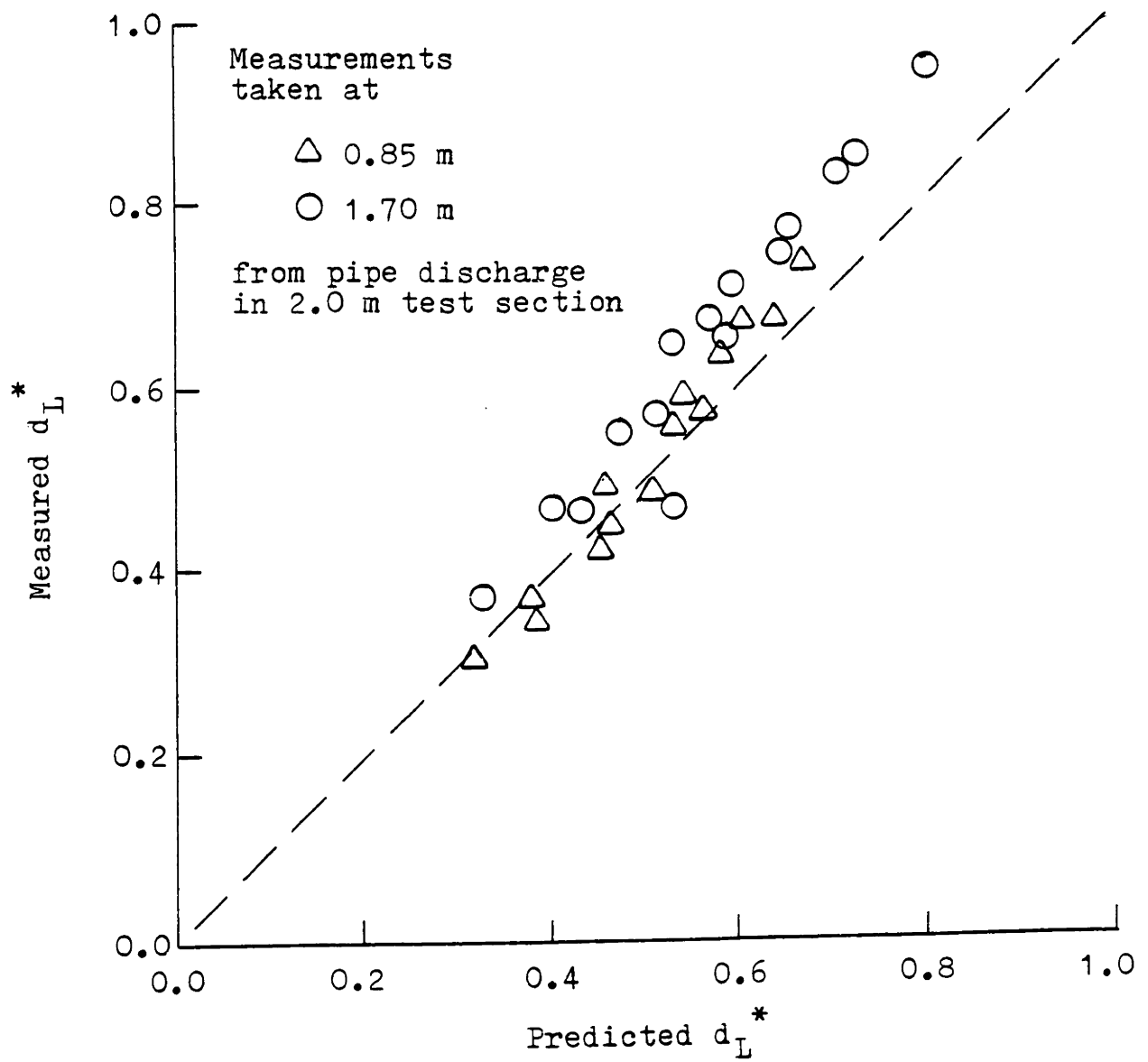


Figure V-1. Comparison of liquid depths predicted by computer model with air-water test data of Table II-1.

flow rates for the initiation of water hammer for the data of Table II-2. Use of $c_1 = 1.0$ in Equations (III-60) and (III-61) greatly overpredicted the critical inlet water flow rates that had been measured. It was decided to find the value of c_1 that gave the best agreement between the predictions of the model and the experimental results. This was found to be $c_1 = 2.5$. The calculations for $c_1 = 2.4$, 2.5, and 2.6 are shown in Appendix B. The criterion used in determining the quality of fit was minimizing the sum of the squares of the percentage deviations, where the percentage deviation is defined as

$$\% \text{ dev.} = 100 \frac{\dot{m}_{\text{LO,crit,meas}} - \dot{m}_{\text{LO,crit,pred}}}{\dot{m}_{\text{LO,crit,pred}}} \quad (\text{V-1})$$

A comparison of measured with predicted critical inlet water flow rates for water hammer initiation is shown in Figure V-2. Good agreement is seen (quantitatively, the rms deviation is 13.6 percent).

3. Liquid exit temperature tests. It has been shown here that modifying the circular pipe equivalent of the Bankoff, et al. (1981) heat transfer coefficient by the factor $c_1 = 2.5$ provides good agreement of the computer model with water hammer initiation data. However, no proof has yet been given that this is physically correct. After all, the criterion for water slug formation, the interfacial shear stress relation, or something else might be in error.

To validate the appropriateness of the heat transfer

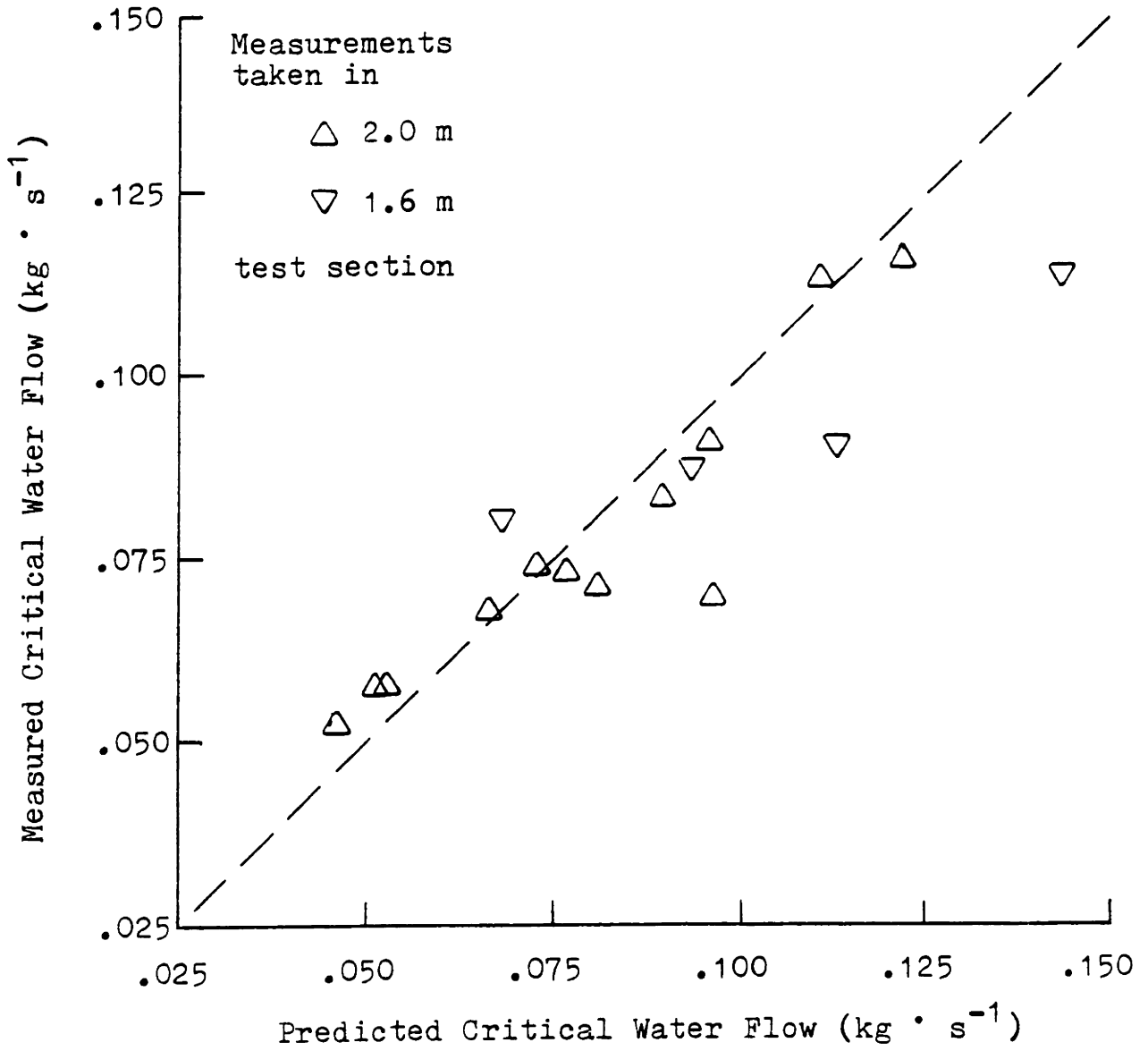


Figure V-2. Comparison of measured with predicted critical inlet water flow rates for water hammer initiation.

coefficient correction, CHOP was run with $c_1 = 2.5$ for the exit liquid temperature test data of Table II-3. The results are shown in Figure V-3 as a comparison of measured with predicted exit liquid temperatures. Good agreement is seen, though the data tend to cross over the correlation line somewhat. This comparison shows that $c_1 = 2.5$ is the proper correction to make, and that the remaining assumptions of the analysis are reasonable approximations. However, the use of Equations (III-60) and (III-61), particularly the latter, with $c_1 = 2.5$ can only be viewed as an estimate of the heat transfer behavior in countercurrent flow of steam and cold water in circular pipes. Detailed and extensive experiments in circular pipes, analogous to the work done by Bankoff, et al. (1982) in rectangular channels would be useful in providing a better correlation. When such a correlation is obtained it should provide useful results when incorporated into the water hammer initiation prediction model described here.

4. Water slug formation location. Two sets of photographs were taken of water slug formation in, respectively, the 2.0 m (Figure II-3) and 1.6 m (Figure II-4) test sections. For the conditions of these photographed tests, CHOP was run to determine the location where water slug formation was first predicted to occur as the inlet water flow was increased. The calculated locations were, respectively, 0.95 m and 0.64 m upstream from the pipe exit in the 2.0 m and 1.6 m test

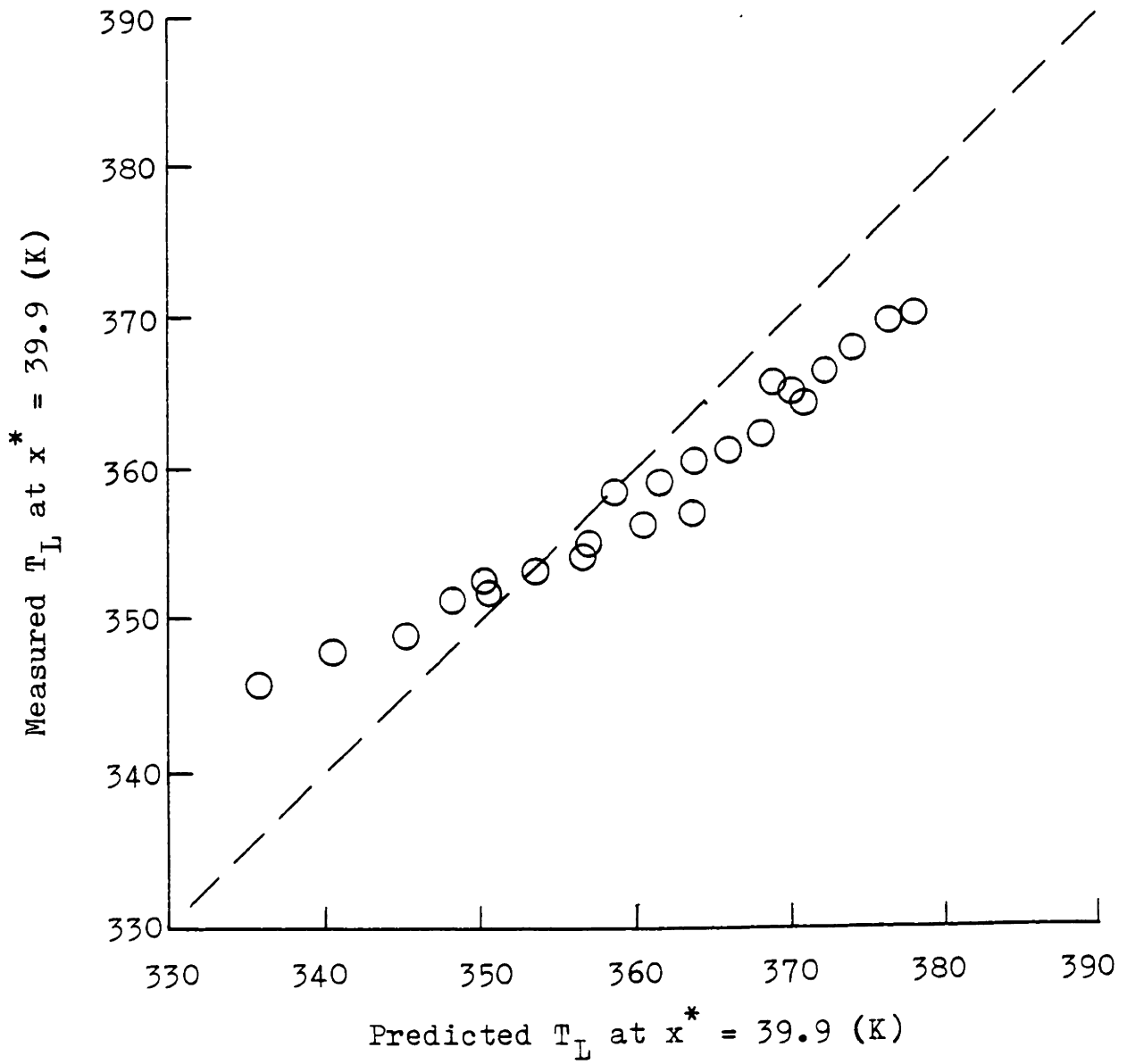


Figure V-3. Comparison of measured with predicted "exit" liquid temperatures, using the CHOP computer program with $c_1 = 2.5$.

sections. These are in reasonable agreement with the photographed locations of roughly 0.7 m and 0.5 m upstream from the pipe exit.

4. Summary. The comparisons of computations of the CHOP computer program with experimental results shown in this section show that the computer model adequately predicts the liquid depth profiles, condensation rates, and critical inlet water flow rates for water hammer initiation in the experimental apparatus of this study. The predicted locations where a water slug first forms are also reasonable.

In the next section (V.B), the CHOP computer program is used to predict the effect of varying different input parameters in turn on the critical inlet water flow rate for water hammer initiation in the low pressure test section used here. Two high pressure nuclear reactor systems which have had water hammer problems are described, and the CHOP program is applied to each.

B. Studies using the computer model

1. Low pressure system. The computer run shown in Figure IV-3 is for a typical set of conditions seen in the experimental apparatus of this study. Plots of the primary dimensionless variables (\dot{m}_S^* , T_L^* , and d_L^*) plus the Taitel-Dukler stability parameter are shown in Appendix C, together with a printout summarizing the results. The conditions of this run are such that the maximum value of N_{TD} is just greater than 1. This case is therefore situated just beyond

the "metastable-unstable limit" and water hammer is expected. As one would expect, \dot{m}_S^* (Figure C-1) and T_L^* (Figure C-2) increase monotonically along the pipe and d_L^* (Figure C-3) decreases monotonically along the pipe and more rapidly as the pipe exit is approached. Figure C-4 shows that the Taitel-Dukler stability parameter goes through a maximum value in the middle of the test section. The location of this maximum is where water slug formation is predicted.

With all the other parameters of Appendix C constant, if $\dot{m}_{SO} = 0.001 \text{ kg} \cdot \text{s}^{-1}$, the critical inlet water flow rate for water hammer initiation is found to be $0.057 \text{ kg} \cdot \text{s}^{-1}$. The printout and plots for this case are shown in Appendix D. The behavior of \dot{m}_S^* , T_L^* , and d_L^* seen in Figures D-1 through D-3 is similar to that of Figures C-1 through C-3 except that the steam flow rate is not zero at $x^* = 0$. However, comparison of Figure D-4 with Figure C-4 shows that the location of water slug formation has moved significantly closer to the water inlet. This is intuitively correct because the vented steam flow tilts the steam flow rate curve, increasing the flow rate near the water inlet (where the liquid depth is greatest) as seen by comparing Figures D-1 and C-1.

Take the computer run shown in Appendix C as a base case. Then, each of the input parameters may be varied individually to provide information on the sensitivity of the critical inlet water flow rate for water hammer initiation to that

parameter. The input parameters varied were pipe length, pipe diameter, pipe inclination, inlet water subcooling, saturation temperature, and vented steam flow. The "meta-stable-unstable limit," "absolute stability limit," and pipe-full limit (in terms of inlet water flow rate) are calculated for each case.

The calculated effect of pipe length on the water hammer region is shown in Figure V-4. Reducing the pipe length is predicted to increase the critical inlet water flow rate. This is intuitively correct because reducing the pipe length reduces the surface area for condensation.

The calculated effect of pipe diameter on the water hammer region is shown in Figure V-5. Increasing the pipe diameter is predicted to increase the critical inlet water flow rate. This is intuitively correct because increasing the pipe diameter reduces the dimensionless liquid depth in the pipe.

The calculated effect of pipe inclination on the water hammer region is shown in Figure V-6. The range of pipe inclinations examined (-0.005 to $+0.005$ radians) is equivalent to roughly \pm one critical depth of the flow over the length of the pipe. For this range of inclinations, increasing the inclination decreases the critical inlet water flow rate. However, the effect is rather small.

The calculated effect of inlet water subcooling on the water hammer region is shown in Figure V-7. Heating of the

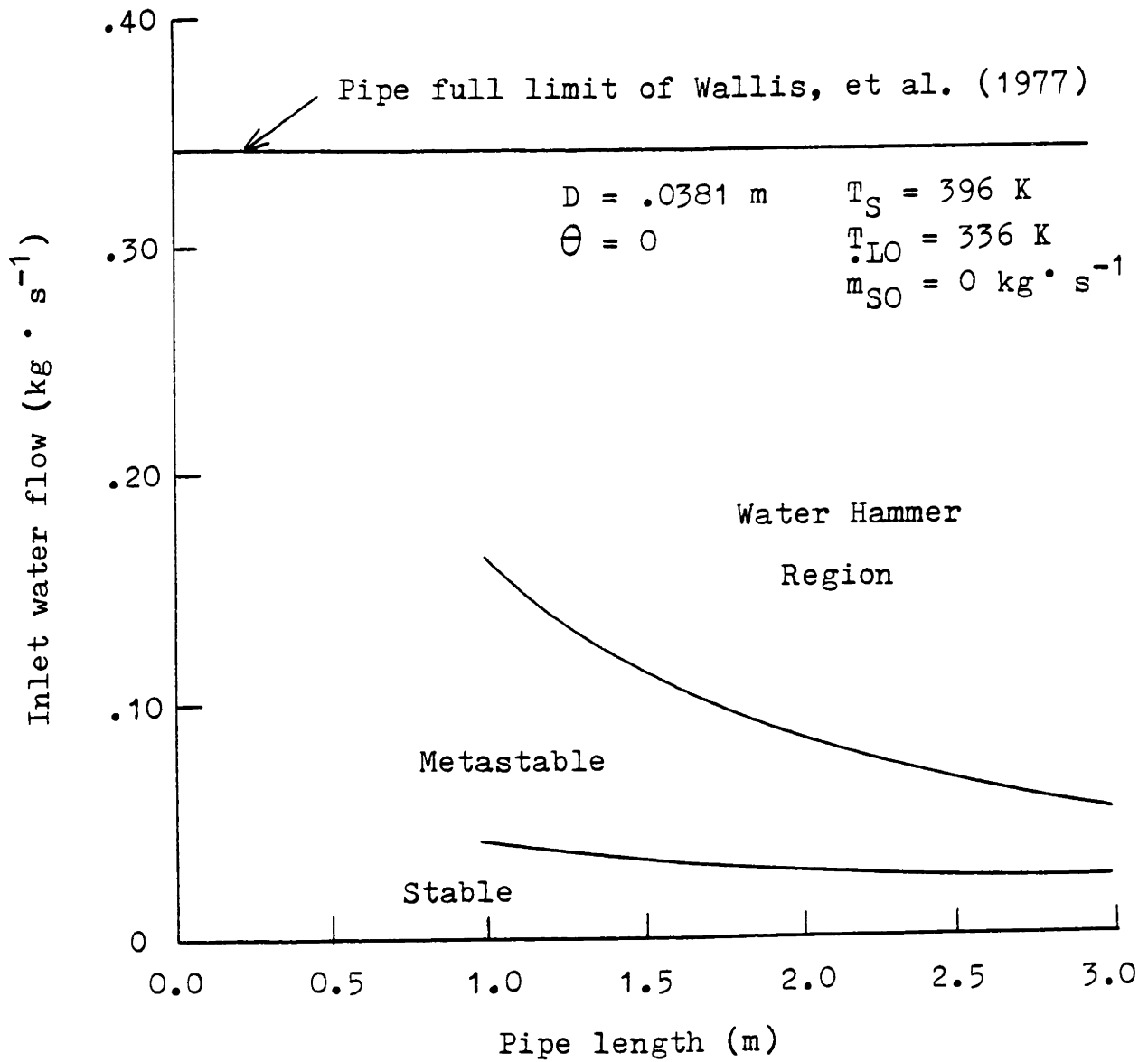


Figure V-4. Calculated effect of pipe length on the water hammer region, low pressure experiments.

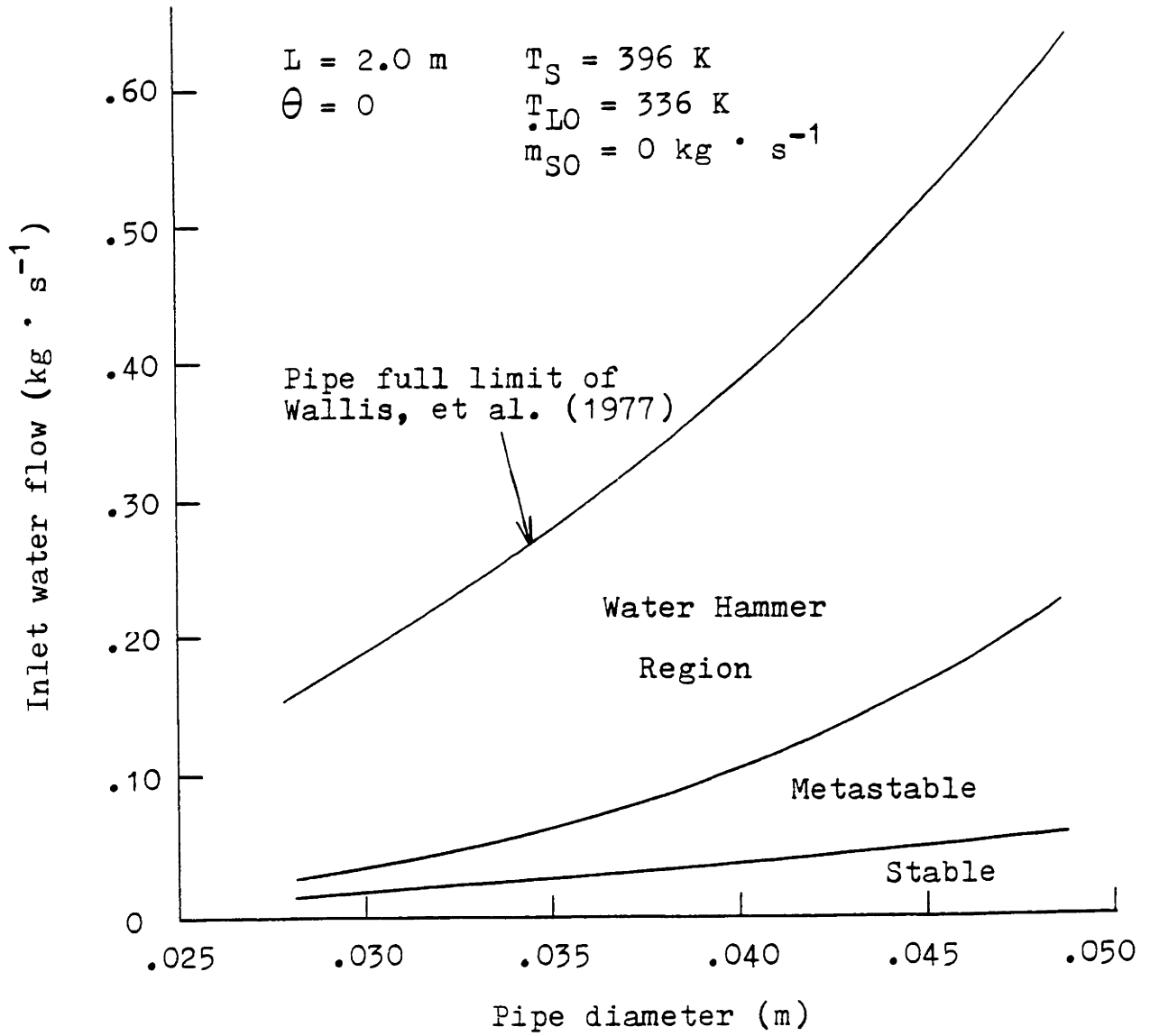


Figure V-5. Calculated effect of pipe diameter on the water hammer region, low pressure experiments.

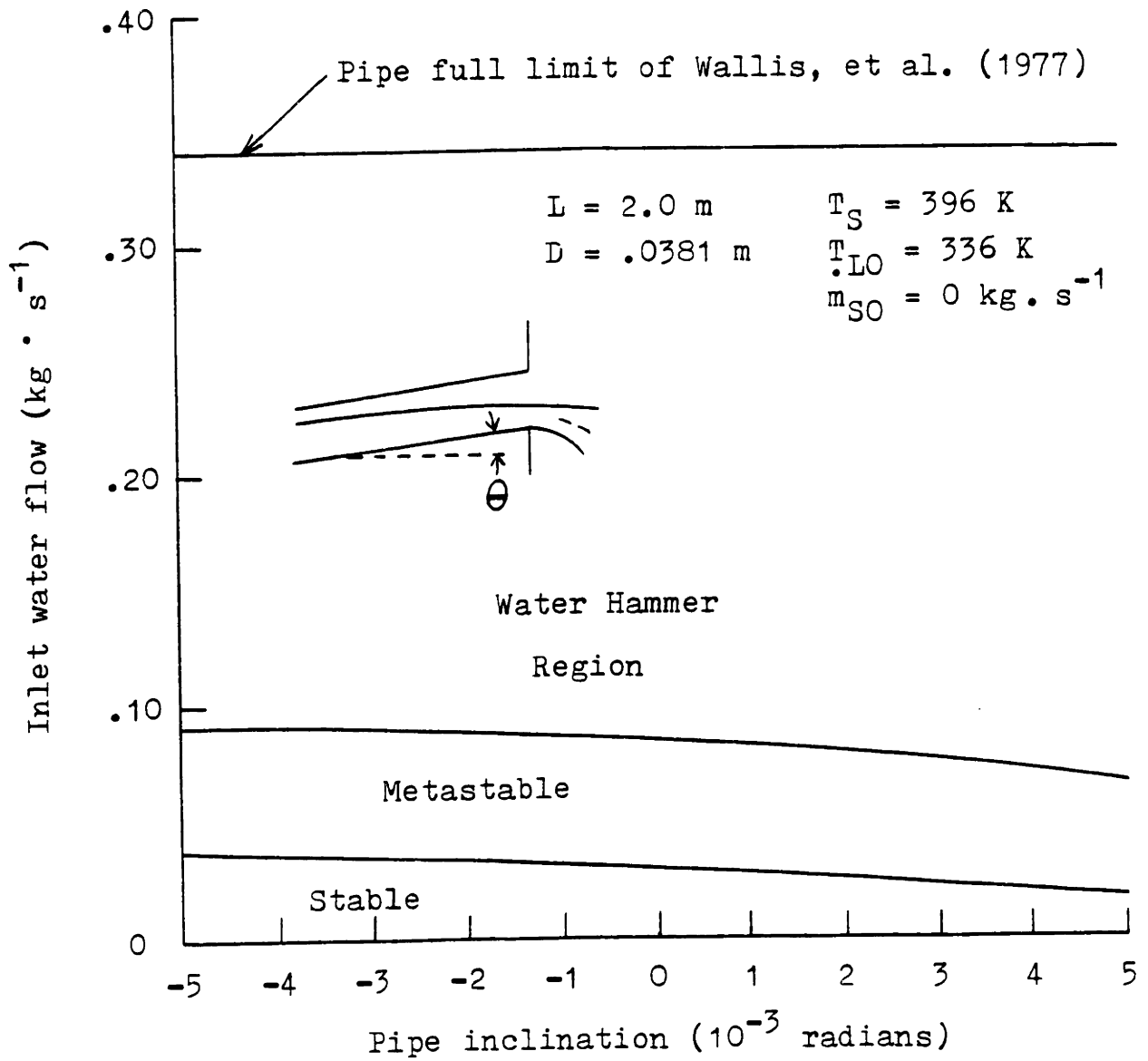


Figure V-6. Calculated effect of pipe inclination on the water hammer region, low pressure experiments.

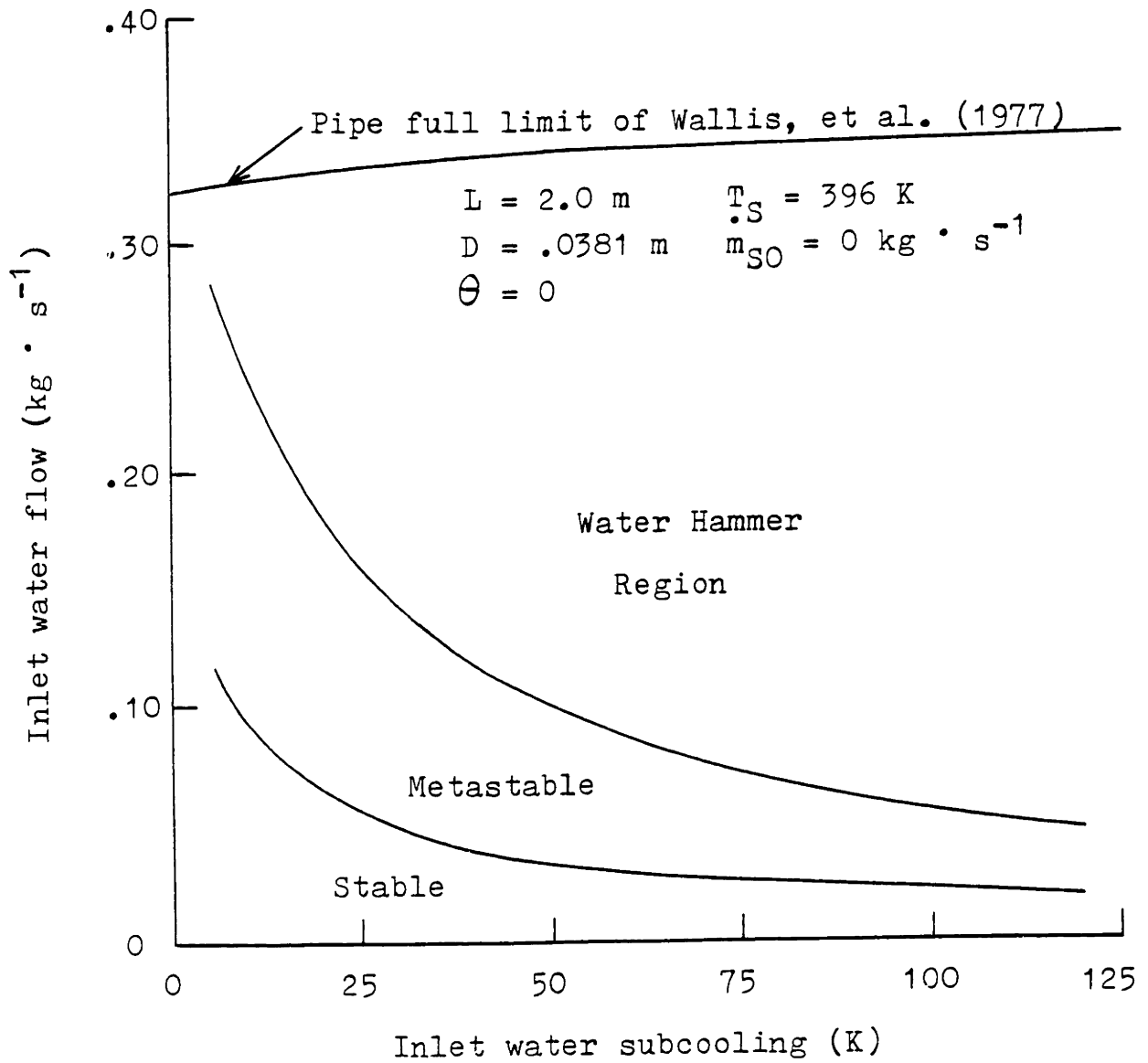


Figure V-7. Calculated effect of inlet water subcooling on the water hammer region, low pressure experiments.

water is predicted to increase the critical inlet water flow rate. This is intuitively correct because heating of the water reduces the temperature difference which drives condensation.

The calculated effect of saturation temperature on the water hammer region is shown in Figure V-8. Increasing the saturation temperature is predicted to increase the critical inlet water flow rate. This is intuitively correct because increasing the saturation temperature increases the steam density and consequently reduces the steam velocity for a given mass flow rate.

The calculated effect of vented steam flow on the water hammer region is shown in Figure V-9. Increasing the vented steam flow is predicted to decrease the critical inlet water flow rate. This is intuitively correct because vented steam increases the steam mass flow rate, thus destabilizing the system.

The sensitivity studies shown here for the low pressure system confirm that the computer model predicts the correct trends. Also, light is shed on which parameters can be effectively modified in order to prevent condensation water hammer.

2. PWR steam generator feed system. Block, et al. (1977) studied the PWR steam generator feed water system consisting of the horizontal feed pipe shown in Figure I-1 and a circumferential feed ring inside the steam generator.

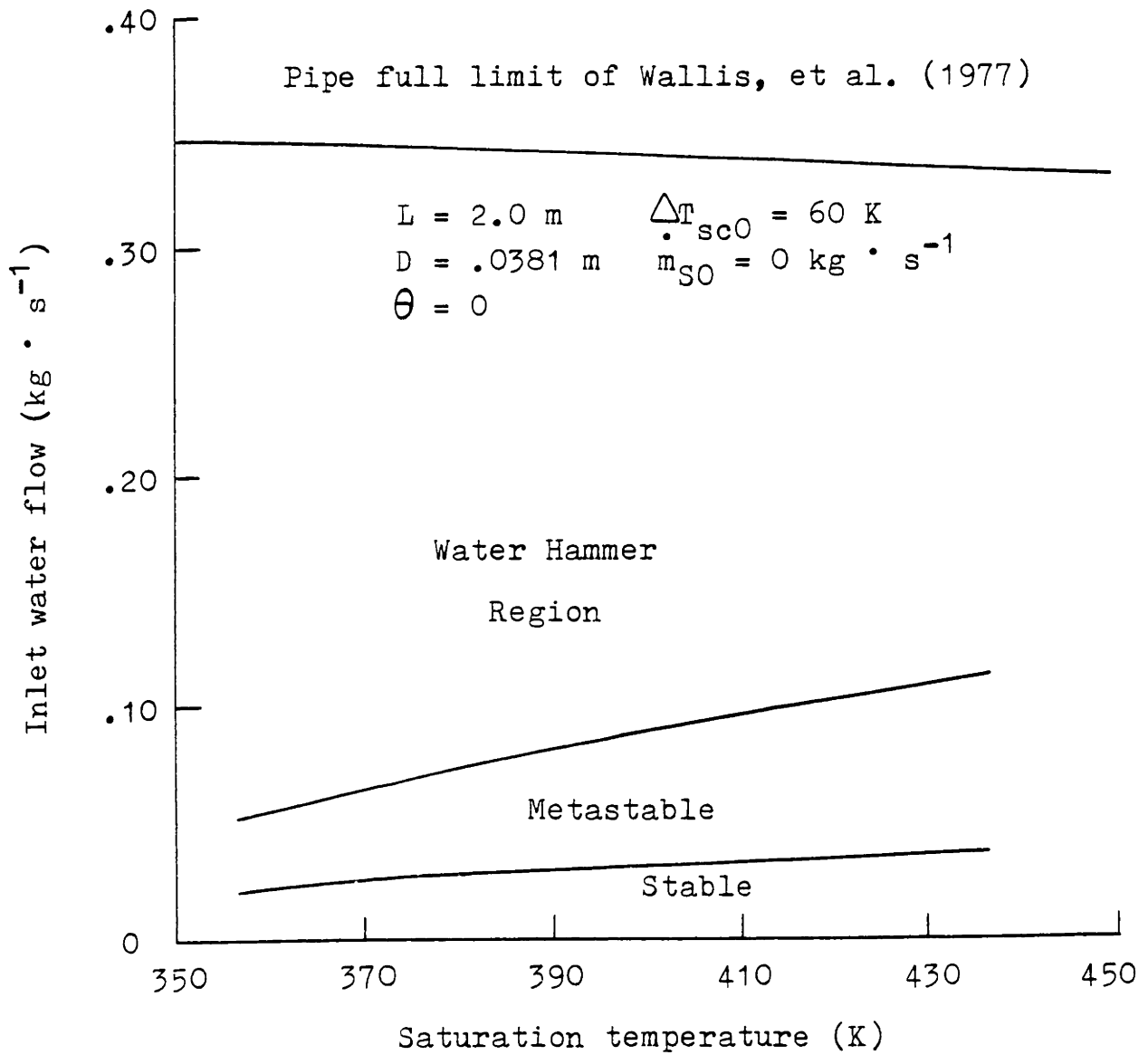


Figure V-8. Calculated effect of saturation temperature on the water hammer region, low pressure experiments.

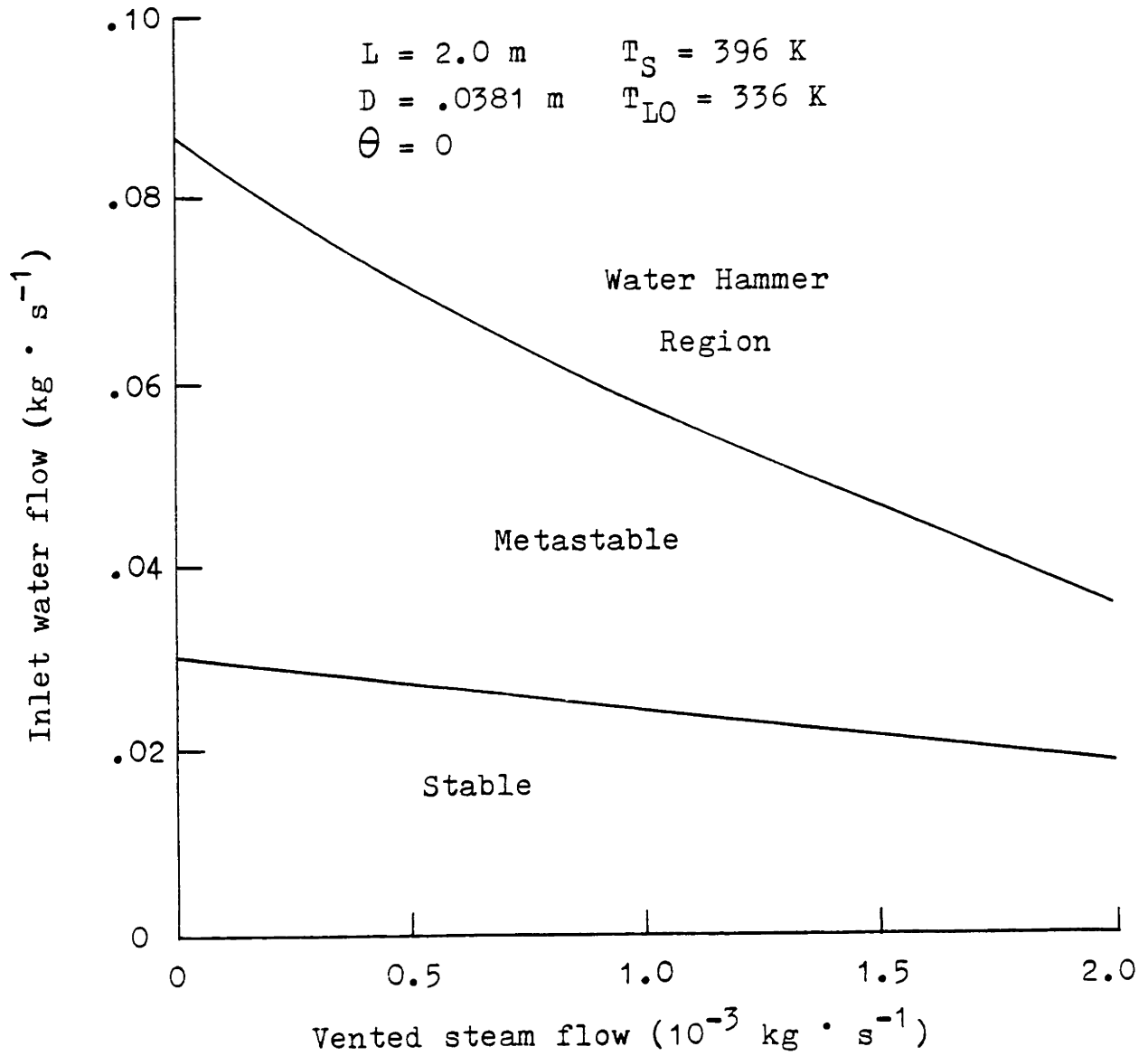


Figure V-9. Calculated effect of vented steam flow on the water hammer region, low pressure experiments.

The feed pipe is 16 inch Schedule 80, with an inside diameter of 0.3636 m.

To apply the present computer model to the PWR steam generator water hammer problem, the feed pipe and feed ring must be replaced by an equivalent length of straight pipe. Appendix E shows a computer printout and plots produced for a 6.0 m pipe length at the critical inlet water flow rate. The most significant difference from the low pressure cases of Appendices C and D is that the liquid reaches saturation temperature part way down the pipe. Near this location, the rough interface expression, Equation (III-61) comes into use. The results are therefore a considerable extrapolation beyond the experimental data base of this study.

Two methods discussed by Block, et al. (1977) for water hammer elimination in the PWR steam generator feed system are reduction in inlet water subcooling and reduction in pipe length. Using the present computer model, sensitivity studies have been done to examine the effects of modifying these parameters on water hammer initiation.

The calculated effect of pipe length on the water hammer region is shown in Figure V-10. As in the low pressure case (Figure V-7), decreasing the pipe length increases the critical inlet water flow rate. A significant difference from the low pressure case is that the "metastable-unstable" and "absolute stability" boundaries are closer together. The pipe-full limit is calculated to be approximately $130 \text{ kg} \cdot \text{s}^{-1}$

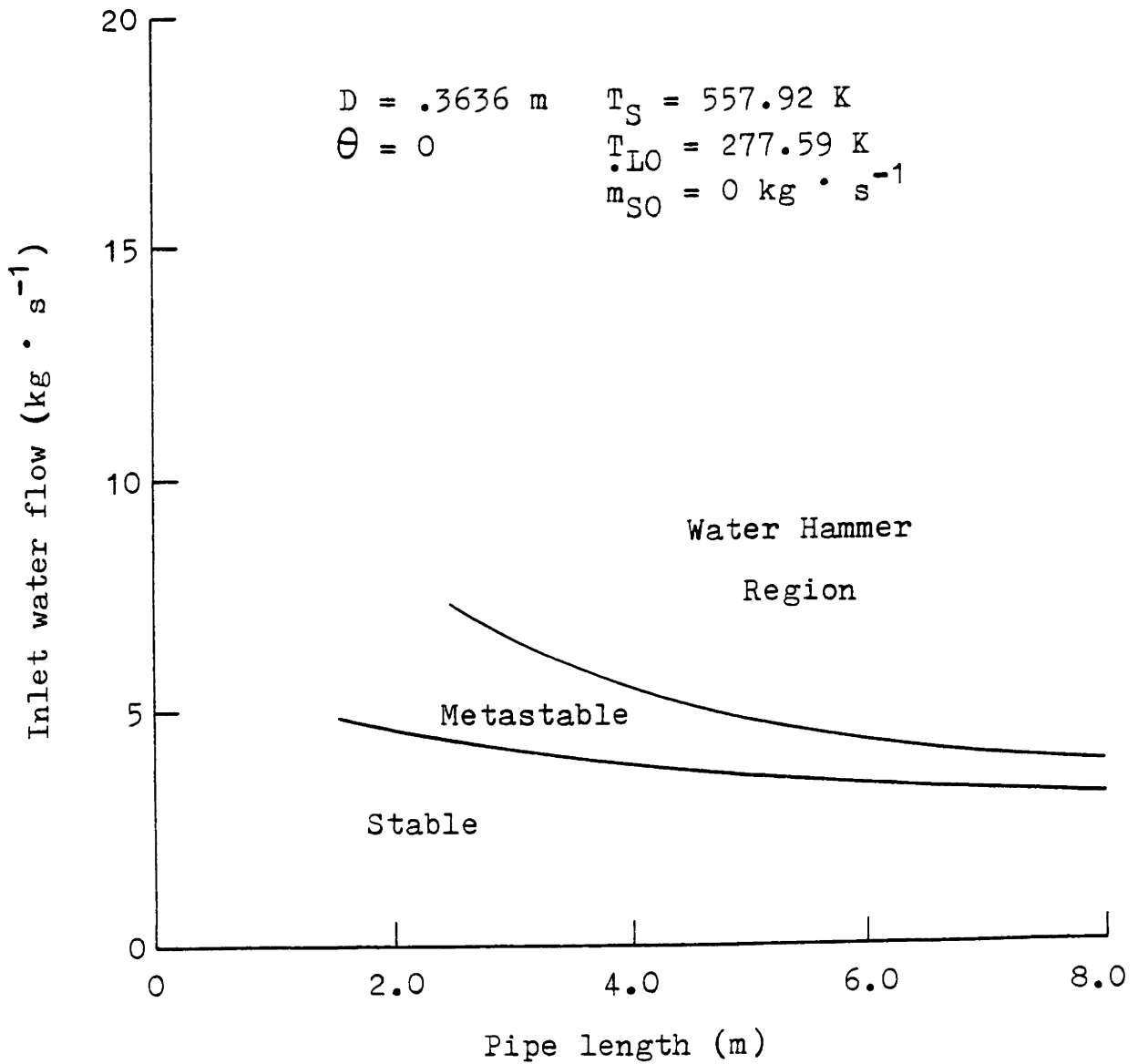


Figure V-10. Calculated effect of pipe length on the water hammer region for the PWR steam generator feed pipe described by Block, et al. (1977).

and hence is not shown on the figure.

The calculated effect of inlet water subcooling on the water hammer region is shown in Figure V-11. Again, the trends are similar to those seen in the low pressure system.

3. Northeast Utilities isolation condenser. The supply line to the isolation condenser of the Millstone #1 nuclear power plant is shown (simplified) in Figure V-12. The reactor vessel contains steam at 561 K and water at 538 K. The water in the isolation condenser is at roughly 300 K. Water hammer events have occurred in this system.

Initially, it was believed that water from the reactor vessel was responsible for the water hammer events. However, application of the present computer model showed that the reactor vessel water temperature was too high to cause a water hammer. The computer model was applied to the 8.23 m horizontal pipe run where water hammer initiation should take place. It was then realized that the only way a water hammer could be initiated was with the cold water from the isolation condenser. Under certain transient operating conditions, it is believed to be possible for the liquid level in the reactor vessel to rise above the isolation condenser supply pipe, thus trapping a steam bubble. If the liquid level in the isolation condenser is high enough, cold water from the isolation condenser can be drawn into the pipe.

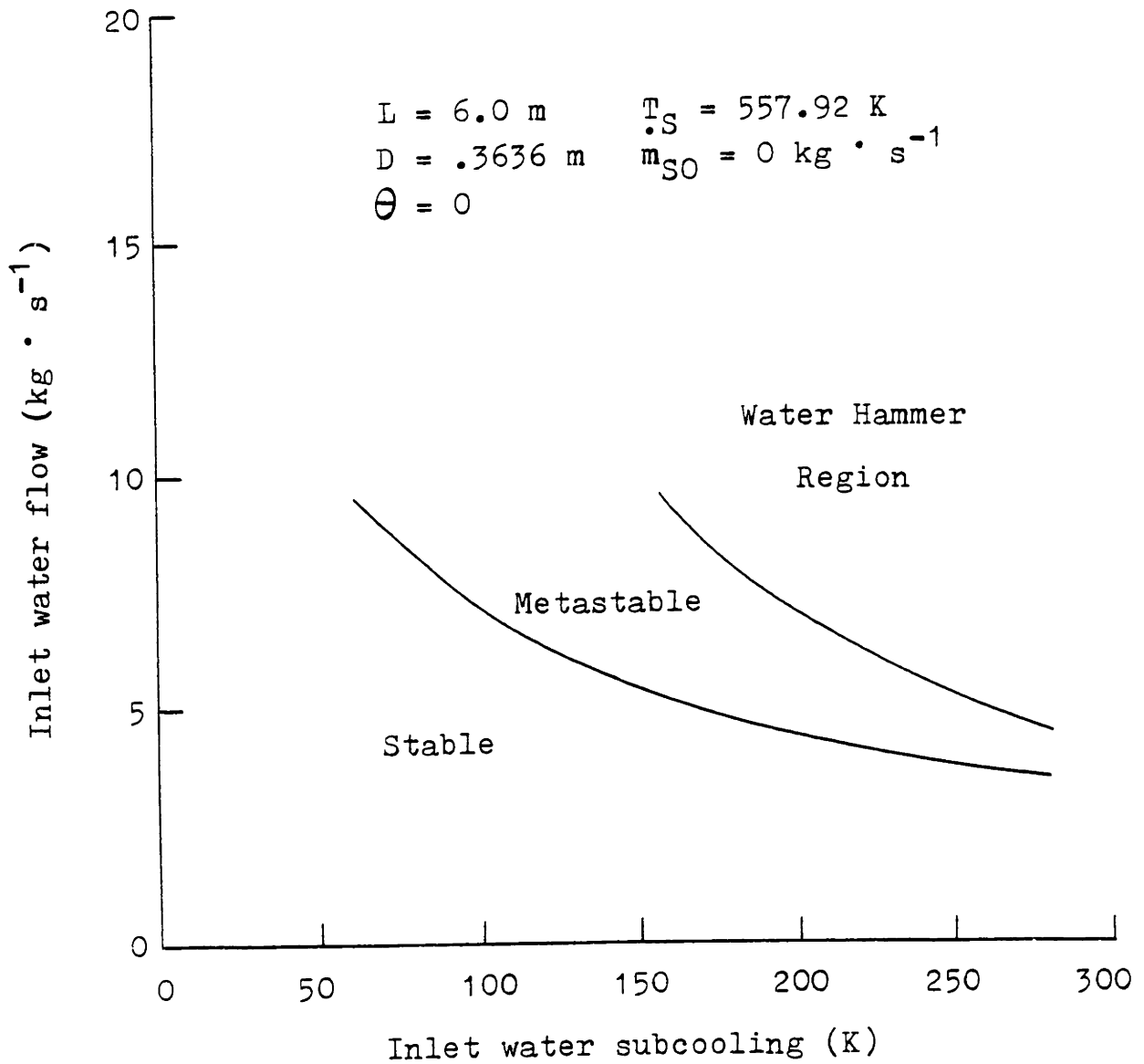


Figure V-11. Calculated effect of inlet water subcooling on the water hammer region for the PWR steam generator feed pipe described by Block, et al. (1977)

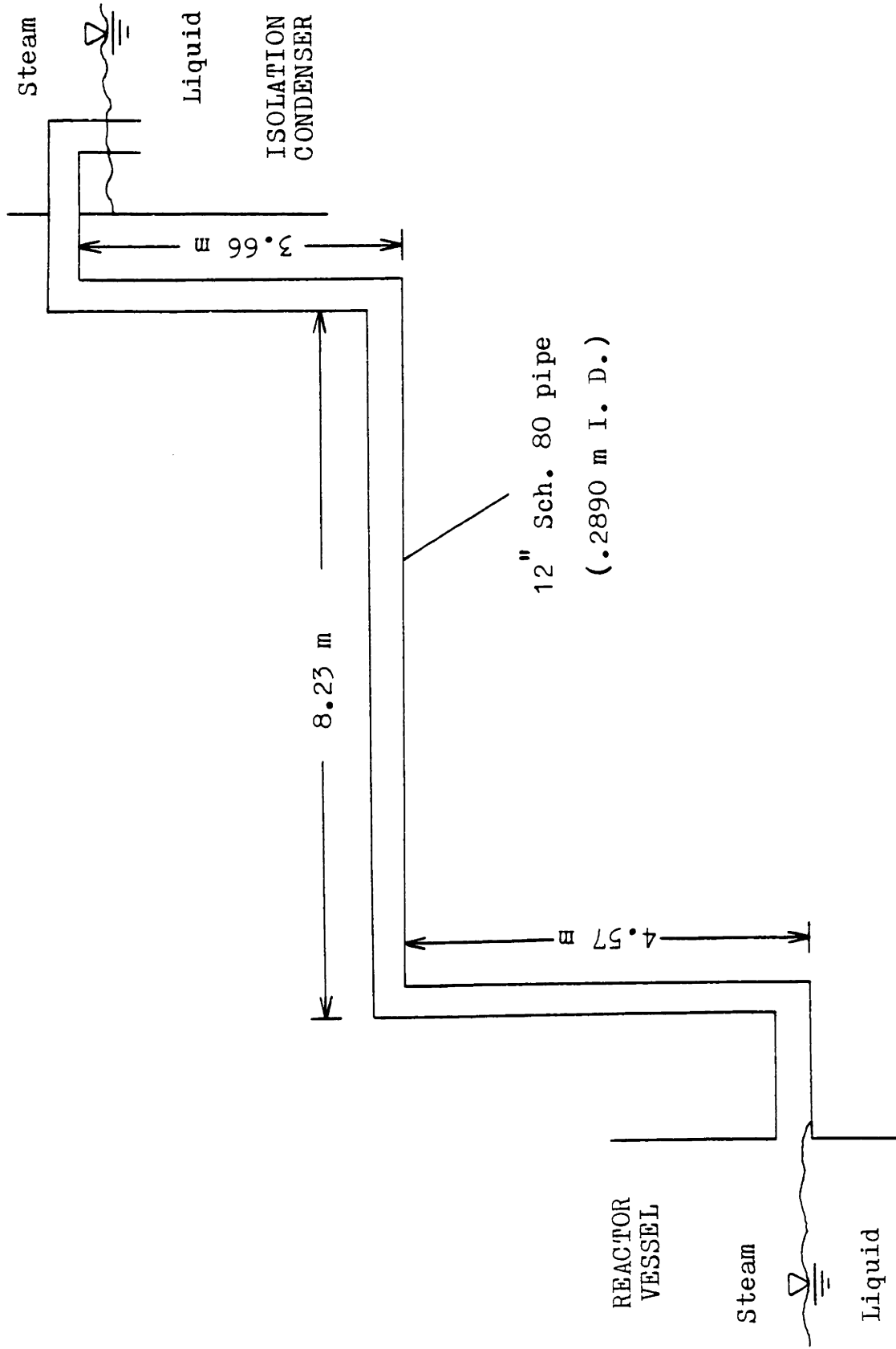


Figure V-12. Simplified diagram of isolation condenser supply line in Millstone #1 nuclear power plant.

The computer model was used to verify that water hammers could be initiated by the presence of water from the isolation condenser in the horizontal pipe run. Assuming the pressure in the pipe is that of the reactor vessel, the critical cold water flow rate for water hammer initiation was calculated to be $2.33 \text{ kg} \cdot \text{s}^{-1}$. A printout and plots of this calculation are shown in Appendix F. The plots are similar to those of the PWR steam generator feed system at its critical inlet water flow rate (Appendix E).

Application of the computer model has shown that cold water from the isolation condenser must be involved for water hammer initiation to occur. Further analysis of the system is needed to discover exactly how this cold water is drawn into the supply piping so that preventive measures may be undertaken.

CHAPTER VI
CONCLUSIONS

An original analytical model has been presented (Chapter III) which predicts the initiation of steam bubble collapse-induced water hammer from an initially stratified flow in a horizontal or nearly-horizontal circular pipe containing steam and subcooled water. Calculations made with this model were shown in Section V.A to compare favorably with measurements of liquid depth, critical inlet water flow rate for water hammer initiation, exit liquid temperature, and the location of water slug formation described in Chapter II. A step-by-step design procedure for applying the model to examine the susceptibility of steam-water systems to condensation water hammer events of the type studied here is shown in Appendix G.

Expressions for the wall and interfacial shear stresses, condensation heat transfer coefficient, and stratified-slug flow regime transition obtained by other researchers have been incorporated into the present model. Beyond multiplying the heat transfer coefficient correlation (which was based on rectangular channel data) by a factor of 2.5, no empiricism was needed. This correction of the heat transfer coefficient was justified by a comparison of predicted and measured exit liquid temperatures. Therefore the model is believed to well approximate the phenomena involved.

The analytical model was applied to two high pressure nuclear reactor systems which had experienced water hammer events. The validity of this extrapolation depends primarily on the validity of the interfacial condensation heat transfer correlation used, which can only be evaluated after further experimental study of condensation rates in countercurrent flow of steam and subcooled water in circular pipes, including large and small pipes over a range of pressures. A correlation based on this data could then be inserted into the model developed here and should improve the reliability of predictions of water hammer initiation in large scale and/or high pressure systems.

Other areas which warrant further investigation include the effects of rapid variations in inlet water flow rate and the presence of noncondensable gas on water hammer initiation. The effect of pipe filling rate can be studied experimentally, using an apparatus similar to that used here. Two results would be of particular interest: (1) the pipe filling rate below which a quasi-steady analysis would apply, and (2) whether the "absolute stability limit" described in Chapter IV is indeed conservative for the case of a rapidly-filling pipe. The presence of noncondensable gas reduces the condensation rate, thus inhibiting water slug formation. In some cases, this may be a practical way to prevent water hammer initiation. However, further experimental work needs to be done to find the amount of noncondensable gas needed.

REFERENCES

- Bakhmeteff, B. A. (1932), Hydraulics of Open Channels, McGraw-Hill, New York.
- Bankoff, S. G. (1980), "Some condensation studies pertinent to LWR safety," Int. J. Multiphase Flow, 6, pp. 51-67.
- Bankoff, S. G., Tankin, R. S., and M. C. Yuen (1981), "Steam-water condensation studies," U. S. NRC Report NUREG/CR-1898, GPO, Washington.
- Bankoff, S. G., Kim, H. J., Tankin, R. S., and M. C. Yuen (1982), "Countercurrent steam-water flow in a flat plate geometry," U. S. NRC Report NUREG/CR-2783, GPO, Washington.
- Bélanger, J. M. (1828), "Essai sur la solution numérique de quelques problèmes, relative au mouvement permanent des eaux courantes," Paris.
- Block, J. A., Crowley, C. J., Rothe, P. H., Wallis, G. B., and L. R. Young (1977), "An evaluation of PWR steam generator water hammer," U. S. NRC Report NUREG-0291, GPO, Washington.
- Block, J. A. (1980), "Condensation-driven fluid motions," Int. J. Multiphase Flow, 6, pp. 113-129.
- Boussinesq, J. (1877), "Essai sur la théorie des eaux courantes," Paris.
- Brumfield, L. K., Houze, R. N., and T. G. Theofanous (1975), "Turbulent mass transfer at free, gas-liquid interfaces, with applications to film flows," Int. J. Heat Mass Transfer, 18, pp. 1077-1081; also Theofanous, Houze, and Brumfield (1976), "Turbulent mass transfer at free, gas-liquid interfaces, with applications to open-channel, bubble and jet flows," Int. J. Heat Mass Transfer, 19, pp. 613-624.
- Cahill, W. J. (1974), "Feedwater line incident report - Indian Point Unit No. 2," Consolidated Edison Co., AEC Docket No. 50-247.
- Chaddock, J. B. (1955), "Film condensation of vapor in horizontal tubes," Sc. D. thesis, MIT Dept. of Mechanical Engineering.

- Chato, J. C. (1960), "Laminar condensation in horizontal and inclined tubes," Ph. D. thesis, MIT Dept. of Mechanical Engineering.
- Chow, V. T. (1959), Open Channel Hydraulics, McGraw-Hill, New York.
- Dittus, F. W., and L. M. K. Boelter (1930), Univ. Calif. Publs. Eng., 2, p. 443.
- Gruel, R. L., Huber, P. W., and W. M. Hurwitz (1981), "Piping response to steam-generated water hammer," ASME J. Pressure Vessel Technology, 103, p. 219.
- Henderson, F. M. (1966), Open Channel Flow, MacMillan, New York.
- Jensen, R. J., and M. C. Yuen (1982), "Interphase transport in horizontal stratified cocurrent flow," U. S. NRC Report NUREG/CR-2334.
- Jones, D. L. (1981), "Horizontal water/steam flow instability," S. B. thesis, MIT Dept. of Mechanical Engineering.
- Kordyban, E. S., and T. Ranov (1970), "Mechanism of slug formation in horizontal two-phase flow," ASME J. Basic Engineering, 92, p. 857.
- Kordyban, E. S. (1977), "Some characteristics of high waves in closed channels approaching Kelvin-Helmholtz instability," ASME J. Fluids Engineering, 99, pp. 339-346.
- Lee, L. Bankoff, S. G., Yuen, M. C., Jensen, R., and R. S. Tankin (1979), "Local condensation rates in horizontal cocurrent steam-water flow," in Nonequilibrium Interfacial Transport Processes, ASME, New York, pp. 79-83.
- Lim, I. S., Bankoff, S. G., Tankin, R. S., and M. C. Yuen (1981), "Cocurrent steam/water flow in a horizontal channel," U. S. NRC Report NUREG/CR-2289.
- Linehan, J. H., Petrick, M., and M. M. El-Wakil (1970), "The condensation of a saturated vapor on a subcooled film during stratified flow," Chem. Engr. Progr. Symp. Series, No. 102, Vol. 66, pp. 11-20.
- Hishima, K., and M. Ishii (1980), "Theoretical prediction of onset of horizontal slug flow," ASME J. Fluids Engineering, 102, pp. 441-445.

- Nusselt, W. (1916), "Die oberflächenkondensation des Wasserdampfes," Zeitschr. Ver. deutsch. Ing., 60, p. 541 and p. 569.
- Rohsenow, W. M., and H. Y. Choi, Heat, Mass, and Momentum Transfer, Prentice-Hall, Englewood Cliffs, NJ.
- Roidt, R. M. (1975), "Steam-water slugging in steam generator feedwater lines," Westinghouse Research Memo No. 74-7E9-FLINE-M1, Pittsburgh.
- Rufer, C. E., and S. P. Kezios (1966), "Analysis of two-phase, one-component stratified flow with condensation," ASME J. Heat Transfer, 88, pp. 265-275.
- Saha, P., Ginsberg, T., Wu, B. J. C., and O. J. Jones, Jr. (1980), "An evaluation of condensation-induced water hammer in preheat steam generators," U. S. NRC Report NUREG/CR-1606.
- Segev, A., and R. P. Collier (1980), "Turbulent steam condensation in a horizontal channel," in Cavitation and Polyphase Flow Forum - 1980, ASME, New York, pp. 45-46.
- Segev, A., Flanigan, L. J., Kurth, R. E., and R. P. Collier (1981), "Experimental study of countercurrent steam condensation," ASME J. Heat Transfer, 103, pp. 307-311.
- Taitel, Y., and A. E. Dukler (1976), "A model for predicting flow regime transitions in horizontal and near horizontal gas-liquid flow," AIChE Journal, 22, pp. 47-55.
- Thomas, R. M. (1979), "Condensation of steam on water in turbulent motion," Int. J. Multiphase Flow, 5, pp. 1-15.
- Wallis, G. B., and J. E. Dobson (1973), "The onset of slugging in horizontal stratified air-water flow," Int. J. Multiphase Flow, 1, pp. 173-193.
- Wallis, G. B., Crowley, C. J., and Y. Hagi (1977), "Conditions for a pipe to run full when discharging liquid into a space filled with gas," ASME J. Fluids Engineering, 99, pp. 405-413.

Appendix A

Computer Program Listings

- I. Main program "CHOP" (Countercurrent
Horizontal Pipe)
- II. Properties functions
- III. Subroutine "EVAL"
- IV. Subroutines "OUTPUT" and "PLOTR"

Main program "CHOP"

```

COMMON DTL(50),DDL(50),DSL(50),XWS,
2  DSS(50),DSI(50),DAL(50),DTAUI(50),DTAUS(50),
3  DNU(50),DTAUL(50),DFR2(50),DX(50),DZETA(50),THETA,
4  XDENL(50),XDENS,XKL(50),XD,XTSAT,XTLO,XWL,XHFG,
5  XVISL(50),XVISS,XPRL(50),PI,XL,XPSAT,NPASS,XCPL(50),
6  OLDDDL(50),OLDDTL(50),DMS(50),DUK(50),DHMOD
C      INPUT DATA
      WRITE(6,1)
1      FORMAT(' ENTER L,D,DZETAOUT,TDAMP,DMAX')
      READ(5,*)XL,XD,DZETAOUT,TDAMP,DMAX
      WRITE(6,2)
2      FORMAT(' ENTER TSAT, TLO, WL, WS, THETA, DHMOD')
      READ(5,*) XTSAT,XTLO,XWL,XWS,THETA,DHMOD
      XPSAT=PSAT(XTSAT)
C      CALCULATE STEAM PROPERTIES AT SATURATION
101     XDENS=DENS(XTSAT)
        XVISS=VISS(XTSAT)
        XHFG=HFG(XTSAT)
C      DEFINE PI
        PI=3.141592654
C      INITIALIZE VARIABLES
        DO 300 I = 1,50
          DTL(I)=0.
          DDL(I)=0.5
          DMS(I)=.000001+XWS/XWL
          OLDDDL(I)=0.5
          OLDDTL(I)=0.
          CALL EVAL(I)
300     CONTINUE
        DO 380 I=1,40
          DX(I)=(I-1.)*(XL/XD)/40.
380     CONTINUE
        DO 381 I=41,50
          DX(I)=(I-40.)*(XL/XD)/400.+DX(40)
381     CONTINUE
          NPASS=0
304     CONTINUE
          IF(NPASS.GE.100)GOTO 305
          NPASS=NPASS+1
C      CALCULATE LIQUID TEMPERATURES AND
C      STEAM AND LIQUID FLOW RATES
        DO 303 I=1,49
          XDHL=PI*XD*DAL(I)/(DSL(I)+DSI(I))
          TL=XTLO+DTL(I)*(XTSAT-XTLO)
          DDTL=XKL(I)*DNU(I)*DSI(I)*(XD*XD/XDHL)*(1.-
2         DTL(I))/((1.+DMS(I)-XWS/XWL)*XWL*XCPL(I))*(1.+
3         CPL((XTSAT+TL)/2.)*(XTSAT-TL)/XHFG)
          DTL(I+1)=(DTL(I)+DDTL*(DX(I+1)-DX(I)))*
2         (1.-TDAMP)+DTL(I+1)*TDAMP
          IF(DTL(I+1).GT.1.)DTL(I+1)=1.
          T1=XTLO+(XTSAT-XTLO)*DTL(I+1)

```

```

DMS(I+1)=CPL((T1+XTLO)/2.)*(T1-XTLO)/
2 (XHFG+CPL((XTSAT+T1)/2.)*(XTSAT-T1))+XWS/XWL
CALL EVAL(I+1)
303 CONTINUE
C CALCULATE EXIT LIQUID DEPTH
340 DDL(50)=DDL(50)*(1.+04*(DZETAOUT-DZETA(50)))
IF(DDL(50).GT..98)DDL(50)=.98
IF(DDL(50).LT..02)DDL(50)=.02
CALL EVAL(50)
IF(ABS(DZETA(50)-DZETAOUT).LT..0005)GOTO 341
GOTO 340
341 CONTINUE
C CALCULATE LIQUID DEPTHS
DO 310 J=1,49
M=51-J
XDHL=PI*XD*DAL(M)/(DSL(M)+DSI(M))
DPSI=XDENL(M)/XDENS*DMS(M)/(1.+DMS(M)-XWS/XWL)*
2 (DAL(M)/(1.-DAL(M)))**2
DDDL=(-(DTAUL(M)+DTAUI(M)+DTAUS(M))-THETA+PI/2.*DAL(M))*
2 DFR2(M)/(1.+DMS(M)-XWS/XWL)*(XD*XD/XDHL)*DNU(M)*XKL(M)*
3 (XTSAT-XTLO)*(1.-DTL(M))/(XWL*XHFG)*(DPSI-1.)/DZETA(M)
DDL(M-1)=DDL(M)-DDDL*(DX(M)-DX(M-1))
IF(DDL(M-1).GT.DMAX)DDL(M-1)=DMAX
IF(DDL(M-1).LT..02)DDL(M-1)=.02
IF(DDL(M-1).LT.DDL(50))DDL(M-1)=DDL(50)
CALL EVAL(M-1)
310 CONTINUE
C ITERATION PRINT
WRITE(6,979)NPASS,DDL(1),DTL(50)
979 FORMAT(15,2F12.5)
C TEST FOR CONVERGENCE
LCON=1
TOLD=.0001
TOLT=.0001
DO 330 I=1,50
IF(ABS(DDL(I)-OLDDDL(I)).GT.TOLD)LCON=0
333 IF(DTL(I).EQ.0.) GOTO 334
IF(ABS((DTL(I)-OLDDTL(I))/DTL(I)).GT.TOLT)LCON=0
334 CONTINUE
OLDDDL(I)=DDL(I)
OLDDTL(I)=DTL(I)
330 CONTINUE
IF(LCON.EQ.1)GOTO 305
GOTO 304
C CALCULATE TAITEL-DUKLER PARAMETER
305 DO 370 I=1,50
DUK(I)=DFR2(I)*XDENL(I)/XDENS*(DAL(I)/(1.-DAL(I)))**3*
2 (DMS(I)/(1.+DMS(I)-XWS/XWL))**2/(1.-DDL(I))**2
370 CONTINUE
C PRODUCE PLOTS AND/OR PRINT OF RESULTS
CALL OUTPUT
STOP
END

```

Properties functions

```

function cond1(ts)
  c   Range of Ts is from 273.15 to 623.15 K
      TSY=TS/273.15
      CONDL=(-922.47+2839.5*TSY-1800.7*TSY*TSY+
2     525.77*TSY**3-73.440*TSY**4)/1000.
      return
      end
function cpl(ts)
  C   RANGE OF TS IS FROM 273.15 TO 573.15 K
      CPL=6.7354361E3-1.9475519E1*TS+4.6626211E-2*
2     TS*TS-3.3535899E-5*TS**3
      IF(TS.LE.423.15)RETURN
      CPL=-4.1157172E4+2.9671824E2*TS-
2     6.5200181E-1*TS*TS+4.8357996E-4*TS**3
      return
      end
function den1(ts)
  C   RANGE OF TS IS FROM 273.15 TO 573.15 K
      DENL=9.2357693E2+7.1815435E-1*TS-
2     1.2766493E-3*TS*TS-1.0638178E-6*TS**3
      return
      end
function dens(ts)
  c   Range of Ts is from 373.15 to 623.15 K
      ps=psat(ts)
      phi=ps/ts
      DENS=-3.7369734E-3+2.1956381E-3*PHI
2     +6.6080342E-8*PHI*PHI-1.7785537E-12*PHI**3
      IF(TS.LE.473.15)RETURN
      DENS=-1.8777741E0+2.9588227E-3*PHI
2     -3.1936217E-8*PHI*PHI+3.1629508E-12*PHI**3
      RETURN
      END
FUNCTION HFG(TS)
  C   RANGE OF TS IS FROM 373.15 TO 623.15 K
      TI=1./TS
      HFG=-9.7431967E6+1.2840218E10*TI
2     -4.7267100E12*TI*TI+5.9945373E14*TI**3
      IF(TS.LE.523.15)RETURN
      HFG=-8.0807554E7+1.2571814E11*TI
2     -6.4543889E13*TI*TI+1.1174109E16*TI**3
      return
      end
function prl(ts)
      PRL=VISL(TS)*CPL(TS)/CONDL(TS)
      RETURN
      END
FUNCTION PSAT(T)
      TTC=T/647.3
      PHI=1.-TTC
      PSI=((20.9750676*PHI+4.16711732)*PHI+1.)*TTC

```

```

PPC=EXP((((64.23285504-(PHI*118.9646225))
2 *PHI-168.1706546)*PHI-26.08023696)*PHI-7.691234564)
3 *PHI/PSI-PHI/(1.E9*PHI*PHI+6.))
PSAT=2.21199996E7*PPC
RETURN
END
FUNCTION TSAT(XP)
C      TAKES PRESSURE IN PA, RETURNS TSAT IN K.
C      CONVERT P INTO PSIA
P=XP/6894.7572
PLN=LOG(P)
TOLD=.0362144*PLN**4+.0502405*PLN**3+2.31548*PLN*PLN
2 +33.8215*PLN+101.575
DTDPLN=.1448576*PLN**3+.1507215*PLN*PLN
2 +4.63096*PLN+33.8215
1 TK=(5./9.)*(TOLD+459.67)
PP=PSAT(TK)
PNEW=PP/6894.7572
CALPLN=LOG(PNEW)
TNEW=TOLD-DTDPLN*(CALPLN-PLN)
CONV=ABS(TNEW/TOLD-1.)
IF(CONV.LT..0001)GOTO 2
TOLD=TNEW
GOTO 1
C      Convert t into K
2 tsat=(5./9.)*(tnew+459.67)
return
end
function visl(ts)
C      RANGE OF TS IS FROM 273.15 TO 573.15 K
VISL=241.4E-7*10**(247.8/(TS-140))
RETURN
END
function viss(ts)
C      RANGE OF TS IS FROM 373.15 TO 623.15 K
tss=sqrt(ts)
VISS=-7.9250439E-5+1.0743852E-5*TSS
2 -4.5646298E-7*TSS*TSS+7.5055862E-9*TSS**3
IF(TS.LE.523.15)RETURN
VISS=4.1111312E-6+2.1373386E-5*TSS
2 -1.8279052E-6*TSS*TSS+4.0194973E-8*TSS**3
RETURN
END

```

Subroutine "EVAL"

```

SUBROUTINE EVAL(I)
COMMON DTL(50),DDL(50),DSL(50),XWS,
2 DSS(50),DSI(50),DAL(50),DTAUI(50),DTAUS(50),
3 DNU(50),DTAUL(50),DFR2(50),DX(50),DZETA(50),THETA,
4 XDENL(50),XDENS,XKL(50),XD,XTSAT,XTLO,XWL,XHFG,
5 XVISL(50),XVISS,XPRL(50),PI,XL,XPSAT,NPASS,XCPL(50),
6 OLDDDL(50),OLDDTL(50),DMS(50),DUK(50),DHMOD
TL=DTL(I)*(XTSAT-XTLO)+XTLO
XDENL(I)=DENL(TL)
XVISL(I)=VISL(TL)
XCPL(I)=CPL(TL)
XKL(I)=CONDL(TL)
XPRL(I)=PRL(TL)
BETA=ACOS(1.-2.*DDL(I))
DSL(I)=BETA
DSS(I)=PI-BETA
DSI(I)=SIN(BETA)
DAL(I)=(2.*BETA-SIN(2.*BETA))/(2.*PI)
DFR2(I)=(XWL*(1.+DMS(I))-XWS)**2*64.*DSI(I)/
2 (9.80665*XDENL(I)**2*DAL(I)**3*PI**3*XD**5)
DPHI=XDENL(I)/XDENS*(DMS(I)/(1.+DMS(I)-XWS/XWL))**2*
3 (DAL(I)/(1.-DAL(I)))**3
DZETA(I)=1.-DFR2(I)*(1.+DPHI)
IF(DZETA(I).LT.DZETA(50))DZETA(I)=DZETA(50)
XDHL=PI*XD*DAL(I)/(DSL(I)+DSI(I))
REL=(4./PI)*(1.+DMS(I)-XWS/XWL)*XWL*XDHL/(XVISL(I)*
2 DAL(I)*XD*XD)
DTAUL(I)=.08164*(XWL*(1.+DMS(I))-XWS)**2*DSL(I)/
2 (9.80665*XDENL(I)**2*DAL(I)**3*XD**5)/REL**.25
XDHS=PI*XD*(1.-DAL(I))/(DSS(I)+DSI(I))
RES=(4./PI)*DMS(I)*XWL*XDHS/(XVISS*(1.-DAL(I))*
2 XD*XD)
DTAUS(I)=.08164*(XWL*DMS(I))**2*DSS(I)/
2 (9.80665*XDENL(I)*XDENS*(1.-DAL(I))**3*XD**5)/
3 RES**.25
DNU(I)=.236*RES**.027*REL**.49*XPRL(I)**.42
Y=1.17E-10*RES**2.1*REL**.56*XPRL(I)**1.16
IF(Y.GT.DNU(I))DNU(I)=Y
DNU(I)=DNU(I)*DHMOD
IF(DNU(I).LT.1.E-10)DNU(I)=1.E-10
DTAUI(I)=DSI(I)/(9.80665*XDENL(I)*XDENS*DAL(I)*
2 (1.-DAL(I))**2*XD**3)*((1.254E-6*REL+.01352)*
3 (XWL*DMS(I))**2/(XD*XD*(1.-DAL(I)))+1.6211*
4 XWL*DMS(I)*DNU(I)*XKL(I)*(XTSAT-XTLO)*(1.-DTL(I))/
5 (XHFG*XDHL))
400 RETURN
END

```

Subroutines "OUTPUT" and "PLOTTR"

```

SUBROUTINE OUTPUT
COMMON DTL(50),DDL(50),DSL(50),XWS,
2 DSS(50),DSI(50),DAL(50),DTAUI(50),DTAUS(50),
3 DNU(50),DTAUL(50),DFR2(50),DX(50),DZETA(50),THETA,
4 XDENL(50),XDENS,XKL(50),XD,XTSAT,XTLO,XWL,XHFG,
5 XVISL(50),XVISS,XPRL(50),PI,XL,XPSAT,NPASS,XCPL(50),
6 OLDDDL(50),OLDDTL(50),DMS(50),DUK(50),DHMOD
CHARACTER*9 DAT
CHARACTER*8 TIM
CHARACTER*6 PLQ
C      DETERMINE OUTPUT INFORMATION
CALL PLOTTR
WRITE(6,50)
50  FORMAT(' DO YOU WISH A PRINT?')
    READ(5,*) PLQ
    IF(PLQ.NE.'YES')RETURN
    OPEN(UNIT=4,TYPE='NEW',FORM='FORMATTED',
2     NAME='CHOPOUT.DAT')
    CALL DATE(DAT)
    CALL TIME(TIM)
    WRITE(4,51)DAT,TIM
51  FORMAT('////////'          RUN IDENTIFICATION:',
2     A14,A12/)
    WRITE(4,52)
52  FORMAT('////'          ',
2     'INPUT DATA'//)
    WRITE(4,53)NPASS,DZETA(50)
53  FORMAT('          NO. OF PASSES =',I4,
2     '          DZETAOUT =',F6.3)
    WRITE(4,54)XL,XD
54  FORMAT('          L =',F10.3,' M',
2     '          D =',F10.4,' M')
    WRITE(4,55)XTSAT,XTLO
55  FORMAT('          TSAT =',F10.2,' K',
2     '          TLIN =',F10.2,' K')
    WRITE(4,56)XPSAT
56  FORMAT('          PSAT =',E12.4,' PA',
2     '          N =',50,' INTERVALS')
    WRITE(4,57)XWL,THETA
57  FORMAT('          INLET WATER FLOW =',F7.4,' KG/S',
2     '          PIPE SLOPE =',F9.5)
    WRITE(4,90)DHMOD,XWS
90  FORMAT('          DHMOD =',F9.3,
2     '          STEAM VENTED =',F10.5,' KG/S')
    WRITE(4,58)
58  FORMAT('////////'          ',
2     'CALCULATED PROPERTIES'//)
    WRITE(4,59)XDENL(1)
59  FORMAT('          INLET LIQUID DENSITY =',F8.1,' KG/M3')
    WRITE(4,60)XDENS
60  FORMAT('          STEAM DENSITY =',F8.3,' KG/M3')

```

```

WRITE(4,61)XVISL(1)
61  FORMAT('          INLET LIQUID VISCOSITY =',E12.4,' KG/M*S')
WRITE(4,62)XVISS
62  FORMAT('          STEAM VISCOSITY =',E12.4,' KG/M*S')
WRITE(4,63)XCPL(1)
63  FORMAT('          INLET LIQUID SPECIFIC HEAT =',F9.1,' J/KG*K')
WRITE(4,64)XKL(1)
64  FORMAT('          INLET LIQUID THERMAL COND. =',F9.4,
2    ' W/M*K')
WRITE(4,65)XPRL(1)
65  FORMAT('          INLET LIQUID PRANDTL NO. =',F10.3)
WRITE(4,72)XHFG
72  FORMAT('          ENTHALPY OF VAPORIZATION =',E12.4,
2    ' J/KG'////////)
WRITE(4,76)
76  FORMAT('          ,
2    ' ABBREVIATIONS OF DIMENSIONLESS VARIABLES'//)
WRITE(4,77)
77  FORMAT('          X*          AXIAL LOCATION')
WRITE(4,78)
78  FORMAT('          DL*         LIQUID DEPTH')
WRITE(4,79)
79  FORMAT('          TL*         LIQUID TEMPERATURE')
WRITE(4,80)
80  FORMAT('          MS*         STEAM MASS FLOWRATE')
WRITE(4,81)
81  FORMAT('          DAL          LIQUID FLOW AREA')
WRITE(4,82)
82  FORMAT('          DUKLER       TAITEL-DUKLER PARAMETER')
WRITE(4,83)
83  FORMAT('          DNU          CONDENSATION ',
2    ' NUSSELT NUMBER')
WRITE(4,84)
84  FORMAT('          DTAUL        LIQUID WALL SHEAR STRESS')
WRITE(4,85)
85  FORMAT('          DTAUI        INTERFACIAL SHEAR STRESS')
WRITE(4,86)
86  FORMAT('          DTAUS        STEAM WALL SHEAR STRESS'
2    '//)
WRITE(4,51)DAT,TIM
784  FORMAT('/'          RUN IDENTIFICATION:',
2    A14,A12/)
WRITE(4,66)
66  FORMAT('          ,
2    ' DIMENSIONLESS VARIABLES I'//)
WRITE(4,67)
67  FORMAT('          X*          DL*
2    ' TL*          MS*
3    ' DAL          DUKLER '//)
DO 97 I=1,50
DUKLIM=DUK(I)
IF(DUKLIM.GT.10.)DUKLIM=10.

```

```

WRITE(4,68)DX(I),DDL(I),DTL(I),DMS(I),DAL(I),DUKLIM
68  FORMAT(' ',F9.3,F10.4,F10.4,E14.4,F10.4,F10.4)
97  CONTINUE
DO 96 I=1,4
WRITE(4,87)
87  FORMAT(' ')
96  CONTINUE
WRITE(4,784)DAT,TIM
WRITE(4,71)
71  FORMAT(' ',
2    ' DIMENSIONLESS VARIABLES II'//)
WRITE(4,69)
69  FORMAT(' X* ', ' DNU ',
2    ' DTAUL ',
3    ' DTAUI ', ' DTAUS '//)
DO 98 I=1,50
WRITE(4,70)DX(I),DNU(I),DTAUL(I),DTAUI(I),DTAUS(I)
70  FORMAT(' ',F9.3,E14.4,3E13.4)
98  CONTINUE
DO 88 I=1,8
WRITE(4,89)
89  FORMAT(' ')
88  CONTINUE
CLOSE(UNIT=4)
RETURN
END
SUBROUTINE PLOTR
COMMON DTL(50),DDL(50),DSL(50),XWS,
2  DSS(50),DSI(50),DAL(50),DTAUI(50),DTAUS(50),
3  DNU(50),DTAUL(50),DFR2(50),DX(50),DZETA(50),THETA,
4  XDENL(50),XDENS,KKL(50),XD,XTSAT,XTLO,XWL,XHFG,
5  XVISL(50),XVISS,XPRL(50),PI,XL,XPSAT,NPASS,XCPL(50),
6  OLDDDL(50),OLDDTL(50),DMS(50),DUK(50),DHMOD
CHARACTER*6 PLQ,ABX
CHARACTER*36 ABY
DIMENSION PLOTT(2,50),XSCL(4)
WRITE(6,200)
200  FORMAT(' DO YOU WISH A PLOT?')
READ(5,*) PLQ
IF(PLQ.NE.'YES') RETURN
DO 280 I=1,50
PLOTT(2,I)=DX(I)
280  CONTINUE
ABX='X/D'
XSCL(1)=0
XSCL(2)=DX(50)
WRITE(6,201)
201  FORMAT(' PLOT DMS?')
READ(5,*) PLQ
IF(PLQ.NE.'YES') GOTO 250
DO 281 I=1,50
PLOTT(1,I)=DMS(I)

```



```

281   CONTINUE
      XSCL(3)=0.
      XSCL(4)=DMS(50)
      ABY='DIMENSIONLESS STEAM FLOWRATE'
      CALL QPICTR(PLOTT,2,50,QY(1),QX(2),QLABEL(14),
2     QXLAB(ABX),QYLAB(ABY),QISCL(-2),QXSCL(XSCL))
250   WRITE(6,202)
202   FORMAT(' PLOT DTL?')
      READ(5,*) PLQ
      IF(PLQ.NE.'YES')GOTO 251
      DO 282 I=1,50
      PLOTT(1,I)=DTL(I)
282   CONTINUE
      XSCL(3)=0.
      XSCL(4)=1.
      ABY='DIMENSIONLESS LIQUID TEMPERATURE'
      CALL QPICTR(PLOTT,2,50,QY(1),QX(2),QLABEL(14),
2     QXLAB(ABX),QYLAB(ABY),QISCL(-2),QXSCL(XSCL))
251   WRITE(6,203)
203   FORMAT(' PLOT DDL?')
      READ(5,*) PLQ
      IF(PLQ.NE.'YES')GOTO 252
      DO 283 I=1,50
      PLOTT(1,I)=DDL(I)
283   CONTINUE
      XSCL(3)=0.
      XSCL(4)=1.
      ABY='DIMENSIONLESS LIQUID DEPTH'
      CALL QPICTR(PLOTT,2,50,QY(1),QX(2),QLABEL(14),
2     QXLAB(ABX),QYLAB(ABY),QISCL(-2),QXSCL(XSCL))
252   WRITE(6,204)
204   FORMAT(' PLOT DUKLER?')
      READ(5,*) PLQ
      IF(PLQ.NE.'YES')GOTO 253
      DO 284 I=1,50
      PLOTT(1,I)=DUK(I)
284   CONTINUE
      XSCL(3)=0.
      XSCL(4)=2.
      ABY='TAITEL-DUKLER PARAMETER'
      CALL QPICTR(PLOTT,2,50,QY(1),QX(2),QLABEL(14),
2     QXLAB(ABX),QYLAB(ABY),QISCL(-2),QXSCL(XSCL))
253   RETURN
      END

```

Appendix B

Determination of c_1 from
Critical Inlet Water Flow Rate Data

Run	$\dot{m}_{LO,crit,meas}$	pred ($c_1 = 2.6$)	pred (2.5)	pred (2.4)
J1	0.0573	0.049	0.051	0.054
J2	0.0738	0.070	0.073	0.075
J3	0.0830	0.087	0.090	0.093
J4	0.1130	0.109	0.112	0.116
J5	0.0520	0.044	0.046	0.048
J6	0.0675	0.063	0.066	0.068
J7	0.0704	0.078	0.081	0.083
J8	0.0691	0.095	0.097	0.100
J9	0.0573	0.051	0.053	0.055
J10	0.0728	0.075	0.077	0.080
J11	0.0914	0.094	0.097	0.101
J12	0.1161	0.120	0.123	0.127
M1	0.0807	0.065	0.068	0.071
M2	0.0875	0.091	0.094	0.097
M3	0.0903	0.110	0.113	0.117
M4	0.1077	0.140	0.143	0.147
	$\sum (\%dev)^2$	3,201	2,959	3,197

$\therefore c_1 = 2.5$ provides the best agreement of the model predictions with experimental water hammer initiation data. For $c_1 = 2.5$, the rms deviation is 13.6 percent.

Appendix C

Computed Results for
Low Pressure Sample Case

- I. Computer print of calculations.

- II. Plots of:
 - 1) Dimensionless steam flow rate.
 - 2) Dimensionless liquid temperature.
 - 3) Dimensionless liquid depth.
 - 4) Taitel-Dukler stability parameter.

RUN IDENTIFICATION: 2-JUL-82 10:17:06

INPUT DATA

NO. OF PASSES = 14	DZETAOUT = 0.075
L = 2.000 M	D = 0.0381 M
TSAT = 396.00 K	TLIN = 336.00 K
PSAT = 0.2171E+06 PA	N = 50 INTERVALS
INLET WATER FLOW = 0.0860 KG/S	PIPE SLOPE = 0.00000
DHMOD = 2.500	STEAM VENTED = 0.00000 KG/S

CALCULATED PROPERTIES

INLET LIQUID DENSITY = 980.4 KG/M3
 STEAM DENSITY = 1.220 KG/M3
 INLET LIQUID VISCOSITY = 0.4436E-03 KG/M*S
 STEAM VISCOSITY = 0.1294E-04 KG/M*S
 INLET LIQUID SPECIFIC HEAT = 4183.5 J/KG*K
 INLET LIQUID THERMAL COND. = 0.6562 W/M*K
 INLET LIQUID PRANDTL NO. = 2.828
 ENTHALPY OF VAPORIZATION = 0.2193E+07 J/KG

ABBREVIATIONS OF DIMENSIONLESS VARIABLES

X*	AXIAL LOCATION
DL*	LIQUID DEPTH
TL*	LIQUID TEMPERATURE
MS*	STEAM MASS FLOWRATE
DAL	LIQUID FLOW AREA
DUKLER	TAITEL-DUKLER PARAMETER
DNU	CONDENSATION NUSSELT NUMBER
DTAUL	LIQUID WALL SHEAR STRESS
DTAUI	INTERFACIAL SHEAR STRESS
DTAUS	STEAM WALL SHEAR STRESS

RUN IDENTIFICATION: 2-JUL-82 10:17:06

DIMENSIONLESS VARIABLES I

X*	DL*	TL*	MS*	DAL	DUKLER
0.000	0.6684	0.0000	0.1000E-05	0.7103	0.0000
1.312	0.6678	0.0084	0.8611E-03	0.7096	0.0042
2.625	0.6672	0.0184	0.1889E-02	0.7088	0.0200
3.937	0.6666	0.0285	0.2931E-02	0.7081	0.0475
5.249	0.6659	0.0386	0.3978E-02	0.7073	0.0866
6.562	0.6651	0.0487	0.5026E-02	0.7064	0.1364
7.874	0.6642	0.0588	0.6073E-02	0.7053	0.1961
9.186	0.6632	0.0688	0.7118E-02	0.7040	0.2644
10.499	0.6619	0.0788	0.8160E-02	0.7024	0.3399
11.811	0.6603	0.0888	0.9200E-02	0.7005	0.4206
13.123	0.6584	0.0987	0.1024E-01	0.6983	0.5044
14.436	0.6562	0.1085	0.1127E-01	0.6956	0.5891
15.748	0.6536	0.1183	0.1230E-01	0.6925	0.6720
17.060	0.6507	0.1281	0.1333E-01	0.6889	0.7509
18.373	0.6473	0.1379	0.1436E-01	0.6848	0.8235
19.685	0.6434	0.1476	0.1539E-01	0.6801	0.8877
20.997	0.6391	0.1573	0.1642E-01	0.6748	0.9420
22.310	0.6343	0.1670	0.1745E-01	0.6690	0.9854
23.622	0.6291	0.1766	0.1848E-01	0.6625	1.0173
24.934	0.6234	0.1863	0.1951E-01	0.6555	1.0376
26.247	0.6172	0.1960	0.2055E-01	0.6479	1.0467
27.559	0.6106	0.2057	0.2159E-01	0.6396	1.0454
28.871	0.6035	0.2155	0.2263E-01	0.6308	1.0346
30.184	0.5960	0.2252	0.2368E-01	0.6214	1.0155
31.496	0.5880	0.2350	0.2474E-01	0.6115	0.9893
32.808	0.5797	0.2449	0.2581E-01	0.6010	0.9573
34.121	0.5709	0.2547	0.2688E-01	0.5899	0.9206
35.433	0.5616	0.2647	0.2796E-01	0.5783	0.8802
36.745	0.5520	0.2747	0.2904E-01	0.5661	0.8370
38.058	0.5419	0.2847	0.3014E-01	0.5533	0.7919
39.370	0.5313	0.2949	0.3125E-01	0.5398	0.7454
40.682	0.5202	0.3051	0.3237E-01	0.5257	0.6981
41.995	0.5085	0.3154	0.3350E-01	0.5108	0.6504
43.307	0.4962	0.3258	0.3465E-01	0.4951	0.6023
44.619	0.4830	0.3363	0.3581E-01	0.4784	0.5542
45.932	0.4689	0.3470	0.3699E-01	0.4605	0.5057
47.244	0.4536	0.3578	0.3819E-01	0.4409	0.4567
48.556	0.4363	0.3688	0.3941E-01	0.4192	0.4063
49.869	0.4161	0.3800	0.4066E-01	0.3937	0.3524
51.181	0.3888	0.3916	0.4195E-01	0.3596	0.2875
51.312	0.3860	0.3928	0.4209E-01	0.3561	0.2816
51.444	0.3830	0.3940	0.4222E-01	0.3524	0.2755
51.575	0.3799	0.3952	0.4236E-01	0.3485	0.2692
51.706	0.3765	0.3965	0.4250E-01	0.3444	0.2626
51.837	0.3730	0.3977	0.4264E-01	0.3400	0.2557
51.969	0.3691	0.3989	0.4278E-01	0.3353	0.2484
52.100	0.3649	0.4002	0.4292E-01	0.3301	0.2404
52.231	0.3601	0.4015	0.4306E-01	0.3242	0.2315
52.362	0.3543	0.4027	0.4320E-01	0.3172	0.2211
52.493	0.3348	0.4040	0.4335E-01	0.2935	0.1869

RUN IDENTIFICATION: 2-JUL-82 10:17:06

DIMENSIONLESS VARIABLES II

X*	DNV	DTAUL	DTAUI	DTAUS
0.000	0.6841E+02	0.4638E-03	0.1401E-06	0.4299E-10
1.312	0.8217E+02	0.4651E-03	0.1505E-03	0.5848E-05
2.625	0.8401E+02	0.4663E-03	0.3520E-03	0.2298E-04
3.937	0.8509E+02	0.4675E-03	0.5757E-03	0.4929E-04
5.249	0.8588E+02	0.4688E-03	0.8187E-03	0.8356E-04
6.562	0.8651E+02	0.4703E-03	0.1079E-02	0.1249E-03
7.874	0.8704E+02	0.4721E-03	0.1355E-02	0.1723E-03
9.186	0.8750E+02	0.4742E-03	0.1645E-02	0.2251E-03
10.499	0.8792E+02	0.4768E-03	0.1947E-02	0.2823E-03
11.811	0.8831E+02	0.4799E-03	0.2258E-02	0.3428E-03
13.123	0.8867E+02	0.4836E-03	0.2575E-02	0.4057E-03
14.436	0.8902E+02	0.4880E-03	0.2895E-02	0.4699E-03
15.748	0.8935E+02	0.4932E-03	0.3215E-02	0.5341E-03
17.060	0.8967E+02	0.4994E-03	0.3531E-02	0.5973E-03
18.373	0.8999E+02	0.5065E-03	0.3840E-02	0.6585E-03
19.685	0.9031E+02	0.5148E-03	0.4140E-02	0.7166E-03
20.997	0.9063E+02	0.5243E-03	0.4427E-02	0.7707E-03
22.310	0.9095E+02	0.5352E-03	0.4699E-02	0.8203E-03
23.622	0.9128E+02	0.5476E-03	0.4955E-02	0.8649E-03
24.934	0.9161E+02	0.5616E-03	0.5194E-02	0.9040E-03
26.247	0.9196E+02	0.5774E-03	0.5415E-02	0.9376E-03
27.559	0.9231E+02	0.5952E-03	0.5618E-02	0.9656E-03
28.871	0.9267E+02	0.6152E-03	0.5805E-02	0.9883E-03
30.184	0.9304E+02	0.6376E-03	0.5976E-02	0.1006E-02
31.496	0.9343E+02	0.6626E-03	0.6132E-02	0.1019E-02
32.808	0.9383E+02	0.6907E-03	0.6275E-02	0.1027E-02
34.121	0.9424E+02	0.7223E-03	0.6407E-02	0.1031E-02
35.433	0.9468E+02	0.7578E-03	0.6529E-02	0.1032E-02
36.745	0.9513E+02	0.7979E-03	0.6644E-02	0.1029E-02
38.058	0.9561E+02	0.8434E-03	0.6751E-02	0.1022E-02
39.370	0.9611E+02	0.8953E-03	0.6855E-02	0.1013E-02
40.682	0.9664E+02	0.9549E-03	0.6955E-02	0.1002E-02
41.995	0.9721E+02	0.1024E-02	0.7055E-02	0.9871E-03
43.307	0.9781E+02	0.1106E-02	0.7155E-02	0.9701E-03
44.619	0.9847E+02	0.1203E-02	0.7259E-02	0.9503E-03
45.932	0.9919E+02	0.1321E-02	0.7369E-02	0.9274E-03
47.244	0.9999E+02	0.1470E-02	0.7489E-02	0.9009E-03
48.556	0.1009E+03	0.1666E-02	0.7625E-02	0.8694E-03
49.869	0.1020E+03	0.1946E-02	0.7787E-02	0.8299E-03
51.181	0.1036E+03	0.2438E-02	0.8004E-02	0.7711E-03
51.312	0.1038E+03	0.2498E-02	0.8035E-02	0.7656E-03
51.444	0.1039E+03	0.2564E-02	0.8067E-02	0.7598E-03
51.575	0.1041E+03	0.2636E-02	0.8102E-02	0.7536E-03
51.706	0.1043E+03	0.2715E-02	0.8138E-02	0.7469E-03
51.837	0.1046E+03	0.2803E-02	0.8177E-02	0.7397E-03
51.969	0.1048E+03	0.2903E-02	0.8220E-02	0.7318E-03
52.100	0.1051E+03	0.3018E-02	0.8268E-02	0.7228E-03
52.231	0.1054E+03	0.3157E-02	0.8322E-02	0.7125E-03
52.362	0.1057E+03	0.3335E-02	0.8387E-02	0.6998E-03
52.493	0.1070E+03	0.4047E-02	0.8582E-02	0.6513E-03

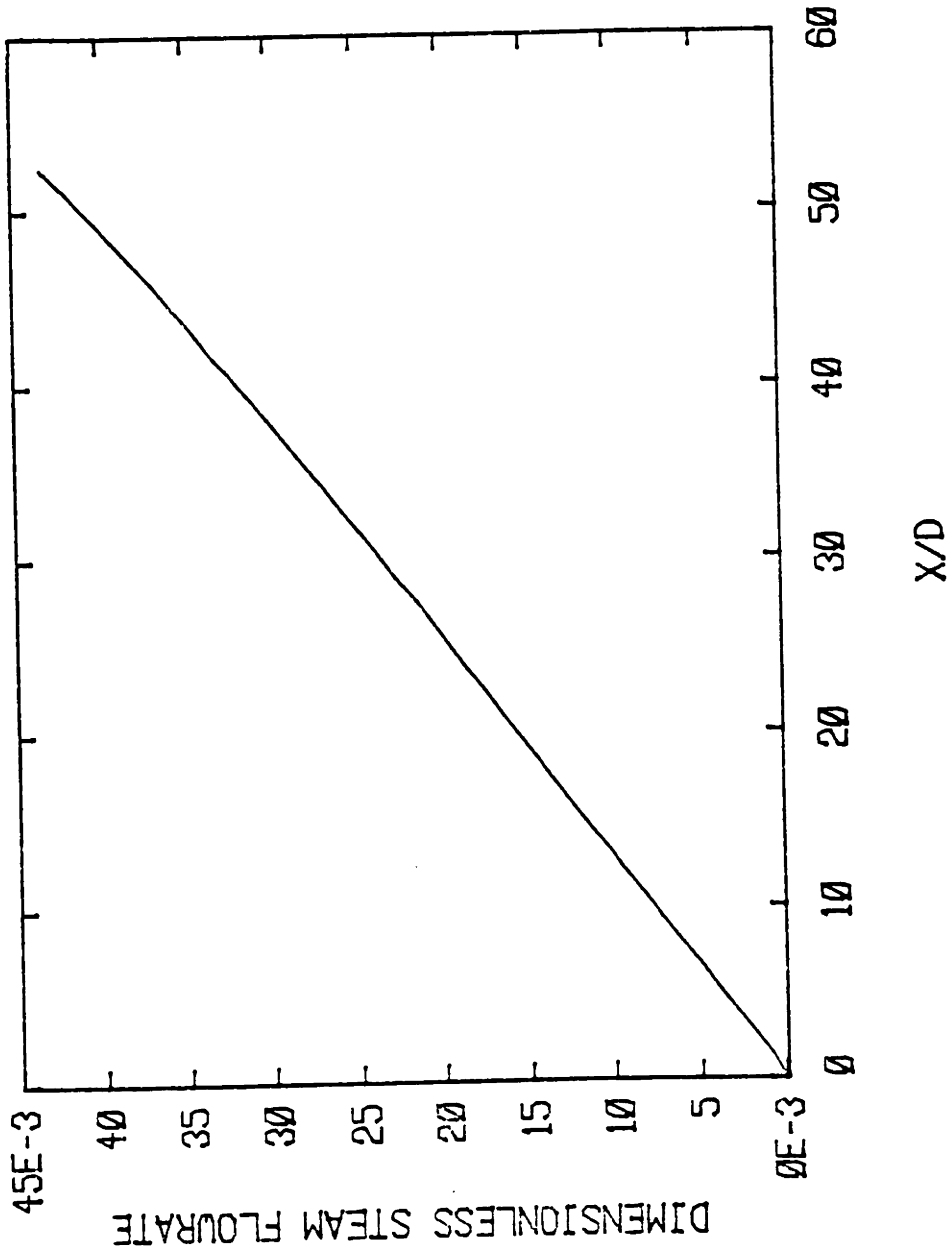


Figure C-1. Dimensionless steam flow rate profile for low pressure sample case.

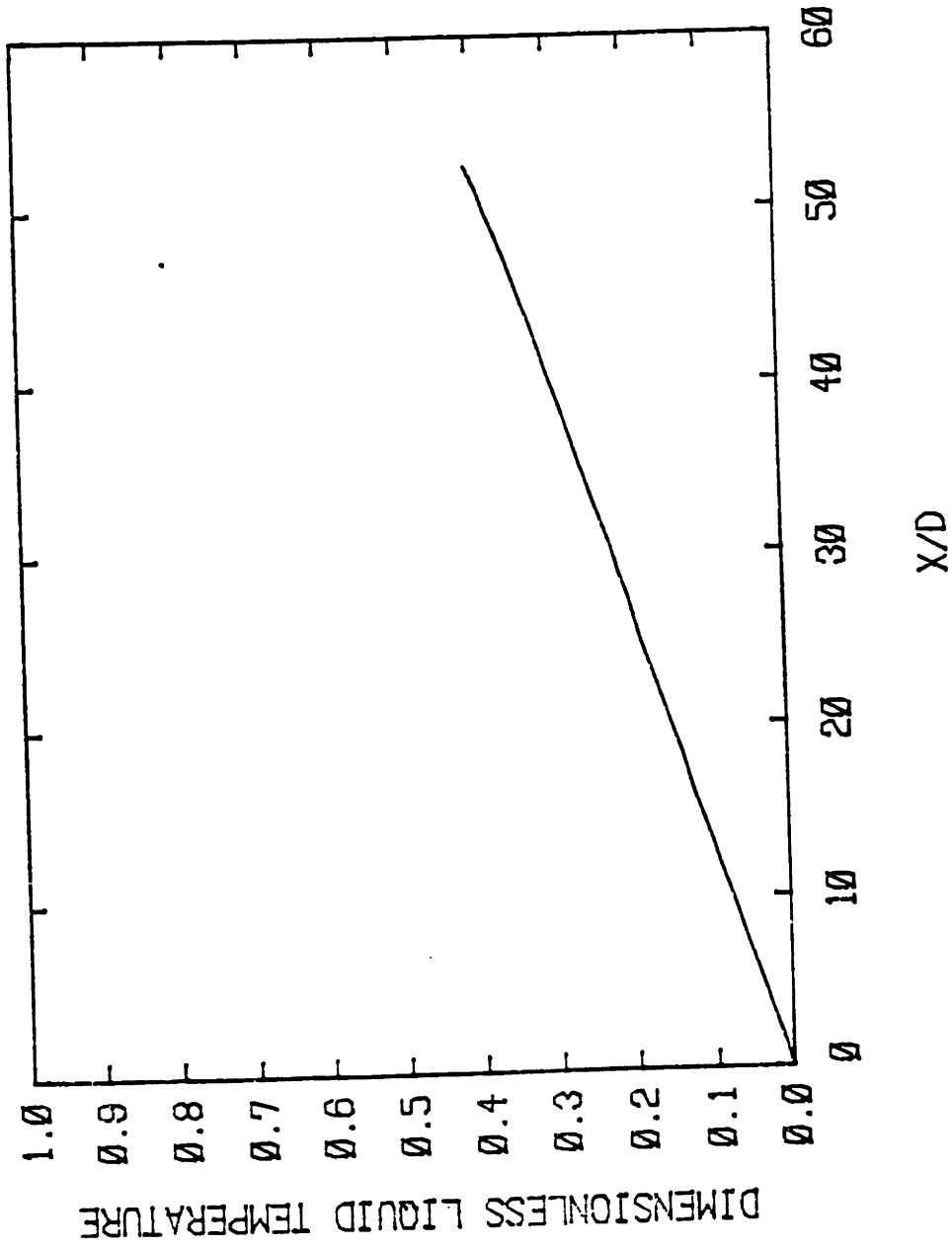


Figure C-2. Dimensionless liquid temperature profile for low pressure sample case.

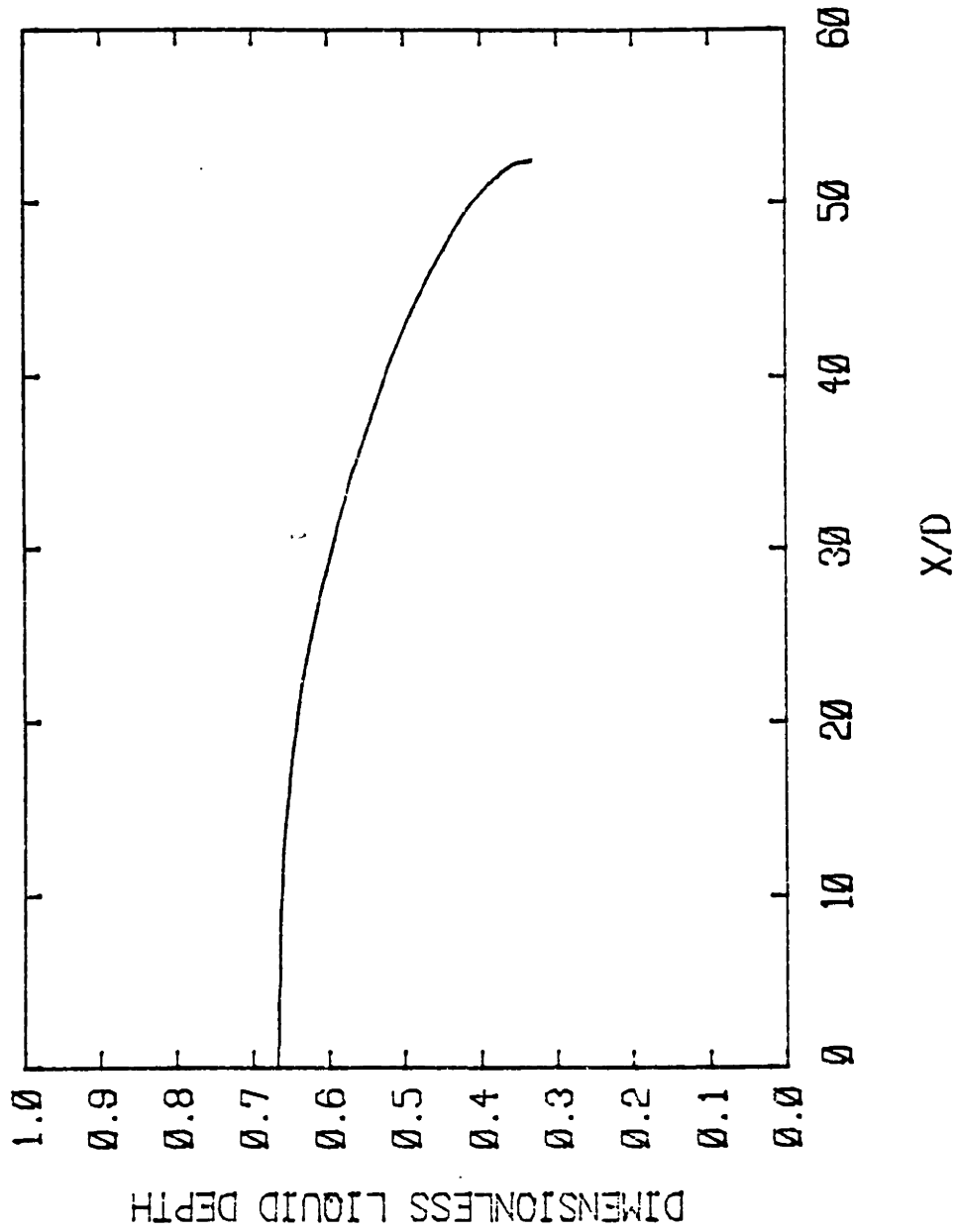


Figure C-3. Dimensionless liquid depth profile for low pressure sample case.

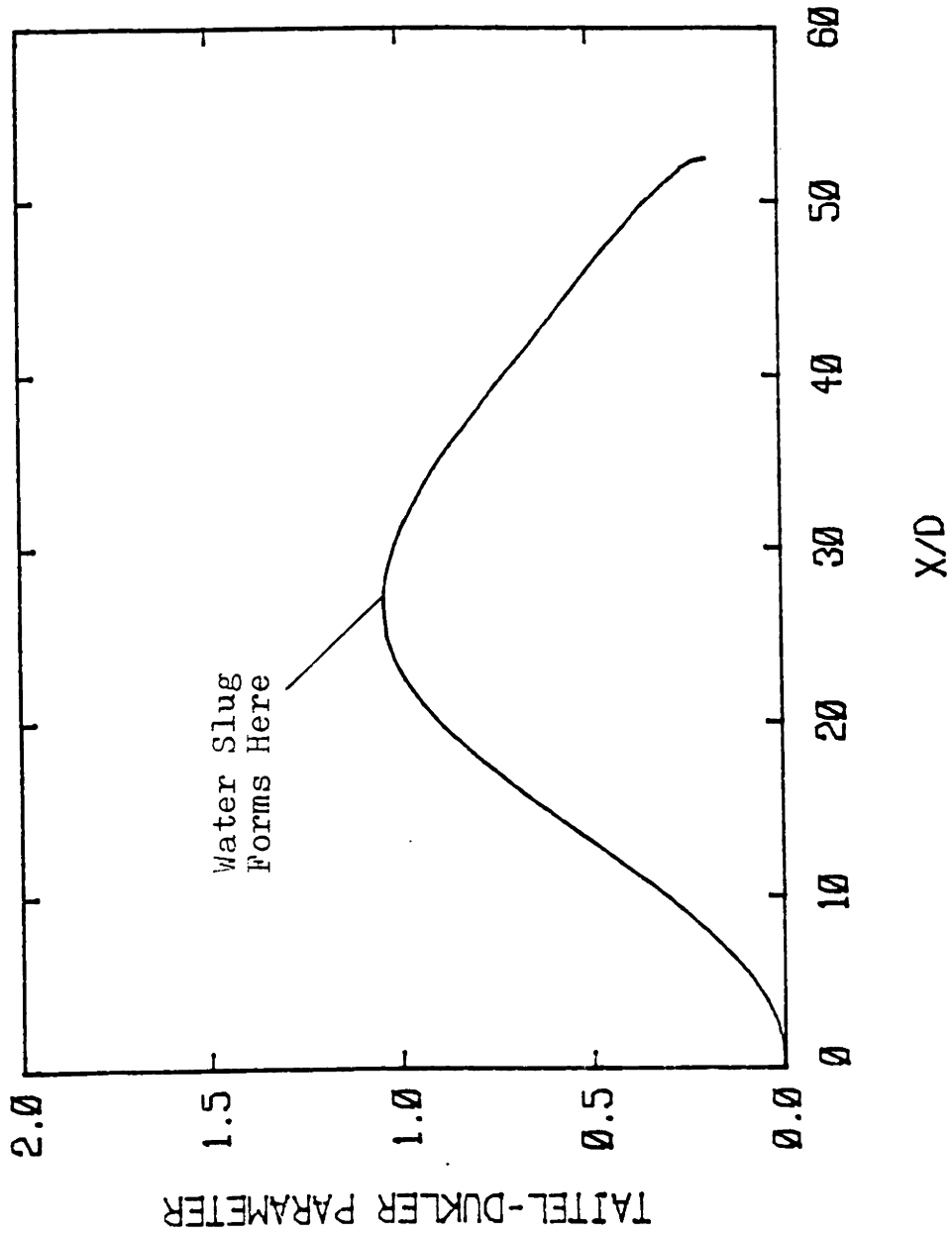


Figure C-4. Taitel-Dukler stability parameter profile for low pressure sample case.

Appendix D

Computed Results for
Low Pressure Sample Case
with Vented Steam

- I. Computer print of calculations.

- II. Plots of:
 - 1) Dimensionless steam flow rate.
 - 2) Dimensionless liquid temperature.
 - 3) Dimensionless liquid depth.
 - 4) Taitel-Dukler stability parameter.

RUN IDENTIFICATION: 2-JUL-82 10:46:55

INPUT DATA

NO. OF PASSES = 12	DZETAOUT = 0.075
L = . 2.000 M	D = 0.0381 M
TSAT = 396.00 K	TLIN = 336.00 K
PSAT = 0.2171E+06 PA	N = 50 INTERVALS
INLET WATER FLOW = 0.0570 KG/S	PIPE SLOPE = 0.00000
DHMOD = 2.500	STEAM VENTED = 0.00100 KG/S

CALCULATED PROPERTIES

INLET LIQUID DENSITY = 980.4 KG/M3
 STEAM DENSITY = 1.220 KG/M3
 INLET LIQUID VISCOSITY = 0.4436E-03 KG/M*S
 STEAM VISCOSITY = 0.1294E-04 KG/M*S
 INLET LIQUID SPECIFIC HEAT = 4183.5 J/KG*K
 INLET LIQUID THERMAL COND. = 0.6562 W/M*K
 INLET LIQUID PRANDTL NO. = 2.828
 ENTHALPY OF VAPORIZATION = 0.2193E+07 J/KG

ABBREVIATIONS OF DIMENSIONLESS VARIABLES

X*	AXIAL LOCATION
DL*	LIQUID DEPTH
TL*	LIQUID TEMPERATURE
MS*	STEAM MASS FLOWRATE
DAL	LIQUID FLOW AREA
DUKLER	TAITEL-DUKLER PARAMETER
DNU	CONDENSATION NUSSELT NUMBER
DTAUL	LIQUID WALL SHEAR STRESS
DTAUI	INTERFACIAL SHEAR STRESS
DTAUS	STEAM WALL SHEAR STRESS

RUN IDENTIFICATION: 2-JUL-82 10:46:55

DIMENSIONLESS VARIABLES I

X*	DL*	TL*	MS*	DAL	DUKLER
0.000	0.6444	0.0000	0.1754E-01	0.6812	0.5123
1.312	0.6426	0.0140	0.1898E-01	0.6790	0.5826
2.625	0.6405	0.0279	0.2042E-01	0.6765	0.6516
3.937	0.6381	0.0417	0.2184E-01	0.6736	0.7176
5.249	0.6354	0.0553	0.2326E-01	0.6702	0.7793
6.562	0.6323	0.0689	0.2467E-01	0.6665	0.8354
7.874	0.6290	0.0824	0.2607E-01	0.6623	0.8849
9.186	0.6252	0.0957	0.2747E-01	0.6578	0.9270
10.499	0.6212	0.1090	0.2886E-01	0.6527	0.9613
11.811	0.6167	0.1222	0.3025E-01	0.6473	0.9874
13.123	0.6120	0.1354	0.3164E-01	0.6414	1.0054
14.436	0.6069	0.1485	0.3303E-01	0.6351	1.0155
15.748	0.6015	0.1615	0.3441E-01	0.6284	1.0182
17.060	0.5958	0.1744	0.3579E-01	0.6212	1.0141
18.373	0.5898	0.1874	0.3717E-01	0.6137	1.0039
19.685	0.5835	0.2003	0.3855E-01	0.6058	0.9883
20.997	0.5769	0.2131	0.3992E-01	0.5975	0.9680
22.310	0.5701	0.2259	0.4130E-01	0.5889	0.9439
23.622	0.5630	0.2387	0.4268E-01	0.5799	0.9166
24.934	0.5556	0.2515	0.4407E-01	0.5706	0.8867
26.247	0.5480	0.2642	0.4545E-01	0.5610	0.8548
27.559	0.5402	0.2769	0.4683E-01	0.5511	0.8215
28.871	0.5321	0.2896	0.4822E-01	0.5408	0.7872
30.184	0.5238	0.3023	0.4961E-01	0.5302	0.7523
31.496	0.5152	0.3150	0.5100E-01	0.5193	0.7171
32.808	0.5064	0.3277	0.5240E-01	0.5081	0.6818
34.121	0.4973	0.3403	0.5379E-01	0.4966	0.6467
35.433	0.4880	0.3530	0.5520E-01	0.4847	0.6119
36.745	0.4783	0.3657	0.5660E-01	0.4724	0.5776
38.058	0.4684	0.3783	0.5802E-01	0.4598	0.5438
39.370	0.4581	0.3910	0.5943E-01	0.4467	0.5106
40.682	0.4473	0.4037	0.6086E-01	0.4331	0.4779
41.995	0.4362	0.4165	0.6229E-01	0.4189	0.4458
43.307	0.4244	0.4292	0.6373E-01	0.4042	0.4141
44.619	0.4120	0.4421	0.6518E-01	0.3886	0.3828
45.932	0.3988	0.4550	0.6664E-01	0.3721	0.3516
47.244	0.3845	0.4679	0.6811E-01	0.3542	0.3203
48.556	0.3685	0.4811	0.6961E-01	0.3345	0.2880
49.869	0.3498	0.4944	0.7113E-01	0.3117	0.2537
51.181	0.3248	0.5079	0.7269E-01	0.2815	0.2122
51.312	0.3222	0.5093	0.7285E-01	0.2784	0.2084
51.444	0.3194	0.5108	0.7301E-01	0.2752	0.2044
51.575	0.3166	0.5122	0.7317E-01	0.2718	0.2003
51.706	0.3136	0.5136	0.7334E-01	0.2682	0.1961
51.837	0.3103	0.5150	0.7350E-01	0.2644	0.1916
51.969	0.3069	0.5165	0.7367E-01	0.2604	0.1868
52.100	0.3031	0.5180	0.7384E-01	0.2559	0.1817
52.231	0.2988	0.5194	0.7401E-01	0.2510	0.1761
52.362	0.2939	0.5209	0.7418E-01	0.2452	0.1696
52.493	0.2726	0.5224	0.7435E-01	0.2208	0.1427

RUN IDENTIFICATION: 2-JUL-82 10:46:55

DIMENSIONLESS VARIABLES II

X*	DNU	DTAUL	DTAUI	DTAUS
0.000	0.7238E+02	0.2485E-03	0.2453E-02	0.4407E-03
1.312	0.7265E+02	0.2504E-03	0.2696E-02	0.4975E-03
2.625	0.7290E+02	0.2527E-03	0.2937E-02	0.5543E-03
3.937	0.7316E+02	0.2553E-03	0.3175E-02	0.6102E-03
5.249	0.7341E+02	0.2583E-03	0.3407E-02	0.6644E-03
6.562	0.7366E+02	0.2618E-03	0.3633E-02	0.7165E-03
7.874	0.7391E+02	0.2657E-03	0.3849E-02	0.7658E-03
9.186	0.7416E+02	0.2702E-03	0.4056E-02	0.8117E-03
10.499	0.7442E+02	0.2752E-03	0.4252E-02	0.8541E-03
11.811	0.7467E+02	0.2807E-03	0.4437E-02	0.8925E-03
13.123	0.7493E+02	0.2869E-03	0.4610E-02	0.9269E-03
14.436	0.7520E+02	0.2938E-03	0.4771E-02	0.9571E-03
15.748	0.7547E+02	0.3014E-03	0.4920E-02	0.9832E-03
17.060	0.7574E+02	0.3098E-03	0.5058E-02	0.1005E-02
18.373	0.7603E+02	0.3190E-03	0.5185E-02	0.1024E-02
19.685	0.7631E+02	0.3292E-03	0.5301E-02	0.1038E-02
20.997	0.7661E+02	0.3403E-03	0.5409E-02	0.1049E-02
22.310	0.7691E+02	0.3525E-03	0.5508E-02	0.1058E-02
23.622	0.7722E+02	0.3658E-03	0.5599E-02	0.1063E-02
24.934	0.7754E+02	0.3805E-03	0.5684E-02	0.1065E-02
26.247	0.7787E+02	0.3966E-03	0.5764E-02	0.1065E-02
27.559	0.7821E+02	0.4143E-03	0.5838E-02	0.1063E-02
28.871	0.7856E+02	0.4338E-03	0.5909E-02	0.1059E-02
30.184	0.7892E+02	0.4553E-03	0.5977E-02	0.1054E-02
31.496	0.7930E+02	0.4791E-03	0.6042E-02	0.1046E-02
32.808	0.7969E+02	0.5056E-03	0.6107E-02	0.1038E-02
34.121	0.8009E+02	0.5350E-03	0.6171E-02	0.1028E-02
35.433	0.8051E+02	0.5681E-03	0.6236E-02	0.1016E-02
36.745	0.8095E+02	0.6053E-03	0.6303E-02	0.1004E-02
38.058	0.8140E+02	0.6474E-03	0.6372E-02	0.9906E-03
39.370	0.8189E+02	0.6956E-03	0.6445E-02	0.9761E-03
40.682	0.8240E+02	0.7511E-03	0.6523E-02	0.9605E-03
41.995	0.8294E+02	0.8158E-03	0.6607E-02	0.9438E-03
43.307	0.8352E+02	0.8922E-03	0.6700E-02	0.9259E-03
44.619	0.8415E+02	0.9841E-03	0.6805E-02	0.9066E-03
45.932	0.8484E+02	0.1097E-02	0.6925E-02	0.8855E-03
47.244	0.8561E+02	0.1241E-02	0.7066E-02	0.8622E-03
48.556	0.8650E+02	0.1433E-02	0.7240E-02	0.8356E-03
49.869	0.8757E+02	0.1711E-02	0.7467E-02	0.8034E-03
51.181	0.8909E+02	0.2209E-02	0.7819E-02	0.7573E-03
51.312	0.8926E+02	0.2272E-02	0.7864E-02	0.7529E-03
51.444	0.8944E+02	0.2340E-02	0.7911E-02	0.7483E-03
51.575	0.8962E+02	0.2414E-02	0.7962E-02	0.7435E-03
51.706	0.8982E+02	0.2496E-02	0.8018E-02	0.7383E-03
51.837	0.9003E+02	0.2587E-02	0.8078E-02	0.7327E-03
51.969	0.9026E+02	0.2690E-02	0.8145E-02	0.7266E-03
52.100	0.9052E+02	0.2810E-02	0.8220E-02	0.7199E-03
52.231	0.9081E+02	0.2952E-02	0.8307E-02	0.7122E-03
52.362	0.9115E+02	0.3130E-02	0.8413E-02	0.7030E-03
52.493	0.9265E+02	0.4076E-02	0.8894E-02	0.6584E-03

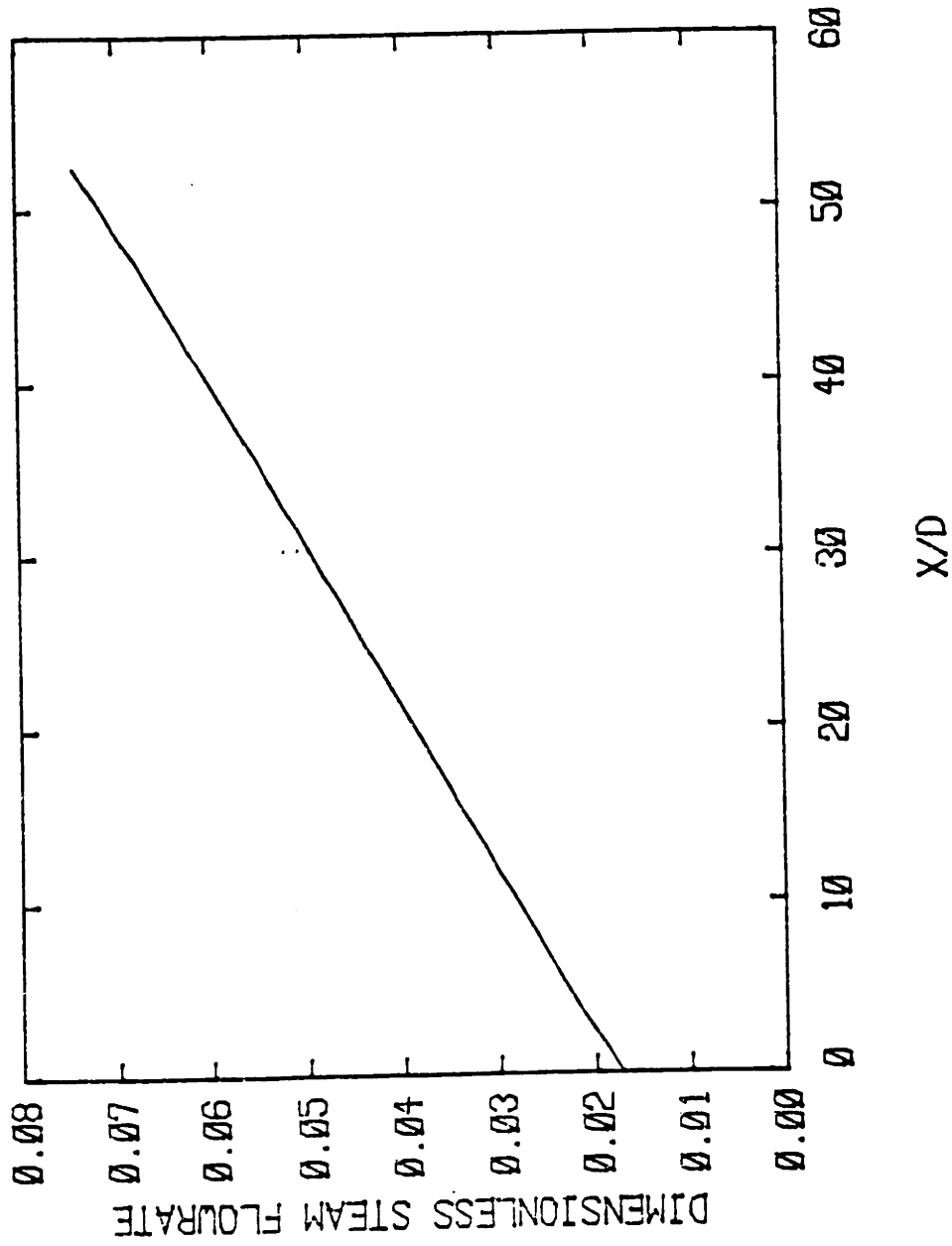


Figure D-1. Dimensionless steam flow rate profile for low pressure sample case with vented steam.

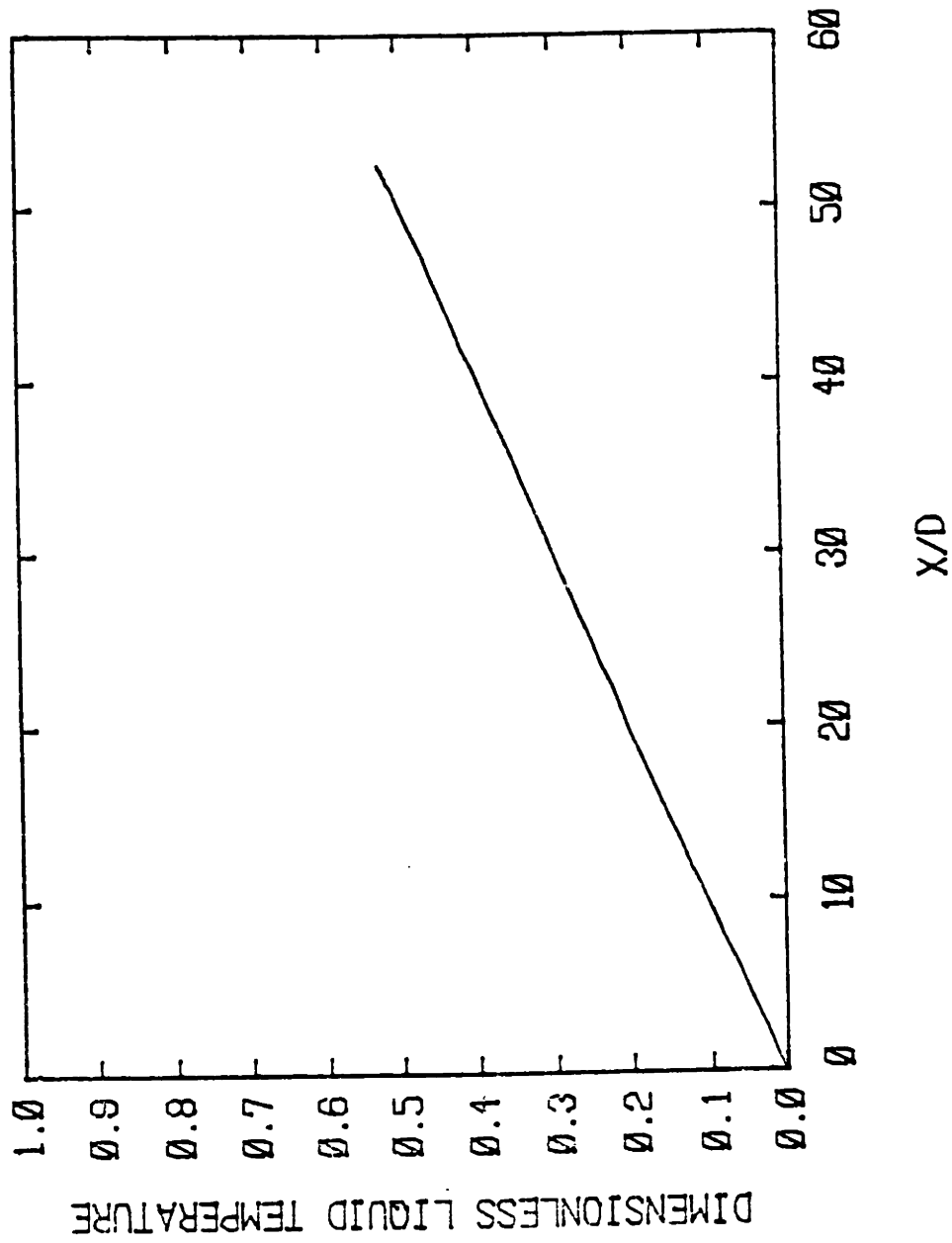


Figure D-2. Dimensionless liquid temperature profile for low pressure sample case with vented steam.

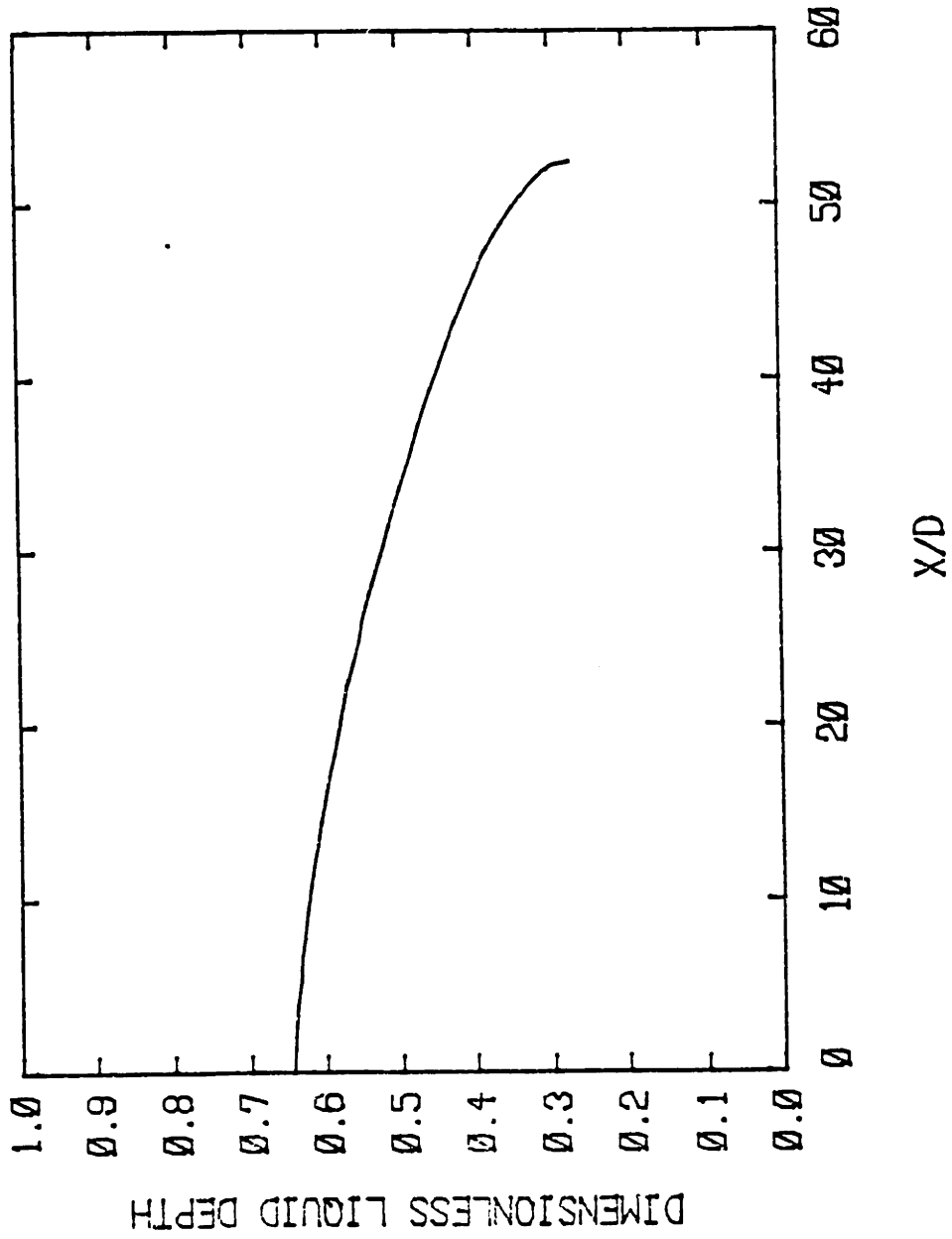


Figure D-3. Dimensionless liquid depth profile for low pressure sample case with vented steam.

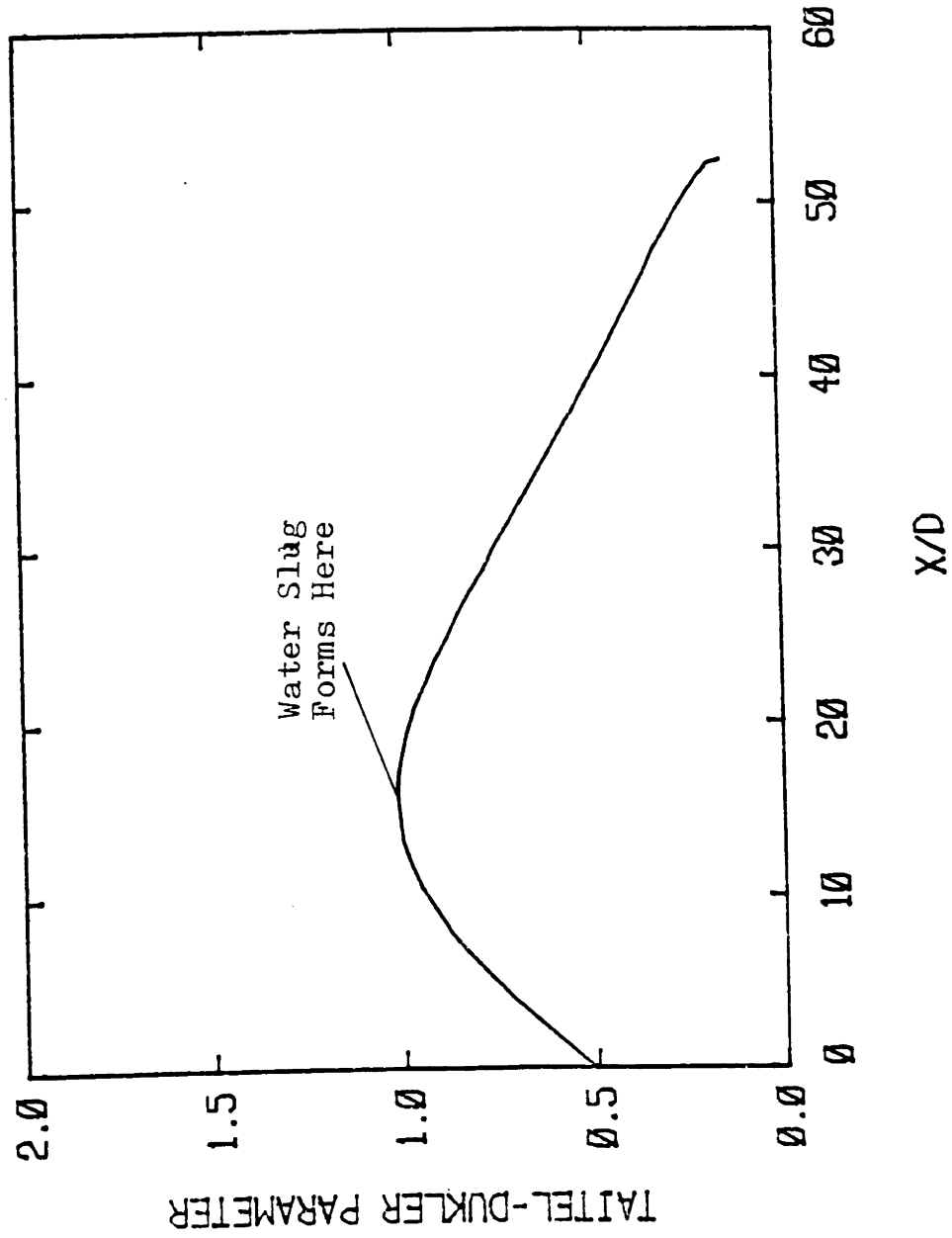


Figure D-4. Taitel-Dukler stability parameter profile for low pressure sample case with vented steam.

Appendix E

Computed Results for
PWR Steam Generator Sample Case

- I. Computer print of calculations.

- II. Plots of:
 - 1) Dimensionless steam flow rate.
 - 2) Dimensionless liquid temperature.
 - 3) Dimensionless liquid depth.
 - 4) Taitel-Dukler stability parameter.

RUN IDENTIFICATION: 2-JUL-82 10:34:11

INPUT DATA

NO. OF PASSES = 20	DZETAOUT = 0.075
L = 6.000 M	D = 0.3636 M
TSAT = 557.92 K	TLIN = 277.59 K
PSAT = 0.6895E+07 PA	N = 50 INTERVALS
INLET WATER FLOW = 4.3100 KG/S	PIPE SLOPE = 0.00000
DHMOD = 2.500	STEAM VENTED = 0.00000 KG/S

CALCULATED PROPERTIES

INLET LIQUID DENSITY = 1001.8 KG/M3
 STEAM DENSITY = 35.781 KG/M3
 INLET LIQUID VISCOSITY = 0.1527E-02 KG/M*S
 STEAM VISCOSITY = 0.1883E-04 KG/M*S
 INLET LIQUID SPECIFIC HEAT = 4204.7 J/KG*K
 INLET LIQUID THERMAL COND. = 0.5770 W/M*K
 INLET LIQUID PRANDTL NO. = 11.126
 ENTHALPY OF VAPORIZATION = 0.1515E+07 J/KG

ABBREVIATIONS OF DIMENSIONLESS VARIABLES

X*	AXIAL LOCATION
DL*	LIQUID DEPTH
TL*	LIQUID TEMPERATURE
MS*	STEAM MASS FLOWRATE
DAL	LIQUID FLOW AREA
DUKLER	TAITEL-DUKLER PARAMETER
DNU	CONDENSATION NUSSELT NUMBER
DTAUL	LIQUID WALL SHEAR STRESS
DTAUI	INTERFACIAL SHEAR STRESS
DTAUS	STEAM WALL SHEAR STRESS

RUN IDENTIFICATION: 2-JUL-82 10:34:11

DIMENSIONLESS VARIABLES I

X*	DL*	TL*	MS*	DAL	DUKLER
0.000	0.6015	0.0000	0.1000E-05	0.6284	0.0000
0.413	0.6015	0.0018	0.7989E-03	0.6284	0.0000
0.825	0.6015	0.0040	0.1756E-02	0.6284	0.0000
1.238	0.6015	0.0063	0.2735E-02	0.6284	0.0000
1.650	0.6015	0.0086	0.3726E-02	0.6283	0.0000
2.063	0.6015	0.0109	0.4726E-02	0.6283	0.0000
2.475	0.6015	0.0132	0.5733E-02	0.6283	0.0001
2.888	0.6015	0.0155	0.6745E-02	0.6283	0.0001
3.300	0.6015	0.0178	0.7763E-02	0.6283	0.0001
3.713	0.6015	0.0201	0.8785E-02	0.6283	0.0002
4.125	0.6014	0.0224	0.9810E-02	0.6283	0.0002
4.538	0.6014	0.0249	0.1092E-01	0.6283	0.0002
4.950	0.6014	0.0280	0.1229E-01	0.6282	0.0003
5.363	0.6014	0.0319	0.1402E-01	0.6282	0.0004
5.776	0.6014	0.0369	0.1624E-01	0.6282	0.0005
6.188	0.6014	0.0436	0.1921E-01	0.6282	0.0008
6.601	0.6014	0.0526	0.2327E-01	0.6282	0.0011
7.013	0.6013	0.0654	0.2906E-01	0.6281	0.0017
7.426	0.6013	0.0843	0.3774E-01	0.6281	0.0029
7.838	0.6013	0.1138	0.5152E-01	0.6281	0.0055
8.251	0.6013	0.1622	0.7490E-01	0.6280	0.0117
8.663	0.6013	0.2458	0.1177E+00	0.6281	0.0292
9.076	0.6016	0.3939	0.2026E+00	0.6284	0.0895
9.488	0.6016	0.6476	0.3860E+00	0.6284	0.3495
9.901	0.5656	0.9939	0.7842E+00	0.5833	1.0309
10.314	0.5351	1.0000	0.7941E+00	0.5447	0.7144
10.726	0.5090	1.0000	0.7941E+00	0.5115	0.5197
11.139	0.4858	1.0000	0.7941E+00	0.4819	0.3971
11.551	0.4645	1.0000	0.7941E+00	0.4549	0.3138
11.964	0.4447	1.0000	0.7941E+00	0.4298	0.2540
12.376	0.4260	1.0000	0.7941E+00	0.4061	0.2094
12.789	0.4080	1.0000	0.7941E+00	0.3835	0.1749
13.201	0.3905	1.0000	0.7941E+00	0.3617	0.1476
13.614	0.3733	1.0000	0.7941E+00	0.3405	0.1255
14.026	0.3563	1.0000	0.7941E+00	0.3195	0.1072
14.439	0.3390	1.0000	0.7941E+00	0.2986	0.0918
14.851	0.3213	1.0000	0.7941E+00	0.2774	0.0785
15.264	0.3027	1.0000	0.7941E+00	0.2555	0.0669
15.677	0.2823	1.0000	0.7941E+00	0.2318	0.0563
16.089	0.2571	1.0000	0.7941E+00	0.2034	0.0458
16.130	0.2545	1.0000	0.7941E+00	0.2005	0.0448
16.172	0.2519	1.0000	0.7941E+00	0.1976	0.0439
16.213	0.2491	1.0000	0.7941E+00	0.1945	0.0429
16.254	0.2462	1.0000	0.7941E+00	0.1913	0.0419
16.295	0.2431	1.0000	0.7941E+00	0.1880	0.0409
16.337	0.2399	1.0000	0.7941E+00	0.1845	0.0398
16.378	0.2365	1.0000	0.7941E+00	0.1807	0.0387
16.419	0.2327	1.0000	0.7941E+00	0.1767	0.0376
16.460	0.2285	1.0000	0.7941E+00	0.1722	0.0363
16.502	0.2049	1.0000	0.7941E+00	0.1474	0.0301

RUN IDENTIFICATION: 2-JUL-82 10:34:11

DIMENSIONLESS VARIABLES II

X*	DNU	DTAUL	DTAUI	DTAUS
0.000	0.1573E+03	0.1683E-04	0.3006E-09	0.1776E-13
0.413	0.1885E+03	0.1680E-04	0.2923E-06	0.2132E-08
0.825	0.1927E+03	0.1675E-04	0.6688E-06	0.8463E-08
1.238	0.1952E+03	0.1671E-04	0.1074E-05	0.1837E-07
1.650	0.1970E+03	0.1667E-04	0.1503E-05	0.3156E-07
2.063	0.1985E+03	0.1663E-04	0.1955E-05	0.4785E-07
2.475	0.1997E+03	0.1658E-04	0.2430E-05	0.6709E-07
2.888	0.2008E+03	0.1654E-04	0.2926E-05	0.8920E-07
3.300	0.2017E+03	0.1650E-04	0.3445E-05	0.1141E-06
3.713	0.2026E+03	0.1646E-04	0.3986E-05	0.1416E-06
4.125	0.2191E+03	0.1642E-04	0.4845E-05	0.1719E-06
4.538	0.2707E+03	0.1638E-04	0.6570E-05	0.2073E-06
4.950	0.3413E+03	0.1633E-04	0.9192E-05	0.2550E-06
5.363	0.4406E+03	0.1628E-04	0.1335E-04	0.3210E-06
5.776	0.5853E+03	0.1620E-04	0.2027E-04	0.4156E-06
6.188	0.8052E+03	0.1611E-04	0.3255E-04	0.5578E-06
6.601	0.1152E+04	0.1599E-04	0.5564E-04	0.7804E-06
7.013	0.1730E+04	0.1584E-04	0.1030E-03	0.1153E-05
7.426	0.2756E+04	0.1566E-04	0.2101E-03	0.1824E-05
7.838	0.4707E+04	0.1544E-04	0.4814E-03	0.3153E-05
8.251	0.8733E+04	0.1525E-04	0.1265E-02	0.6100E-05
8.663	0.1799E+05	0.1530E-04	0.3886E-02	0.1361E-04
9.076	0.4354E+05	0.1637E-04	0.1417E-01	0.3633E-04
9.488	0.1443E+06	0.2136E-04	0.5923E-01	0.1207E-03
9.901	0.8188E+06	0.4993E-04	0.7818E-01	0.3720E-03
10.314	0.8133E+06	0.5977E-04	0.6057E-01	0.3071E-03
10.726	0.7856E+06	0.6956E-04	0.5333E-01	0.2587E-03
11.139	0.7643E+06	0.8037E-04	0.4828E-01	0.2244E-03
11.551	0.7473E+06	0.9250E-04	0.4459E-01	0.1985E-03
11.964	0.7334E+06	0.1063E-03	0.4178E-01	0.1783E-03
12.376	0.7219E+06	0.1222E-03	0.3962E-01	0.1618E-03
12.789	0.7122E+06	0.1407E-03	0.3793E-01	0.1482E-03
13.201	0.7041E+06	0.1627E-03	0.3661E-01	0.1366E-03
13.614	0.6972E+06	0.1891E-03	0.3561E-01	0.1265E-03
14.026	0.6915E+06	0.2214E-03	0.3487E-01	0.1177E-03
14.439	0.6869E+06	0.2622E-03	0.3439E-01	0.1098E-03
14.851	0.6833E+06	0.3152E-03	0.3416E-01	0.1027E-03
15.264	0.6809E+06	0.3877E-03	0.3423E-01	0.9601E-04
15.677	0.6798E+06	0.4952E-03	0.3468E-01	0.8958E-04
16.089	0.6808E+06	0.6886E-03	0.3585E-01	0.8281E-04
16.130	0.6811E+06	0.7139E-03	0.3601E-01	0.8217E-04
16.172	0.6814E+06	0.7413E-03	0.3619E-01	0.8153E-04
16.213	0.6818E+06	0.7712E-03	0.3639E-01	0.8087E-04
16.254	0.6822E+06	0.8041E-03	0.3661E-01	0.8020E-04
16.295	0.6827E+06	0.8406E-03	0.3685E-01	0.7950E-04
16.337	0.6832E+06	0.8817E-03	0.3712E-01	0.7878E-04
16.378	0.6839E+06	0.9286E-03	0.3742E-01	0.7803E-04
16.419	0.6847E+06	0.9835E-03	0.3778E-01	0.7723E-04
16.460	0.6857E+06	0.1050E-02	0.3821E-01	0.7636E-04
16.502	0.6930E+06	0.1557E-02	0.4124E-01	0.7192E-04

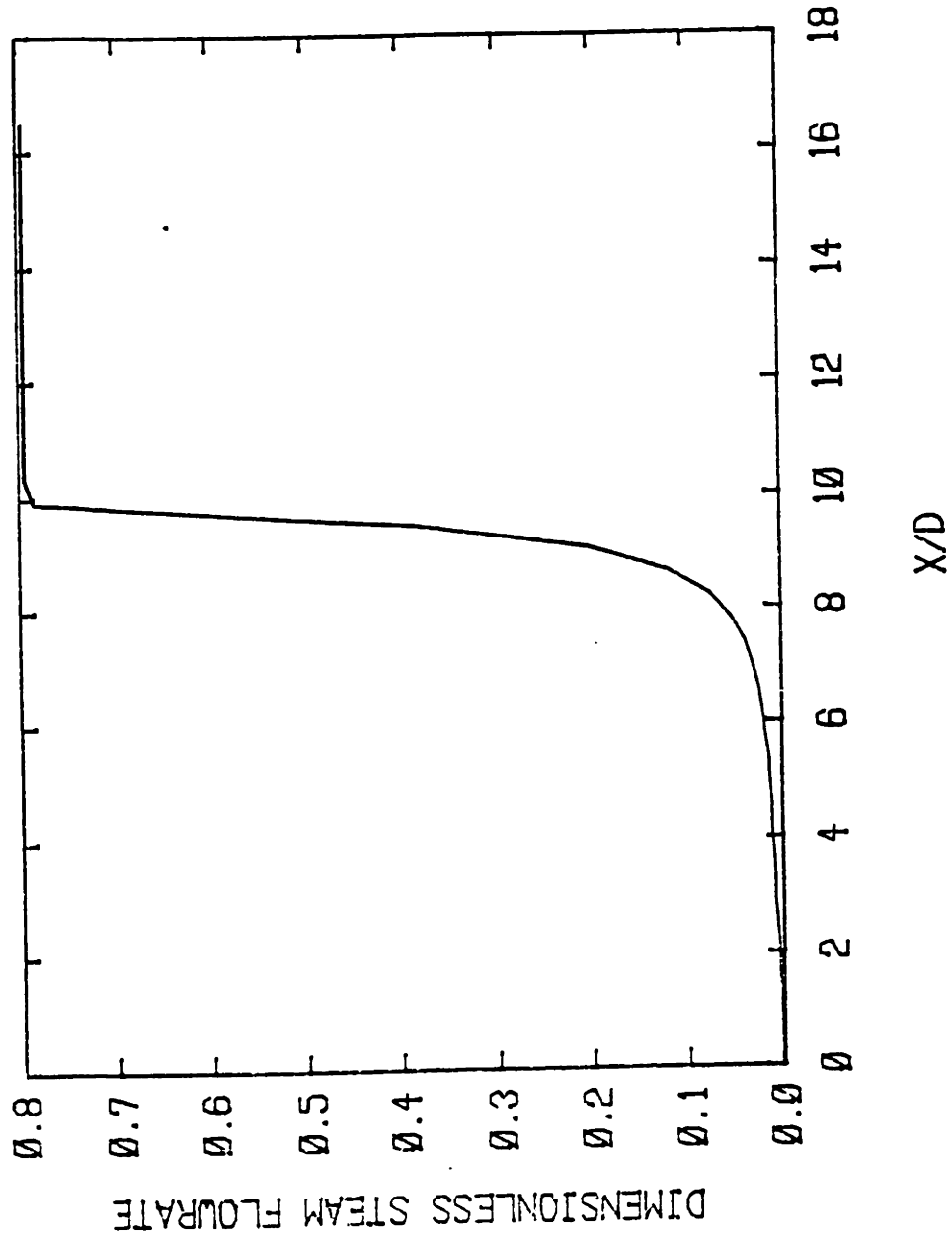


Figure E-1. Dimensionless steam flow rate profile for PWR steam generator sample case.

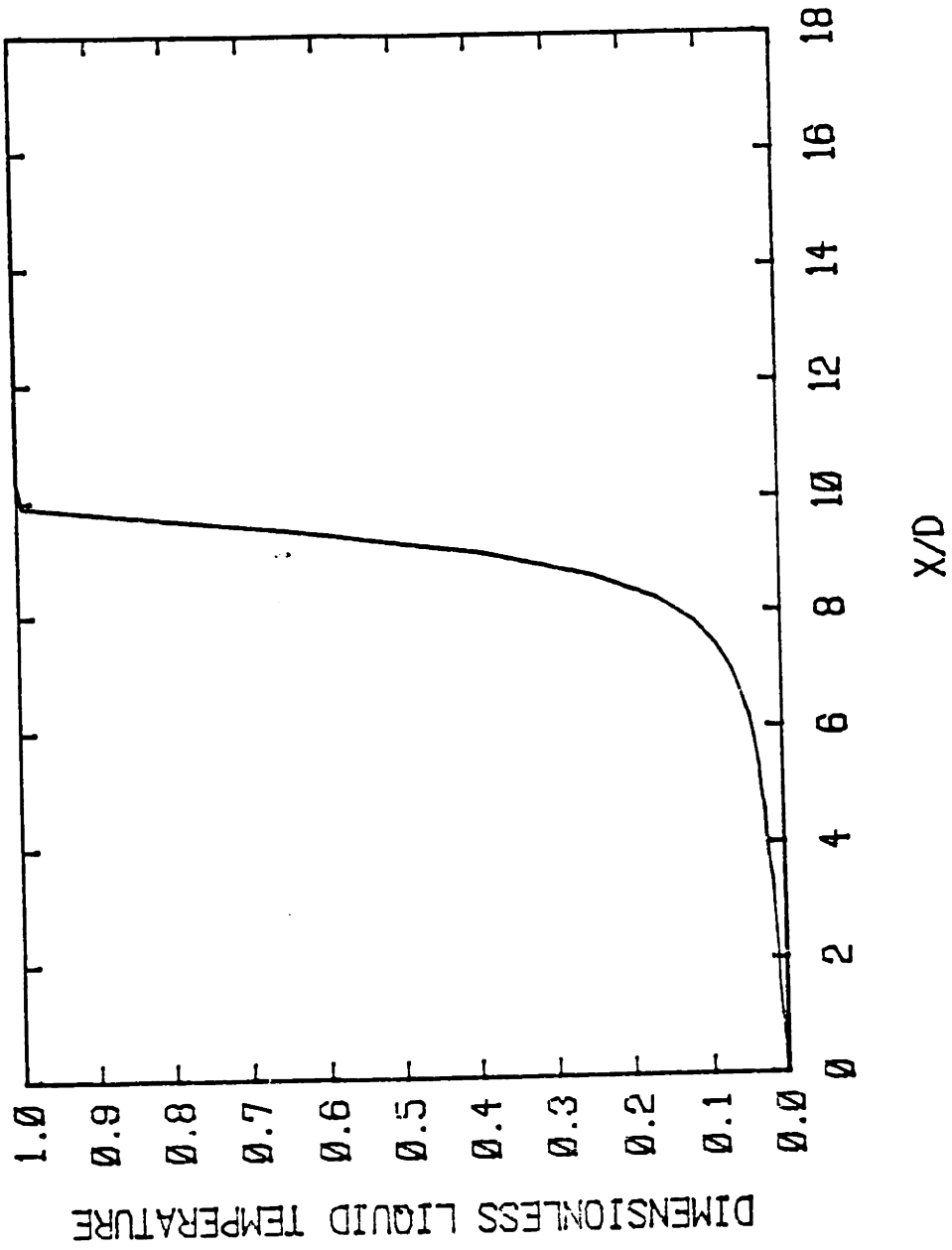


Figure E-2. Dimensionless liquid temperature profile for PWR steam generator sample case.

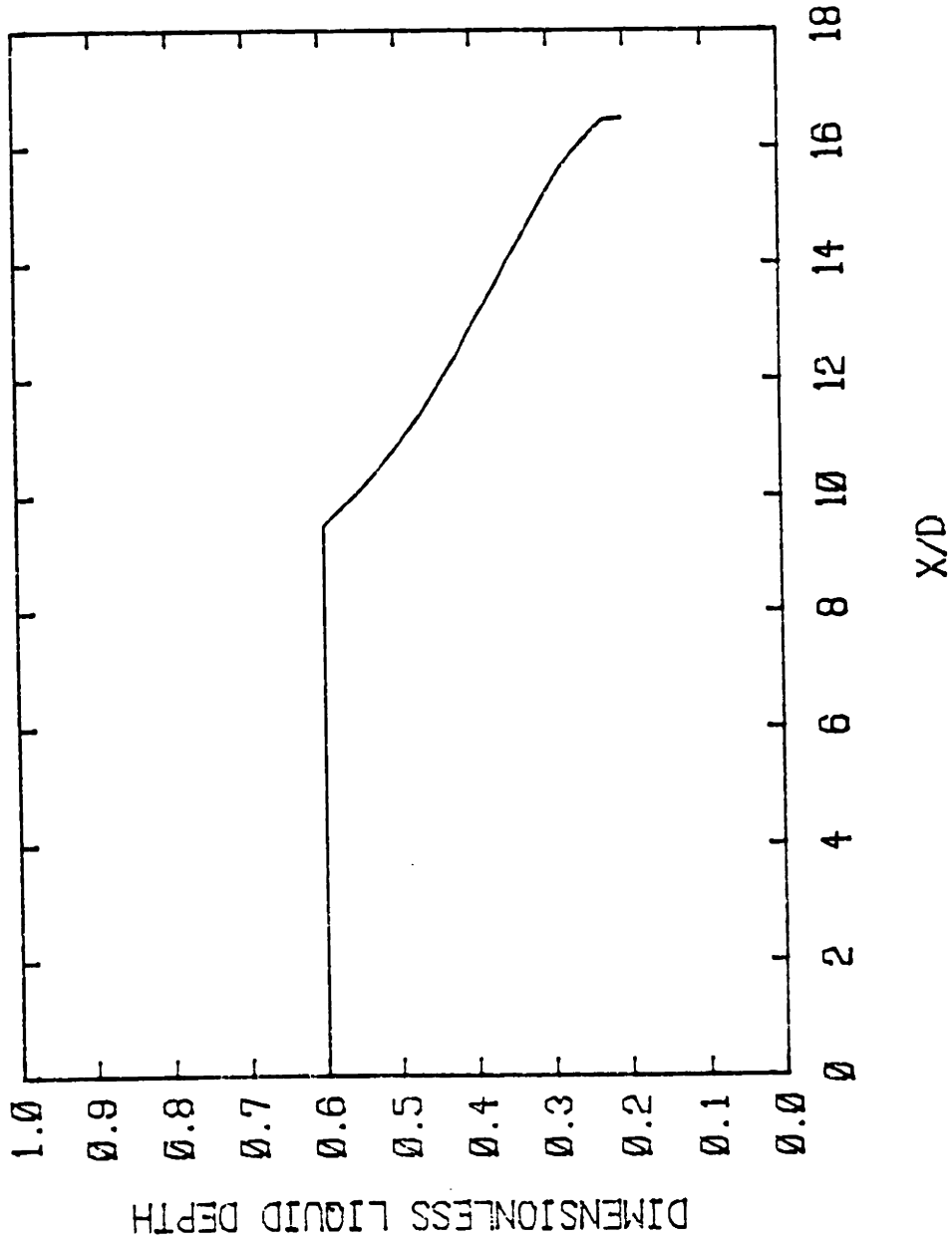


Figure E-3. Dimensionless liquid depth profile for PWR steam generator sample case.

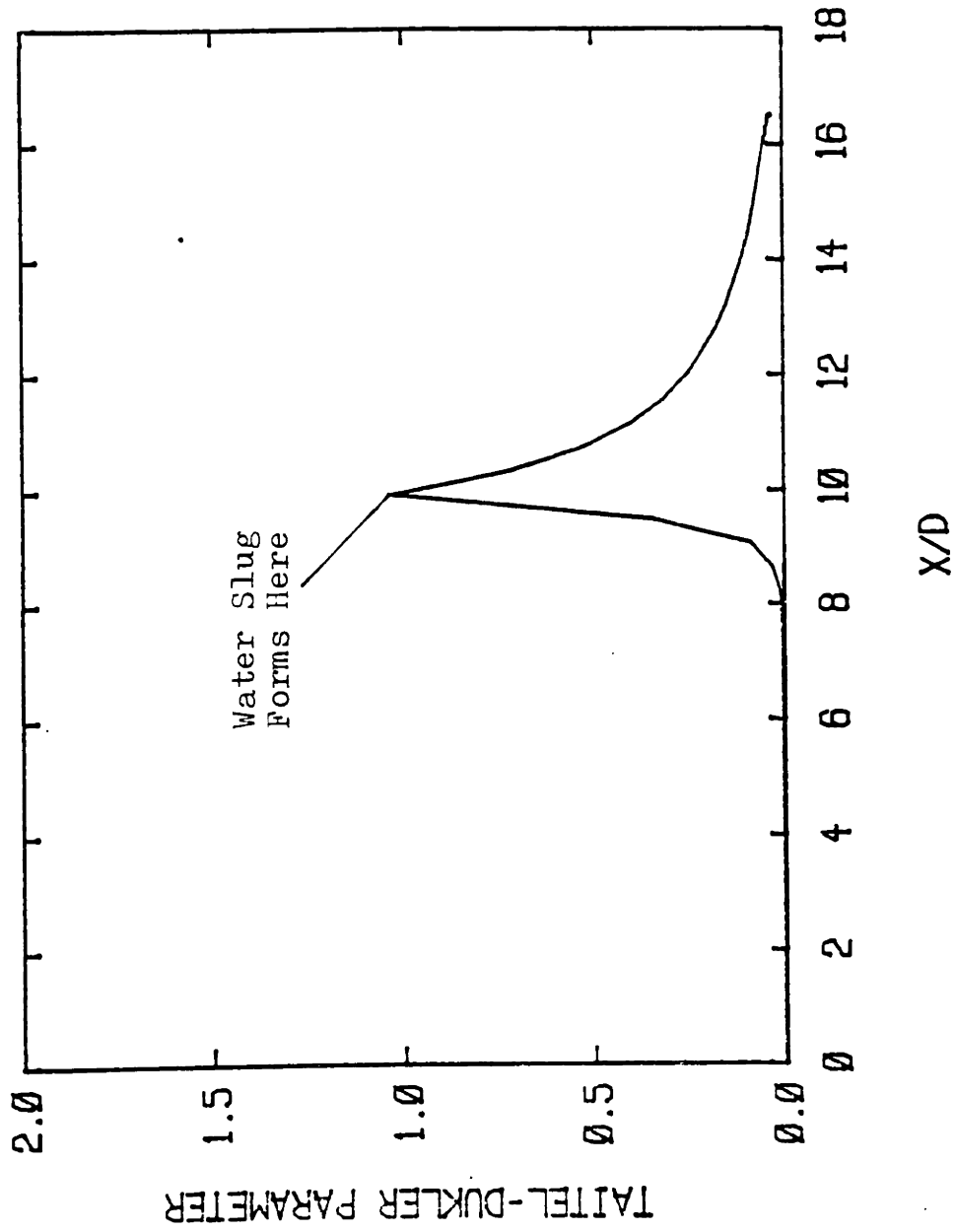


Figure E-4. Taitel-Dukler stability parameter profile for PWR steam generator sample case.

Appendix F

Computed Results for
Millstone #1
Isolation Condenser Sample Case

- I. Computer print of calculations.

- II. Plots of:
 - 1) Dimensionless steam flow rate.
 - 2) Dimensionless liquid temperature.
 - 3) Dimensionless liquid depth.
 - 4) Taitel-Dukler stability parameter.

RUN IDENTIFICATION: 2-JUL-82 10:16:19

INPUT DATA

NO. OF PASSES = 10	DZETAOUT = 0.075
L = 8.230 M	D = 0.2890 M
TSAT = 560.93 K	TLIN = 299.82 K
PSAT = 0.7208E+07 PA	N = 50 INTERVALS
INLET WATER FLOW = 2.3300 KG/S	PIPE SLOPE = 0.00000
DHMOD = 2.500	STEAM VENTED = 0.00000 KG/S

CALCULATED PROPERTIES

INLET LIQUID DENSITY = 995.5 KG/M3
 STEAM DENSITY = 37.583 KG/M3
 INLET LIQUID VISCOSITY = 0.8575E-03 KG/M*S
 STEAM VISCOSITY = 0.1898E-04 KG/M*S
 INLET LIQUID SPECIFIC HEAT = 4183.8 J/KG*K
 INLET LIQUID THERMAL COND. = 0.6135 W/M*K
 INLET LIQUID PRANDTL NO. = 5.848
 ENTHALPY OF VAPORIZATION = 0.1495E+07 J/KG

ABBREVIATIONS OF DIMENSIONLESS VARIABLES

X*	AXIAL LOCATION
DL*	LIQUID DEPTH
TL*	LIQUID TEMPERATURE
MS*	STEAM MASS FLOWRATE
DAL	LIQUID FLOW AREA
DUKLER	TAITEL-DUKLER PARAMETER
DNU	CONDENSATION NUSSELT NUMBER
DTAUL	LIQUID WALL SHEAR STRESS
DTAUI	INTERFACIAL SHEAR STRESS
DTAUS	STEAM WALL SHEAR STRESS

RUN IDENTIFICATION: 2-JUL-82 10:16:19

DIMENSIONLESS VARIABLES I

X*	DL*	TL*	MS*	DAL	DUKLER
0.000	0.6217	0.0000	0.1000E-05	0.6534	0.0000
0.712	0.6217	0.0039	0.1619E-02	0.6534	0.0000
1.424	0.6217	0.0086	0.3596E-02	0.6534	0.0000
2.136	0.6217	0.0134	0.5615E-02	0.6534	0.0001
2.848	0.6216	0.0183	0.7658E-02	0.6533	0.0001
3.560	0.6216	0.0231	0.9716E-02	0.6533	0.0002
4.272	0.6216	0.0280	0.1179E-01	0.6533	0.0003
4.984	0.6216	0.0329	0.1387E-01	0.6533	0.0005
5.696	0.6216	0.0378	0.1595E-01	0.6533	0.0006
6.407	0.6216	0.0427	0.1805E-01	0.6532	0.0008
7.119	0.6216	0.0479	0.2029E-01	0.6532	0.0010
7.831	0.6215	0.0544	0.2311E-01	0.6532	0.0013
8.543	0.6215	0.0627	0.2671E-01	0.6532	0.0018
9.255	0.6215	0.0735	0.3145E-01	0.6532	0.0024
9.967	0.6215	0.0880	0.3788E-01	0.6531	0.0036
10.679	0.6214	0.1081	0.4690E-01	0.6531	0.0055
11.391	0.6214	0.1369	0.6010E-01	0.6530	0.0090
12.103	0.6214	0.1798	0.8041E-01	0.6530	0.0162
12.815	0.6213	0.2463	0.1134E+00	0.6530	0.0326
13.527	0.6214	0.3522	0.1706E+00	0.6530	0.0753
14.239	0.6212	0.5210	0.2761E+00	0.6528	0.2050
14.951	0.6161	0.7698	0.4775E+00	0.6465	0.6192
15.663	0.5782	1.0000	0.7556E+00	0.5992	1.0077
16.375	0.5481	1.0000	0.7556E+00	0.5611	0.6735
17.087	0.5224	1.0000	0.7556E+00	0.5285	0.4880
17.798	0.4996	1.0000	0.7556E+00	0.4995	0.3721
18.510	0.4789	1.0000	0.7556E+00	0.4731	0.2939
19.222	0.4597	1.0000	0.7556E+00	0.4487	0.2380
19.934	0.4416	1.0000	0.7556E+00	0.4258	0.1965
20.646	0.4243	1.0000	0.7556E+00	0.4040	0.1646
21.358	0.4077	1.0000	0.7556E+00	0.3831	0.1394
22.070	0.3915	1.0000	0.7556E+00	0.3629	0.1191
22.782	0.3755	1.0000	0.7556E+00	0.3432	0.1024
23.494	0.3597	1.0000	0.7556E+00	0.3238	0.0885
24.206	0.3439	1.0000	0.7556E+00	0.3045	0.0766
24.918	0.3278	1.0000	0.7556E+00	0.2851	0.0664
25.630	0.3111	1.0000	0.7556E+00	0.2654	0.0575
26.342	0.2935	1.0000	0.7556E+00	0.2448	0.0495
27.054	0.2740	1.0000	0.7556E+00	0.2224	0.0421
27.766	0.2499	1.0000	0.7556E+00	0.1954	0.0345
27.837	0.2474	1.0000	0.7556E+00	0.1927	0.0338
27.908	0.2449	1.0000	0.7556E+00	0.1898	0.0331
27.979	0.2422	1.0000	0.7556E+00	0.1869	0.0324
28.050	0.2394	1.0000	0.7556E+00	0.1839	0.0317
28.122	0.2365	1.0000	0.7556E+00	0.1807	0.0310
28.193	0.2334	1.0000	0.7556E+00	0.1774	0.0302
28.264	0.2301	1.0000	0.7556E+00	0.1738	0.0294
28.335	0.2265	1.0000	0.7556E+00	0.1700	0.0286
28.406	0.2224	1.0000	0.7556E+00	0.1657	0.0277
28.478	0.1989	1.0000	0.7556E+00	0.1413	0.0230

RUN IDENTIFICATION: 2-JUL-82 10:16:19

DIMENSIONLESS VARIABLES II

X*	DNU	DTAUL	DTAUI	DTAUS
0.000	0.1298E+03	0.1367E-04	0.3443E-09	0.2056E-13
0.712	0.1587E+03	0.1364E-04	0.7019E-06	0.8499E-08
1.424	0.1624E+03	0.1361E-04	0.1651E-05	0.3435E-07
2.136	0.1646E+03	0.1358E-04	0.2705E-05	0.7494E-07
2.848	0.1663E+03	0.1355E-04	0.3856E-05	0.1290E-06
3.560	0.1676E+03	0.1352E-04	0.5103E-05	0.1958E-06
4.272	0.1688E+03	0.1349E-04	0.6448E-05	0.2746E-06
4.984	0.1698E+03	0.1347E-04	0.7894E-05	0.3650E-06
5.696	0.1707E+03	0.1344E-04	0.9444E-05	0.4667E-06
6.407	0.1835E+03	0.1342E-04	0.1166E-04	0.5793E-06
7.119	0.2306E+03	0.1340E-04	0.1607E-04	0.7115E-06
7.831	0.2963E+03	0.1338E-04	0.2294E-04	0.8936E-06
8.543	0.3911E+03	0.1335E-04	0.3412E-04	0.1153E-05
9.255	0.5326E+03	0.1332E-04	0.5332E-04	0.1535E-05
9.967	0.7531E+03	0.1329E-04	0.8841E-04	0.2129E-05
10.679	0.1114E+04	0.1327E-04	0.1574E-03	0.3100E-05
11.391	0.1739E+04	0.1327E-04	0.3054E-03	0.4802E-05
12.103	0.2904E+04	0.1335E-04	0.6560E-03	0.8038E-05
12.815	0.5273E+04	0.1363E-04	0.1588E-02	0.1483E-04
13.527	0.1074E+05	0.1445E-04	0.4400E-02	0.3093E-04
14.239	0.2611E+05	0.1681E-04	0.1393E-01	0.7479E-04
14.951	0.8391E+05	0.2431E-04	0.4357E-01	0.2037E-03
15.663	0.2779E+06	0.4704E-04	0.4242E-01	0.3753E-03
16.375	0.2649E+06	0.5499E-04	0.3543E-01	0.3002E-03
17.087	0.2554E+06	0.6350E-04	0.3098E-01	0.2519E-03
17.798	0.2482E+06	0.7277E-04	0.2789E-01	0.2179E-03
18.510	0.2424E+06	0.8303E-04	0.2562E-01	0.1925E-03
19.222	0.2377E+06	0.9450E-04	0.2389E-01	0.1726E-03
19.934	0.2337E+06	0.1075E-03	0.2255E-01	0.1566E-03
20.646	0.2304E+06	0.1223E-03	0.2149E-01	0.1433E-03
21.358	0.2276E+06	0.1394E-03	0.2064E-01	0.1321E-03
22.070	0.2251E+06	0.1594E-03	0.1997E-01	0.1225E-03
22.782	0.2231E+06	0.1831E-03	0.1945E-01	0.1141E-03
23.494	0.2213E+06	0.2117E-03	0.1905E-01	0.1067E-03
24.206	0.2199E+06	0.2467E-03	0.1877E-01	0.1000E-03
24.918	0.2188E+06	0.2908E-03	0.1861E-01	0.9396E-04
25.630	0.2179E+06	0.3481E-03	0.1858E-01	0.8837E-04
26.342	0.2174E+06	0.4266E-03	0.1869E-01	0.8309E-04
27.054	0.2173E+06	0.5431E-03	0.1901E-01	0.7793E-04
27.766	0.2179E+06	0.7530E-03	0.1974E-01	0.7241E-04
27.837	0.2180E+06	0.7803E-03	0.1984E-01	0.7190E-04
27.908	0.2181E+06	0.8100E-03	0.1994E-01	0.7137E-04
27.979	0.2182E+06	0.8423E-03	0.2006E-01	0.7083E-04
28.050	0.2184E+06	0.8779E-03	0.2019E-01	0.7028E-04
28.122	0.2186E+06	0.9175E-03	0.2033E-01	0.6971E-04
28.193	0.2188E+06	0.9619E-03	0.2048E-01	0.6912E-04
28.264	0.2190E+06	0.1013E-02	0.2066E-01	0.6850E-04
28.335	0.2193E+06	0.1072E-02	0.2087E-01	0.6784E-04
28.406	0.2196E+06	0.1143E-02	0.2111E-01	0.6713E-04
28.478	0.2223E+06	0.1714E-02	0.2291E-01	0.6334E-04

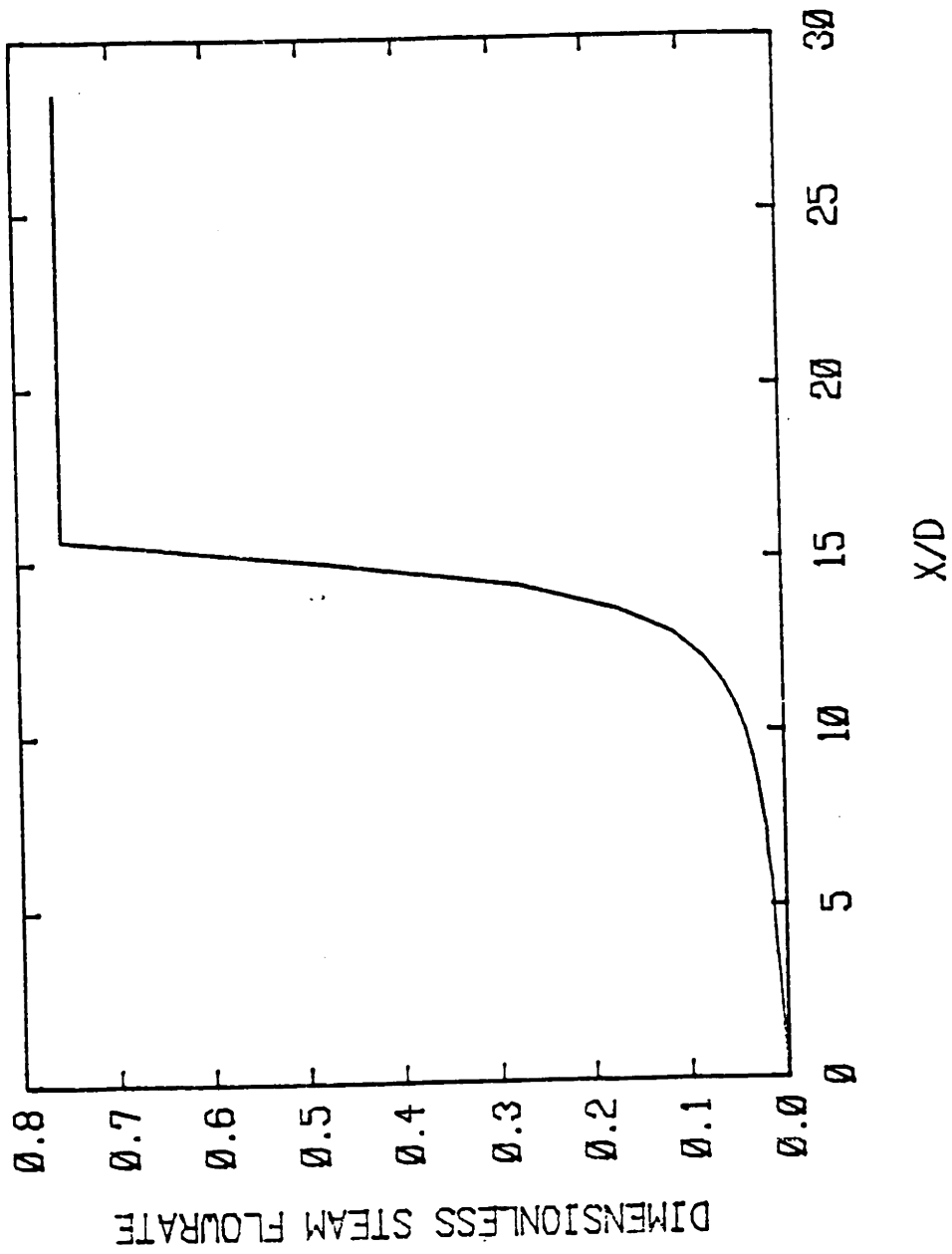


Figure F-1. Dimensionless steam flow rate profile for Millstone #1 isolation condenser sample case.

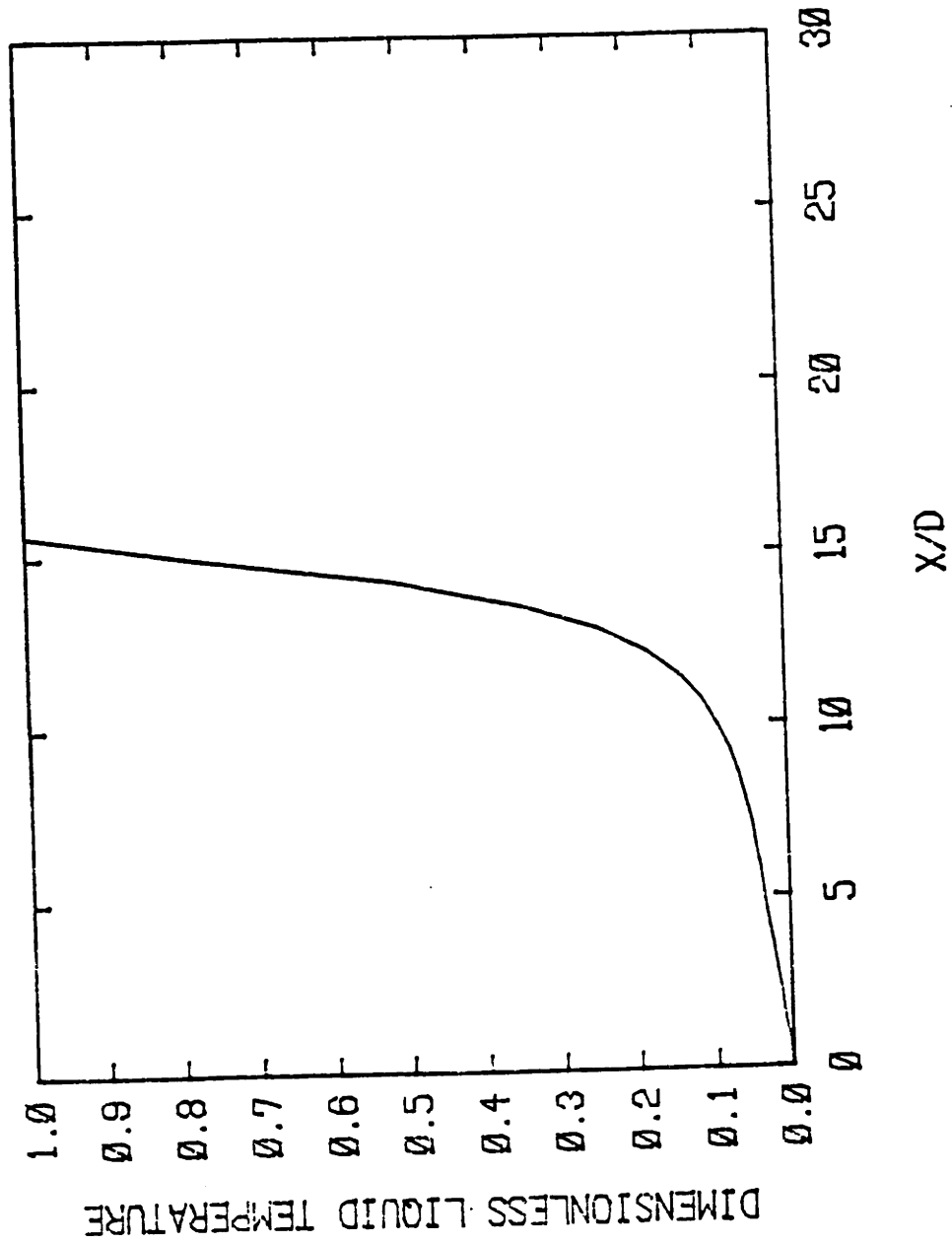


Figure F-2. Dimensionless liquid temperature profile for Millstone #1 isolation condenser sample case.

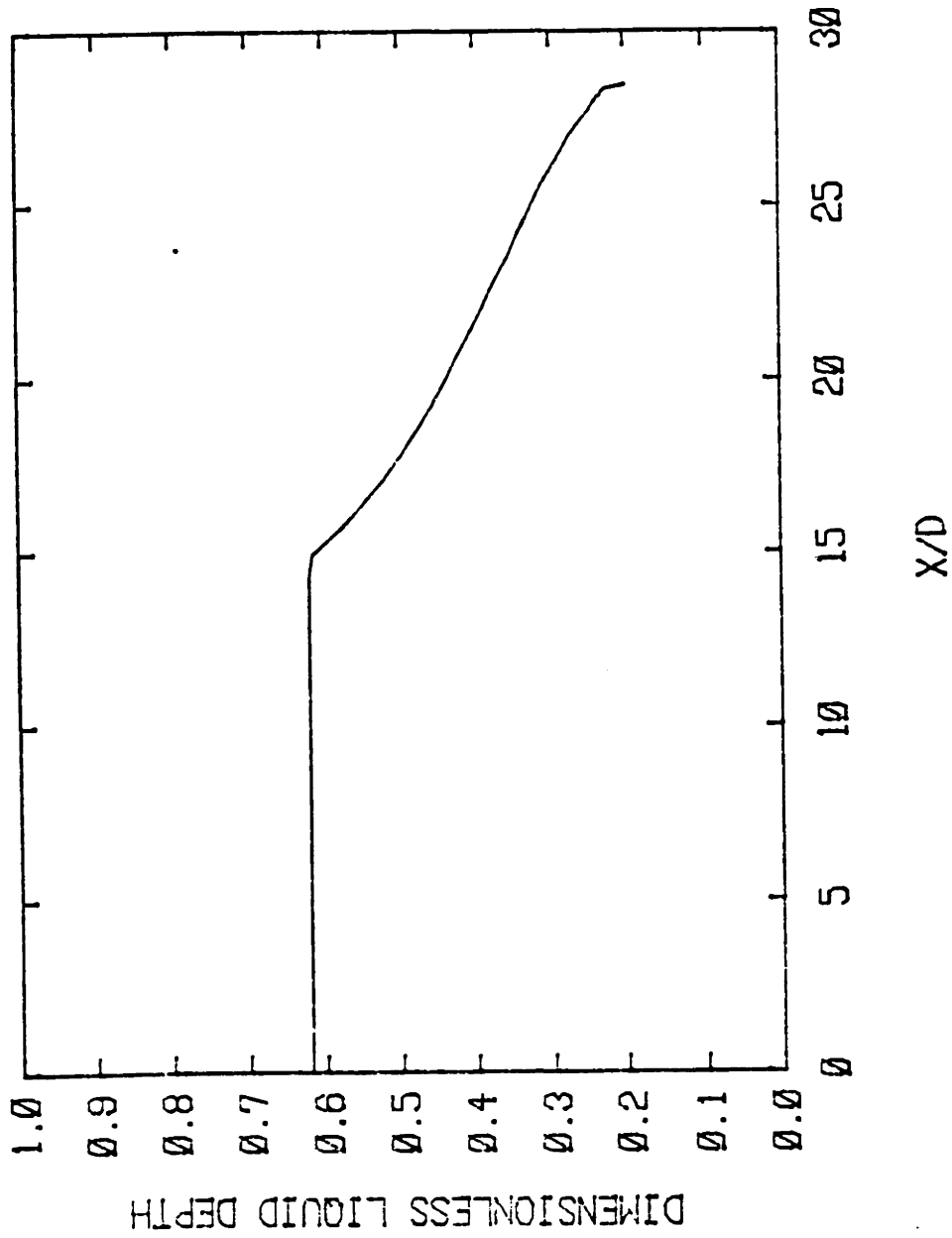


Figure F-3. Dimensionless liquid depth profile for Millstone #1 isolation condenser sample case.

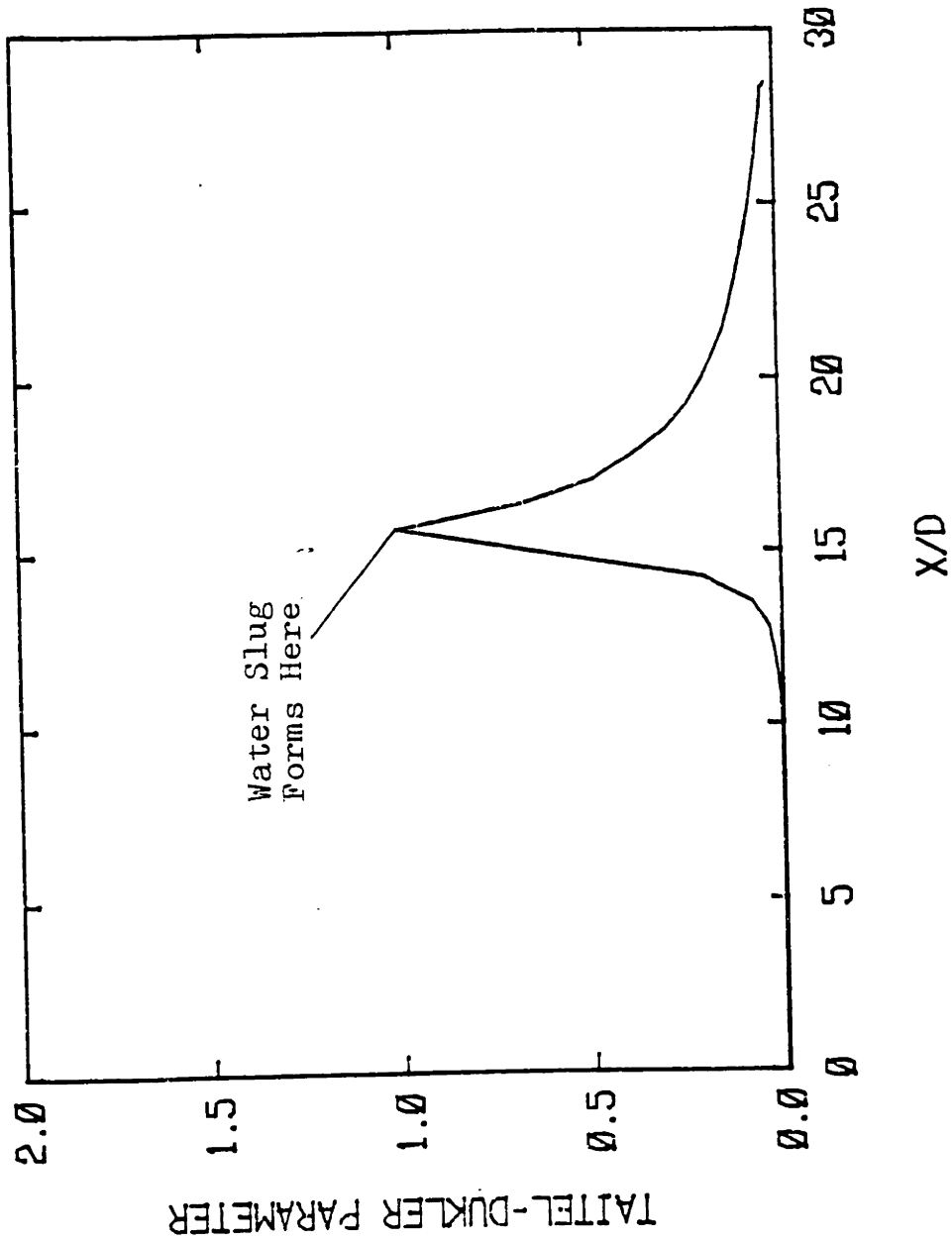


Figure F-4. Taitel-Dukler stability parameter profile for Millstone #1 isolation condenser sample case.

Appendix G

Design Procedure for Water Hammer Avoidance

The procedure to be described is appropriate for use in the flow geometry of Figure II-1. For many practical cases, it will be possible to simplify the actual system to this form.

The following step-by-step procedure may be followed to determine if a piping system has the potential to produce a water hammer event:

1. Determine if there are any horizontal or nearly-horizontal pipe runs in which steam and subcooled water are both present. Abnormal operating conditions and equipment characteristics (e.g., leaking valves) should be considered. If there are no such pipe runs, the condensation water hammer studied here cannot occur.
2. Use Equation (III-67) to determine if the pipe will run full for all flow rates and system conditions possible. If it will, the condensation water hammer studied here cannot occur.
3. Use the "absolute stability limit" model (the CHOP program, with $DHMOD = c_1 = 10,000$) for the worst flow rates and system conditions possible. If the Taitel-Dukler stability parameter cannot be made to exceed 1.0, the condensation water hammer studied here is not expected.

4. Use the CHOP program, with $DHMOD = c_1 = 2.5$ (the "metastable-unstable limit") for the worst flow rates and system conditions possible. If the Taitel-Dukler stability parameter cannot be made to exceed 1.0, condensation water hammer is unlikely, though possible. The proximity of operating conditions to the "metastable-unstable limit" compared with the "absolute stability limit" should be considered. If the Taitel-Dukler stability parameter does exceed 1.0, water hammer problems are anticipated.

If a water hammer problem appears likely, the following actions may be considered in an attempt to eliminate the problem:

1. Reduce the inlet water subcooling.
2. Reduce the pipe length.
3. Increase the pipe diameter, raising the "absolute stability" and "metastable-unstable" critical inlet water flow rates.
4. Decrease the pipe diameter, hoping to ensure the pipe always runs full.
5. Modify system operational characteristics to keep the system out of the water hammer region.
6. Add valves or other devices to prevent the establishment of stratified flow.
7. Modify the piping layout to eliminate the

horizontal run or place it where it will always be full of liquid.

The effects of these modifications may be found by use of the CHOP computer program.

Two other actions may also be considered:

1. Add noncondensable gas to the system, reducing the condensation rate and also reducing the effect of steam bubble collapse, should it occur.
2. Tilt the pipe upward to reduce the steam-water interfacial area.

These modifications cannot be evaluated using the methods described here. As pointed out in Chapter VI, further work is needed in these areas.